Optomechanics in the Quantum Regime

Max Ludwig

München 2008

Optomechanics in the Quantum Regime

Max Ludwig

Diploma thesis
at the Faculty of Physics
Ludwig–Maximilians–Universität
München

München,
November 28, 2008

First reviewer: Dr. Florian Marquardt
Second reviewer: Prof. Dr. Theodor W. Hänsch

Contents

Introduction

Imagine the pressure the sun exerts on your skin if you stand outside on a sunny day. Certainly you have never noticed it. The power of the sunlight at earth's distance, about $1.4\,\mathrm{kW}$ per square meter, translates into a radiation pressure of $10^{-5}\,\mathrm{N/m^2}$. This pressure is very small compared to the atmospheric pressure of $10^{5}\,\mathrm{N/m^2}$.

On the other hand, the sun's radiation pressure might be strong enough to replace the conventional propulsion of spacecrafts on interplanetary missions some day in the future. The idea of using large, reflective structures to sail through space is in fact nearly 400 years old. At that time, Johannes Kepler had observed tails of comets to be deflected by what he believed was a kind of "solar breeze". This was the first reported observation of radiation pressure acting on a mechanical object. Subsequently, Kepler suggested to build "ships and sails proper for heavenly air" in his "Dissertatio com Nuncio Sidereo" (Venice, 1610). The current development of solar sails (see figure 1b), as carried out by NASA and other research institutes, focuses on unmanned, lightweight spaceships. Indeed, a very light solar sail should be able to cover immense distances in a very fast and efficient manner. The radiation pressure of the sun when exerted on a sail, presumably with a total area of $1\,km^2$, is equivalent to a force of $9\,\mathrm{N}$. The acceleration on a solar spacecraft would then be comparable to the acceleration due to the gravitational force close to the earth's surface, i.e around $9\,m\,s^{-2}$ for a spacecraft with a mass of $1\,\mathrm{kg}$. As long as the solar sail stays close enough to the sun, its velocity is steadily increased and can reach values about five times higher than those of conventional rockets. It has even been proposed to push the sail with a very strong laser beam, that would then allow for interstellar missions.

Down on earth, one finds a prominent application of radiation pressure that followed the advent of laser technology: Using the force of laser light to slow down and cool ions or neutral atoms. The theoretical groundwork of this field was laid out in the mid 1970s [1, 2]. Major experimental progress was achieved in the 1980s reaching temperatures in the $\mu\mathrm{K}$ range and even observing the ground state of mechanical motion. These achievements allowed to measure atomic spectra more precisely and to improve atomic clocks and eventually led to the 1997 Nobel prize for Philips, Chu and Cohen-Tannoudji. As laser cooling techniques advanced, even lower temperatures were reached in the 1990s and thereby provided one of the key steps in the 1995 realization of Bose-Einstein condensation [3, 4].

Let us now come closer to the actual subject of this thesis, which is the coupling of a small, but still macroscopic mechanical device to an optical cavity field. The effects of radiation pressure on a relatively large mechanical element were already observed in the group of H. Walther at the MPQ [5] in the 1980s. Their setup used an optical cavity to enhance the light intensity resonantly. One of the cavity's end mirrors was suspended to swing as a pendulum. Hence the motion of the movable mirror was coupled to the cavity field via radiation pressure. At an even earlier stage, the Russian scientist V. Braginsky had considered and performed similar experiments [6, 7].

More recently, the advances in microfabrication led to a miniaturization of such optomechanical

setups: Instead of a macroscopic end mirror, state-of-the-art optomechanical experiments use cantilevers, as otherwise used for atomic force microscopy (see figure 1e), doubly clamped beams, microtoroids or other micromechanical elements that can be affected by light. The fact that their dimensions are in the range of micrometers diminishes the surface area on which the radiation pressure can act. Nevertheless, the small masses ($\sim 10^{-9}\,\mathrm{kg}$) and high quality factors of the mechanical devices, the use of focused laser beams and the enhancement by high-finesse cavities allow for the observation of strong radiation-pressure induced effects. If we assume a laser power of $1\,\mathrm{W}$ focused on a micro-gram mirror with a surface area of $(10\,\mu\mathrm{m})^2$, the radiation pressure exerts a force of roughly $7 \cdot 10^{-9}\,\mathrm{N}$. The acceleration due to this force would then be of the order of $10\,\mathrm{m\,s^{-2}}$ - comparable to the acceleration we assumed for the solar sail above.

Regardless of the specific implementation and geometry, all the just mentioned optomechanical setups share the same basic principle: They consist of a cavity whose resonance frequency depends on the position of some mechanical oscillator. If the radiation pressure of the cavity field deflects the mechanical element, the cavity will in turn be detuned. The cavity can not react instantaneously on the position of the mechanical oscillator. This can be understood by observing, that photons, once they impinged the cavity, stay there for an average time given by the inverse of the cavity decay rate. The time-delayed cavity-induced forces acting on the mechanical oscillator can lead to an additional damping. This effect can be used to cool down the thermal motion of the mechanical element. Note that the small dimension and high mechanical sensitivity of the commonly used micromechanical resonators makes them very susceptible to the fluctuations of the environment. Optomechanical cooling of the thermal motion of a mechanical oscillator has already been demonstrated in a number of experiments [8, 9, 10, 11, 12, 13, 14]. The fundamental mode of the mechanical motion has been cooled down to temperatures up to a few mK starting from room temperature (see for example [14]). Optomechanical cooling may eventually be used to reach the ground state of mechanical motion [15, 16] and several groups aim at reaching this goal. This is indeed a luring aspect of this field: The optomechanical coupling should one day allow to observe the zero-point uncertainty of a macroscopic object consisting of roughly 10^{-20} atoms and observe fundamental aspects of quantum mechanics on scales where they could not be measured so far. The quantum effects that might become observable in optomechanical systems are a main issue of this thesis.

On the other hand, the light-induced forces can also amplify the response of the mechanical oscillator to the noise of its environment and heat up its thermal motion. Moreover, when the power of the laser pumping is increased above a certain threshold, an instability occurs. The mechanical oscillator starts to oscillate at approximately its eigenfrequency with an amplitude that at first grows exponentially and finally settles to a constant value. The instability and the corresponding self-sustained oscillations have been observed in a number of experiments [17, 18, 19, 20]. A theoretical analysis of the coupled system of cavity and mechanical oscillator allows to predict the system's dynamics in form of an intricate attractor diagram [21]. This attractor diagram predicts multistable attractors, i.e. the possibility of multiple solutions of the mechanical oscillation amplitude for a single set of system parameters. A recent comparison of this theory to experimental data which was attained in the group of K. Karrai at LMU, led to a good agreement and revealed the unexpected feature of the simultaneous excitation of several mechanical modes [20]. Note that both the instability as well as the multistable behaviour are common features of coupled nonlinear systems.

The multistable behaviour of optomechanical systems might one day be exploited for a highly-sensitive force measurement. Already today, optomechanical systems similar to the ones discussed here but with much larger dimensions, are employed in the observation of gravitational waves,

for example in the LIGO (Large Interferometer Gravitational Wave Observatory). In such detectors, heavy mechanical elements ($\sim 10\,\mathrm{kg}$) are exposed to radiation pressure in the $4\,\mathrm{km}$ long interferometer arms.

In the past few years it also became apparent that the basic features of optomechanical setups can also be observed in system which contain no optical elements at all. These nanoelectromechanical systems include driven LC circuits coupled to cantilevers [22] or single electron transistors

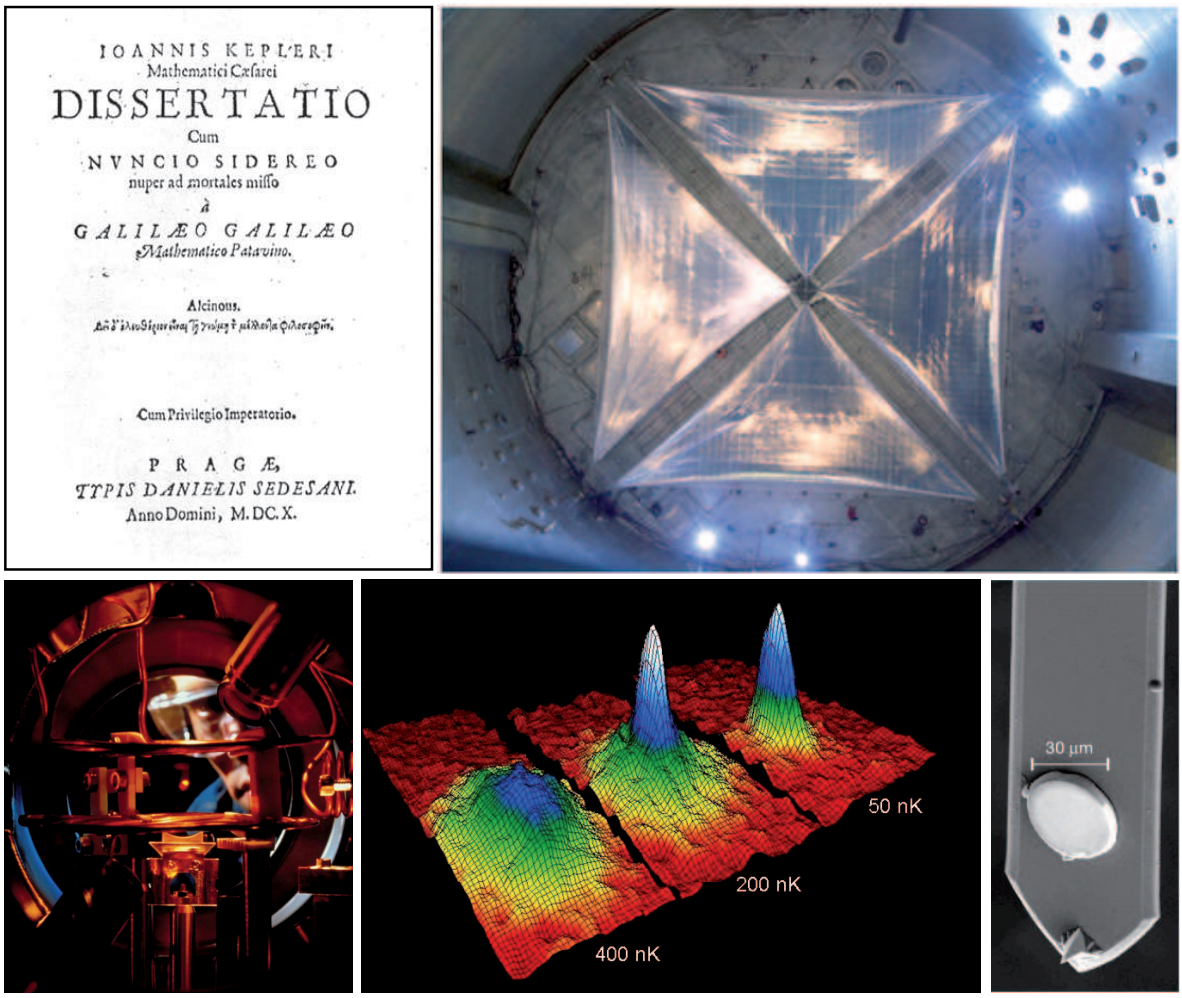

Figure 1: (a) Title page of "Dissertatio cum nuncio sidereo nuper ad mortales misso a Galilaeo Galilaeo" by Johannes Kepler (1571-1630). This work was a reply to Galileo's book "Sidereus Nuncius", issued in Venice in 1610, that had been enthusiastically received by Kepler. (b) A solar sail ($20 \times 20\,m$), developed at the NASA Glenn Research Center. (Source: NASA) (c) View on a sample of cold sodium atoms (bright spot at the center). The atoms are in a magneto-optical trap at a temperature of less than $1\,\mathrm{mK}$. (Picture taken by H. M. Helfer/NIST) (c) The emergence of Bose-Einstein condensation in a cloud of ultra-cold Rubidium atoms as observed by Cornell and Wieman in 1995 [3]. (Source: Mike Matthews, JILA) (d) A cantilever with a micro-meter mirror attached close to its tip as implemented in the setup of the Bouwmeester group. (Picture taken from the publication [11])

and microwave cavities coupled to nanobeams [23, 24, 25, 26, 27, 28, 29, 30].

Another modification of the basic optomechanical setup directs us towards another main issue of this thesis: The idea is to replace the solid mechanical object of conventional setups by a cloud of cold atoms coupled to a single optical cavity mode. The collective motion of the atoms couples to the light intensity in a similar way as the mechanical element. Hence the basic principles of optomechanical systems can be applied directly to these setups. "Optomechanics with cold atoms" might enhance the capabilities in the field of optomechanics and lead towards new regimes. It is an issue of ongoing research and first results were presented quite recently [31, 32, 33, 34]. The number of atoms involved in these setups is of the order of 10^5. Accordingly the total mass of the atomic cloud ($\sim 10^{-20}\,kg$) lies somewhere between the mass of conventional nanobeams ($\sim 10^{-9}\,\mathrm{kg}$) and the limiting case of a single atom ($\sim 10^{-25}\,\mathrm{kg}$) where the quantum regime of ground state cooling has already been extensively studied in ion and atom traps.

It is in a way fascinating to see the wide range of length scales and weights that can be assessed via radiation pressure. In this introduction we discussed a variety of objects that can be affected by the photon pressure of some light source: macroscopic devices, such as (virtual) spacecrafts or test masses in gravitational wave detectors, as well as mesoscopic mechanical oscillators, a cloud of cold atoms or even a single ion or atom. The dimensions of these systems cover mulitple length scales: The detectors at LIGO, even though stretching over a length of $4\,\mathrm{km}$, have to resolve changes in the length of one interferometer arm of about $10^{-18}\,\mathrm{m}$ in order to detect gravitational waves. A conventional cantilever has dimensions on the scale of a few tens of micrometers. While it is already challenging to fabricate such a small mechanical device and incorporate it into a cavity setup, the goal of ground-state cooling is even more ambitious: The zero-point amplitude of the cantilever motion is about $10^{-15}\,\mathrm{m}$, which is roughly the size of the nucleus of a hydrogen atom.

In this thesis we will focus on the lower end of this scale and characterize features of optomechanical systems in the quantum regime. We will consider a generic optomechanical system consisting of a cavity and a movable mirror attached to a cantilever. A fully quantum mechanical treatment based on the numerical simulation of a master equation will be employed to analyze the dynamics of the system. We will discuss the occurrence of the instability in this picture and compare it to the predictions of the attractor diagram which relies on a purely classical approach. This comparison allows to discuss the influence of quantum fluctuations on the coupled cavity-cantilever system and to identify a "quantum-parameter" that keeps track of this quantum-to-classical transition. The dimensionless quantum parameter is given by the ratio between the mechanical zero-point fluctuation amplitude (a quantum parameter $\propto \sqrt{\hbar}$) and the width of the optical resonance (a classical lengthscale). For a large value of the quantum parameter, i.e. in the "quantum regime", the photon shot noise of the cavity and the mechanical zero-point fluctuations affect the system substantially. To reach this regime in experiment one would first of all have to reduce the influence of the (thermal) environment, which could for example be achieved by cooling the cantilever in a preliminary step using the light field. As we will see, the system moreover has to feature both a strong cavity-cantilever coupling and a high cavity finesse, in order to reach a high value of the quantum parameter. Generic optomechanical systems have not reached this regime yet.

Optomechanics with cold atoms however, as realized in the group of D. Stamper-Kurn at Berkeley [32] and in the group of T. Esslinger in Zürich [33], show a substantial quantum parameter $\zeta \sim 1$ already today. In the second part of the thesis we therefore turn towards systems of this kind. In our model setup we combine the concept of the Berkeley setup, i.e. an atomic cloud coupled to a single cavity mode, with a generic optomechanical system consisting of a cavity and a cantilever. Hence we aim at coupling a single cavity mode, a mechanical cantilever and a

cloud of cold atoms. For the interaction between the cantilever and the center-of-mass motion of the atoms, we can identify two basic coupling mechanisms: The cantilever position determines the spatial structure of the cavity field, and therefore can shift the position of the atomic cloud. Apart from this direct coupling, virtual transitions via the cavity mode can induce a second-order coupling between the cantilever and the atomic motion that turns out to be much stronger. Once such relatively strong coupling is eventually realized, it will open up interesting possibilities: One may for example observe the coupled dynamics of the cantilever and the atomic collective mode as the oscillation energy is swapped between the two elements. Even though this beating behaviour is a general feature of coupled oscillators, it should certainly be of main interest to observe this phenomenon on such small devices.

This thesis has the following structure: The first chapter introduces the model of a generic optomechanical setup and discusses its Hamiltonian and the system parameters. In the second chapter, we will analyse the dynamics of the coupled cavity-cantilever system, in particular the occurrence of the instability, by employing a fully quantum mechanical treatment. In the second part of this thesis we will focus on optomechanical systems that involve the collective motion of a cloud of cold atoms. The third chapter introduces basic concepts of the description of trapped Bose-condensed gases. These concepts will be used in the fourth chapter where we consider a model setup consisting of a cavity, a cantilever and a cloud of ultracold atoms and analyse the coupling mechanisms of this model. At the end we will summarize the content of the thesis and discuss further extensions and perspectives. Some details on the numerical methods used in this work are given in the appendix.

Chapter 1

The basic optomechanical setup

This chapter presents the basic model of an optomechanical system consisting of an optical cavity with a movable end mirror. We will discuss both the Hamiltonian and the main features of this setup and identify a set of six parameters that determine the system completely. In particular, we introduce a quantum parameter, which does not show up in the classical description of the system. In the chapter subsequent to this one, we will see that this parameter determines the crossover from classical to quantum behavior of the system's dynamics.

1.1 The model

To begin with, we attempt to illustrate the basic mechanism of a generic optomechanical system: The basic setup consists of a driven, one-sided cavity and a movable end mirror. We imagine this end mirror to be made of a cantilever that is suspended to swing like a pendulum and that reflects the light due to an attached mirror or a coated surface. When a laser pumps light resonantly into the cavity, a standing wave of relatively high intensity builds up. The light field exerts a radiation pressure force on the cantilever and deflects it. Hence the cavity is detuned from resonance by the cantilever motion and the light field diminishes. Correspondingly, the radiation pressure force decreases, allows the cantilever to swing back and the whole cycle can start again.

We consider the following Hamiltonian to describe the system:

$$\hat{H} = \hbar\left(-\Delta + g_M\left(\hat{b}+\hat{b}^\dagger\right)\right)\hat{c}^\dagger\hat{c} \;+\; \hbar\omega_M\hat{b}^\dagger\hat{b} \;+\; \hbar\alpha_L(\,\hat{c}+\hat{c}^\dagger\,) \;+\; \hat{H}_\kappa \;+\; \hat{H}_{\Gamma_M}\,, \qquad (1.1)$$

which is written in the rotating frame of the driving laser field whose frequency is denoted by ω_L and whose amplitude is set by α_L. The laser is detuned by $\Delta = \omega_L - \omega_{\mathsf{cav}}$ with respect to the optical cavity mode which is described by photon annihilation and creation operators $\hat{c}$ and $\hat{c}^\dagger$, and a photon number $\hat{n}_{\mathrm{cav}} = \hat{c}^\dagger\hat{c}$. The cantilever (or, in general, mechanical element) has frequency ω_M and mass m_M, and its displacement is given as $\hat{x}_M = x_{\mathsf{ZPF}}(\hat{b}+\hat{b}^\dagger)$, with the mechanical zero-point amplitude of $x_{\mathsf{ZPF}} = \sqrt{\hbar/(2m_M\omega_M)}$. The optomechanical coupling, between the optical field and the mechanical displacement, is characterized by the parameter g_M. In the simplest case, with a movable, fully reflecting mirror at one end of an optical cavity of length L, we have $g_M = -\omega_{\mathrm{cav}}x_{\mathrm{ZPF}}/L$, and thus $g_M(\hat{b}+\hat{b}^\dagger) = -\omega_{\mathrm{cav}}\hat{x}_M/L$. The radiation pressure force corresponding to this coupling term is given by $\hat{F}_{\mathsf{rad}} = -\hbar g_M\hat{c}^\dagger\hat{c}/x_{\mathsf{ZPF}} = \hbar\omega_{\mathsf{cav}}\hat{c}^\dagger\hat{c}/L$. The decay of a photon and the mechanical damping of the cantilever are captured by $\hat{H}_\kappa$ and $\hat{H}_{\Gamma_M}$, respectively. They describe coupling to a bath leading to a cavity damping rate κ and mechanical damping Γ_M. Note that each of the parameters Δ, g_M, ω_M, α_L has the dimension of a frequency.

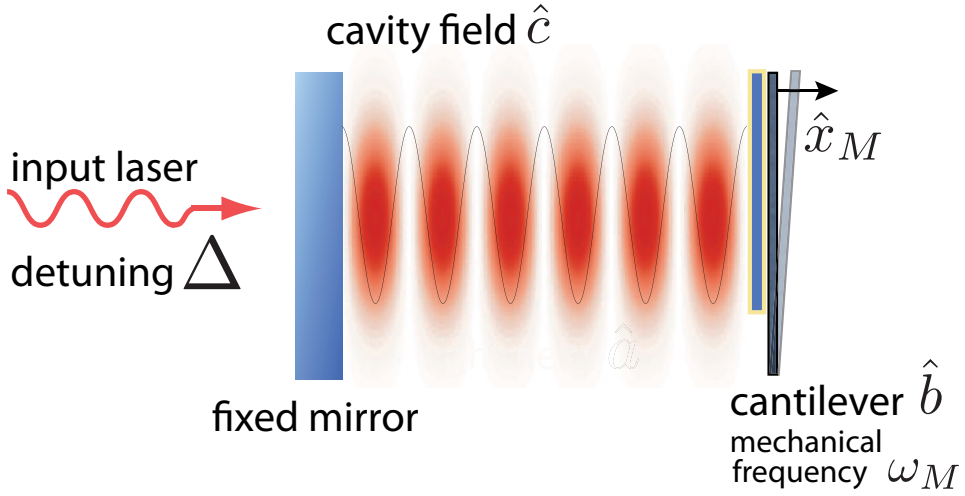

Figure 1.1: The basic optomechanical setup: A cavity consisting of two mirrors one of whom is free to oscillate. Common implementations involve a cantilever with an attached mirror or gold coated beams. The cavity is driven by an incoming laser.

Even though the basic back-action scheme illustrated above is relatively simple, the features of the coupled cavity-cantilever system are quite intricate. Depending on the detuning Δ of the laser with respect to the cavity, the motion of the cantilever is either amplified or cooled down by the light field. In the resolved sideband regime, where the cavity decay is small compared to the mechanical eigenfrequency ($\kappa \ll \omega_M$), the cooling (heating) is especially effective at the sidebands, i.e. for $\Delta = n\,\omega_M$, $n\,\epsilon\,\mathbb{Z}$. This can be understood by analogy to the Raman-scattering process: When a photon enters the cavity with a frequency that is red-detuned with respect to the cavity resonance at exactly $\Delta = -\omega_M$, it will likely absorb a phonon of the cantilever's motion of energy ω_M and hence meet the resonance frequency of the cavity again. On the other hand, a blue-detuned laser will rather emit phonons to the cantilever and thereby heat it up. Note that the resolved sideband regime has been reached in experiment recently [35].

If the system is in the regime of amplification, an increase of the laser input power above a certain threshold can lead to an instability: The mechanical oscillation amplitude starts to increase at first exponentially and the cantilever settles eventually into a regime of self-induced oscillations where the cantilever swings with a constant amplitude at its eigenfrequency. The occurrence of an instability is a basic feature of nonlinear dynamical system. In view of the Hamiltonian (1.1) the nonlinearity arises from the coupling of the cantilever position to the squared amplitude of the cavity field given by the term $\propto \hat{x}_M \hat{c}^\dagger \hat{c}$. When we discuss the dynamics of the coupled cavity-cantilever system in chapter 2, we will focus on the regime of self-induced oscillations. On the one hand it allows to compare the quantum mechanical approach that we will employ to the solution of the classical system [21]. On the other hand we expect the quantum effects to be most pronounced beyond the threshold of the instability.

1.2 Reduction to a set of dimensionless and independent parameters

We now identify the dimensionless parameters the system dynamics depends on. Expressed in terms of the mechanical oscillator frequency ω_M, the parameters describing the classical system are

$$\begin{aligned} \text{mechanical damping} &: \Gamma_M/\omega_M \\ \text{cavity decay} &: \kappa/\omega_M \\ \text{detuning} &: \Delta/\omega_M \\ \text{driving strength} &: \mathcal{P} = 8|\alpha_L|^2 g_M^2/\omega_M^4 = \omega_{\text{cav}}\kappa^2 E_{\max}^{\text{cav}}/(\omega_M^5 m_M L^2). \end{aligned} \tag{1.2}$$

Here $E_{\max}^{\text{cav}}$ is the light energy circulating inside the cavity when the laser is in resonance with the optical mode.

The quantum mechanical nature of the system is described by the "quantum parameter" ζ, comparing the magnitude of the cantilever's zero-point fluctuations, x_{ZPF}, with the full width at half maximum (FWHM) of the cavity (translated into a cantilever displacement x_{FWHM})

$$\text{quantum parameter} : \zeta = \frac{x_{\text{ZPF}}}{x_{\text{FWHM}}} = \frac{g_M}{\kappa}\,. \tag{1.3}$$

The resonance width of the cavity can be expressed as $x_{FWHM} = \kappa L/\omega_{\text{cav}}$, where L is the cavity's length. The quantum parameter ζ vanishes in the classical limit $\hbar \to 0$, as the zero-point fluctuations x_{ZPF} of the cantilever go to zero. The magnitude of ζ determines the effect of quantum fluctuations on the dynamics of the coupled cavity-cantilever system.

We note that there is an alternative way to introduce the quantum parameter (1.3). Here we made use of the two characteristic length scales of the system. Alternatively, we could compare the zero-point momentum fluctuations of the cantilever to the impulse a single intracavity photon transfers to the cantilever. When the photon is reflected at the cantilever, it transfers an impulse of $2\hbar k$. This process is repeated after one cavity round-trip time $\frac{2L}{c}$ for as long as the photon stays inside the cavity, i.e. for a span of time given by κ^{-1}. The total transfer of momentum is therefore given by $p_{\text{phot}} = \hbar k \frac{c}{L}\kappa^{-1} = \frac{\hbar\omega_{\text{cav}}}{\kappa L}$. The strength of the zero-point momentum fluctuations is given by $p_{\text{ZPF}} = \sqrt{\frac{\hbar m_M \omega_M}{2}} = \frac{\hbar}{2x_{\text{ZPF}}}$. Taking the ratio of these to quantities leads directly to the quantum parameter:

$$\frac{p_{\text{phot}}}{p_{\text{ZPF}}} = \frac{2x_{\text{ZPF}}}{\kappa L/\omega_{\text{cav}}} = 2\zeta. \tag{1.4}$$

We see that for a large quantum parameter a single phonon of the cantilever causes a detectable shift of the cavity resonance as well as a single photon causes the cantilever to change its momentum noticeably. Finally we note, that in a recent article Murch et al., introduced a so called granularity parameter to describe the impact of a single photon on the collective motion of ultracold atoms [32]. It directly corresponds to the quantum parameter (1.3), as we will see in section (4.3) of this thesis.

In the following section we will discuss the dynamics of the cantilever due to the driving of the cavity both in a quantum mechanical and a classical treatment. The quantum parameter will turn out to be very suitable for this analysis which will focus on the system's most characteristic quantities, in particular the number of photons in the cavity and the energy of the cantilever's oscillation. There are a few words to be said about the mechanical oscillation energy.

In the classical picture we can obtain a solution of the oscillation amplitude A as a function of the system parameters. This solution has been given in [21] and will be briefly reviewed at the beginning of the subsequent chapter. The expression for the mechanical oscillation energy follows directly from this solution as $E_{M,\mathsf{cl}} = \frac{1}{2}m\omega_M^2 A^2$. The quantum mechanical treatment on the other hand allows to get E_M from the expectation value of the cantilever's occupation number: $E_{M,\mathsf{qm}} = \hbar\omega_M\langle\hat{n}_M\rangle$, where we exclude the zero-point energy. We note that there is one peculiarity in our definition of the phonon occupation number $\langle\hat{n}_M\rangle$. If we would define $\hat{n}_M = \hat{c}^\dagger\hat{c}$, a static displacement of the cantilever, i.e. $\langle\hat{x}_M\rangle \neq 0$, would already yield a non-zero occupation number, even in the absence of any oscillations. In order to exclude these contributions, we shift the position operator by its expectation value and introduce $\hat{x}'_M = \hat{x}_M - \langle\hat{x}_M\rangle$. Correspondingly we obtain shifted annihilation and creation operators $\hat{b}' = \frac{1}{2x_{\mathsf{ZPF}}}(\hat{x}'_M + \frac{i}{m\omega_M}\hat{p}_M)$ and $\hat{b}'^\dagger = \frac{1}{2x_{\mathsf{ZPF}}}(\hat{x}'_M - \frac{i}{m_M\omega_M}\hat{p}_M)$, where $\hat{p}_M = i\sqrt{\frac{\hbar m_M\omega_M}{2}}(\hat{b}^\dagger - \hat{b})$ is the momentum operator of the cantilever. The phonon number operator can now be defined as

$$\begin{aligned}\hat{n}_M &= \hat{b}'^\dagger\hat{b}' \\ &= \frac{1}{4x_{\mathsf{ZPF}}^2}(\hat{x}_M^2 + \frac{\hat{p}_M^2}{m_M^2\omega_M^2}) + \frac{1}{4x_{\mathsf{ZPF}}^2}(\langle\hat{x}_M\rangle^2 - 2\hat{x}_M\langle\hat{x}_M\rangle) \\ &= \hat{b}^\dagger\hat{b} + \frac{1}{4x_{\mathsf{ZPF}}^2}(\langle\hat{x}_M\rangle^2 - 2\hat{x}_M\langle\hat{x}_M\rangle) \qquad (1.5)\end{aligned}$$

Its expectation value is given by $\langle\hat{n}_M\rangle = \langle\hat{b}'^\dagger\hat{b}'\rangle = \langle\hat{b}^\dagger\hat{b}\rangle - \frac{1}{4x_{\mathsf{ZPF}}^2}\langle\hat{x}_M\rangle^2$ and directly corresponds to the oscillation energy $E_{M,\mathsf{qm}}$.

In order to obtain a dimensionless quantity for our comparison, we divide the cantilever energy E_M by a characteristic classical energy scale of the system. To set this characteristic energy scale, we take the energy $E_0 = \frac{1}{2}m\omega_M^2 x_{\mathsf{FWHM}}^2$ associated with an oscillation amplitude x_{FWHM} of the mechanical cantilever which moves the cavity just out of its resonance. It follows that $E_M/E_0 = (A/x_{\mathrm{FWHM}})^2$ in the classical case, and $E_M/E_0 = 4\zeta^2\langle\hat{n}_M\rangle$ in the quantum version.

Chapter 2

The optomechanical instability in the quantum regime

In this chapter we focus on the question of how the optomechanical instability changes due to quantum effects. To answer this question at least partially, we will employ a fully quantum mechanical treatment of the system, based on the numerical solution of a quantum master equation. We will concentrate on the case of blue-detuned pumping of the cavity, where the cantilever can settle into self-induced oscillations once the input power is increased beyond some threshold value. The results of the quantum mechanical treatment can then readily be compared to the classical solution [21]. Below the threshold of the instability, we can check the results of a simple rate equation approach against the results of the master equation. This rate equation approach captures the amplification behaviour of the coupled system and catches the effects of photon shot noise on the cantilever motion [15]. The full quantum mechanical treatment can describe the crossover from the regime below the threshold of instability to the regime of self-induced oscillation. Moreover, the comparison to the classical solution allows to observe the effects of the quantum fluctuations. In this analysis, the quantum parameter $\zeta = x_{\mathrm{ZPF}}/x_{\mathrm{FWHM}}$ will be the most important quantity as it governs the quantum-to-classical transition.

We note, that the main results of this chapter have already been discussed in:

- Max Ludwig, Björn Kubala, Florian Marquardt: "The optomechanical instability in the quantum regime", New Journal of Physics, volume 10, 095013.

2.1 Classical solution

In the following we will briefly review the classical treatment of the system as given in ([21]). It allows to find an analytic solutions for the coupled cavity and cantilever dynamics. In particular one can find the amplitude of the self-induced oscillations as a function of the system parameters.

The Hamiltonian (2.16) introduced in the previous chapter allows to readily derive the Heisenberg equations of motion for the cavity operator $\hat{a}$ and the cantilever position operator $\hat{x}$.. To investigate the purely classical dynamics of the coupled cavity-cantilever system, we replace the operator $\hat{a}(t)$ by the complex light amplitude $\alpha(t)$ and the position operator of the cantilever $\hat{x}$ by its classical counterpart. We thus arrive at:

$$\dot{\alpha} = [i(\Delta + g\frac{x_M}{x_{\mathrm{ZPF}}}) - \frac{\kappa}{2}]\,\alpha - i\alpha_L \tag{2.1}$$

$$\ddot{x} = -\omega_M^2 x + \frac{\hbar g}{m x_{\mathsf{ZPF}}} |\alpha|^2 - \Gamma_M \dot{x}_M \,. \tag{2.2}$$

Here fluctuations (both the photon shot noise as well as intrinsic mechanical thermal fluctuations) have been neglected, to obtain the purely deterministic classical solution. The variables t, x and α can be rescaled [21] as $\tilde{t} = \omega_M t$; $\tilde{\alpha} = i\alpha\omega_M/(2\alpha_L)$; $\tilde{x} = gx/(\omega_M x_{\mathsf{ZPF}})$, so that the coupled equations of motion contain only the dimensionless parameters $\mathcal{P}$, Δ/ω_M, κ/ω_M, and Γ_M/ω_M:

$$\begin{aligned} \frac{d\tilde{\alpha}}{d\tilde{t}} &= [i(\frac{\Delta}{\omega_M} + \tilde{x}) - \frac{1}{2}\frac{\kappa}{\omega_M}]\tilde{\alpha} + \frac{1}{2} \\ \frac{d^2\tilde{x}}{d\tilde{t}^2} &= -\tilde{x} + \mathcal{P}\,|\tilde{\alpha}|^2 - \frac{\Gamma_M}{\omega_M}\frac{d\tilde{x}}{d\tilde{t}} \,. \end{aligned} \tag{2.3}$$

Crucially, the quantum parameter ζ cannot and does not feature in these equations.

Apart from a static solution $x(t) \equiv \mathrm{const}$, this system of coupled differential equations can show self-induced oscillations. In such solutions, the cantilever conducts an approximately sinusoidal oscillation at its eigenfrequency, $x(t) \approx \bar{x} + A\cos(\omega_M t)$. The light amplitude then shows the dynamics of a damped, driven oscillator, which is swept through its resonance, see equation (2.1); an exact solution for the light amplitude $\alpha(t)$ can be given as a Fourier series containing harmonics of the cantilever frequency ω_M [21]:

$$|\tilde{\alpha}(\tilde{t})| = \left| \sum_n \tilde{\alpha}_n e^{in\tilde{t}} \right|, \tag{2.4}$$

with

$$\tilde{\alpha}_n = \frac{1}{2}\frac{J_n(-\tilde{A})}{in + \kappa/(2\omega_M) - i(\bar{\tilde{x}} + \Delta/\omega_M)} \,. \tag{2.5}$$

The dependence of oscillation amplitude, A, and average cantilever position, $\bar{x}$, on the dimensionless system parameters can be found by two balance conditions: Firstly, the total force on the cantilever has to vanish on average, and, secondly, the power input into the mechanical oscillator by the radiation pressure on average has to equal the friction loss.

The force balance condition determines the average position of the oscillator, yielding an implicit equation for $\bar{x}$,

$$\langle \ddot{x} \rangle \equiv 0 \quad \Leftrightarrow \quad m\omega_M^2 \bar{x} = \langle F_{\mathrm{rad}} \rangle = \frac{\hbar g}{m x_{\mathsf{ZPF}}} \langle |\alpha(t)|^2 \rangle \,, \tag{2.6}$$

where the average radiation force, $\langle F_{\mathsf{rad}} \rangle$ is a function of the parameters $\bar{x}$ and A.

The balance between the mechanical power gain due to the light-induced force, $P_{\mathrm{rad}} = \langle F_{\mathrm{rad}} \dot{x} \rangle$, and the frictional loss $P_{\mathrm{fric}} = \Gamma_M \langle \dot{x}^2 \rangle$ follows from

$$\langle \dot{x}\ddot{x} \rangle \equiv 0 \quad \Leftrightarrow \quad \langle F_{\mathsf{rad}} \dot{x} \rangle = \Gamma_M \langle \dot{x}^2 \rangle. \tag{2.7}$$

For each value of the oscillation amplitude A we can now plot the ratio between radiation power input and friction loss, $P_{\mathrm{rad}}/P_{\mathrm{fric}} = \langle F_{\mathsf{rad}} \dot{x} \rangle / (\Gamma_M \langle \dot{x}^2 \rangle)$, after eliminating $\bar{x}$ using equation 2.6. This is shown in figure 2.1. Power balance is fulfilled if this ratio is one, corresponding to the contour line $P_{\mathrm{rad}}/P_{\mathrm{fric}} = 1$. If the power input into the cantilever by radiation pressure is larger

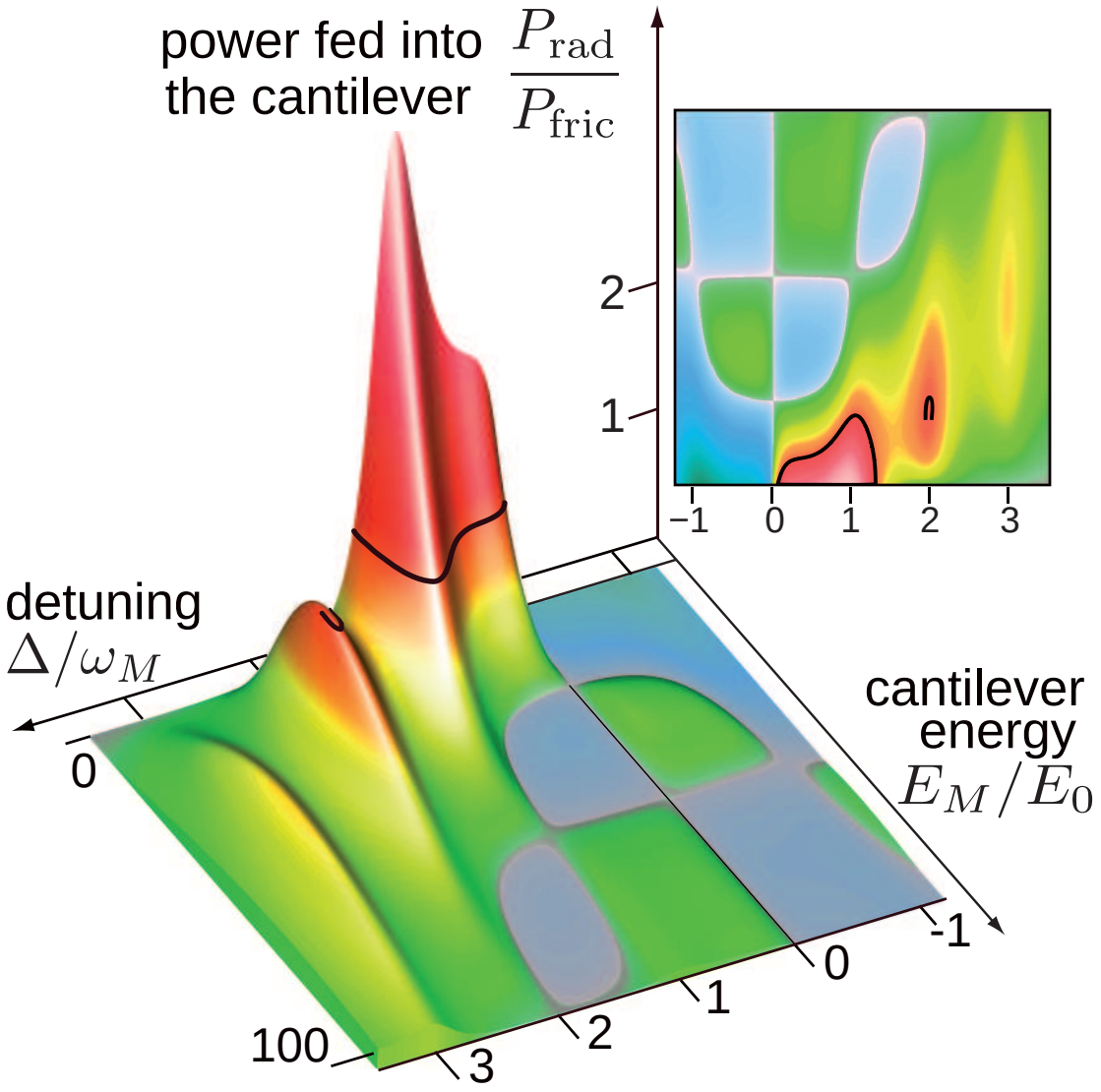

Figure 2.1: Classical self-induced oscillations of the coupled cavity-cantilever system. The radiation pressure acting on the cantilever provides an average mechanical power input of $P_{\rm rad}$. The ratio $P_{\rm rad}/P_{\rm fric}$ of this power $P_{\rm rad}$ vs. the loss due to mechanical friction, $P_{\rm fric}$, is shown as a function of the detuning Δ and the cantilever's oscillation energy E_M, at fixed laser input power $\mathcal{P}$. The oscillation energy $E_M = m\omega_M^2 A^2/2$ is shown in units of E_0, where $E_M/E_0 = (A/x_{\rm FWHM})^2$. Self-induced oscillations require $P_{\rm rad} = P_{\rm fric}$. This condition is fulfilled along the horizontal cut at $P_{\rm rad}/P_{\rm fric} = 1$ (see black line and the inset depicting the same plot, viewed from above). These solutions are stable if the ratio $P_{\rm rad}/P_{\rm fric}$ decreases with increasing oscillation amplitude A. The blue regions at the floor of the plot indicate that $P_{\rm rad}$ is negative, resulting in cooling. The cavity decay rate is $\kappa = 0.5\omega_M$, the mechanical damping is chosen as $\Gamma_M/\omega_M = 1.47 \cdot 10^{-3}$, and the input power as $\mathcal{P} = 6.05 \cdot 10^{-3}$; these parameters are also used in figures 2.2, 2.3, 2.4, and 2.6, and will be referred to as Γ_M^* and $\mathcal{P}^*$.

than frictional losses (i.e., for a ratio larger than one), the amplitude of oscillations will increase, otherwise it will decrease. Stable solutions (dynamical attractors) are therefore given by that part of the contour line where the ratio decreases with increasing oscillation amplitude (energy), as shown in figure 2.1.

Changing the (dimensionless) mechanical damping rate Γ_M/ω_M will scale the plot in figure 2.1 along the vertical axis, so that the horizontal cut at one yields a different contour line of stable solutions [a changed input power $\mathcal{P}$ gives a similar scaling, but leads to further changes in the solution, as $\mathcal{P}$ also enters the force balance condition, equation (2.6)]. Decreasing mechanical damping or increasing the power input will increase the plot height in figure 2.1, so that the amplitude/energy of oscillation of the stable solution increases.

While the surface or contour plots in figure 2.1 allow a discussion of general features of the self-induced oscillations, such as the multistabilities discussed in Ref. [21], a slightly different representation of the classical solution is more amenable to an easier understanding of the particular dynamics of the system for a certain set of fixed system parameters. Figure 2.2 shows the cantilever energy $E_{M,\mathrm{cl}} = \frac{1}{2}m\omega_M^2 A^2$ in terms of the classical energy scale $E_0 = \frac{1}{2}m\omega_M^2 x_{\mathrm{FWHM}}^2$ as function of driving $\mathcal{P}$ and detuning Δ/ω_M. These are the parameters that can typically be varied in a given experimental setup.

For sufficiently strong driving, self-induced oscillations appear around integer multiples of the cantilever frequency, $\Delta \approx n\omega_M$. For a cavity decay rate $\kappa = 0.5\omega_M$ assumed in figure 2.2, the different bands are distinguishable at lower driving; for larger κ (or for stronger driving), the various 'sidebands' merge. For the lower-order sidebands, the nonzero amplitude solution connects continuously to the zero amplitude solution, which becomes unstable. This is an example of a (super-critical) Hopf bifurcation into a limit cycle.

The vertical faces, shown gray in figure 2.2, for $\Delta \approx 2\omega_M$ and $\Delta \approx 3\omega_M$ are connected to the sudden appearance of attractors with a finite amplitude. For example, while approaching the detuning of $\Delta = 2\omega_M$ at fixed $\mathcal{P}$ (the solid line in figure 2.2 refers to $\mathcal{P} = 1.47 \cdot 10^{-3}$), a finite amplitude solution appears, although $A = 0$ remains stable. In Ref. [21] the existence of higher-amplitude stable attractors and, correspondingly, dynamic multistability were discussed.

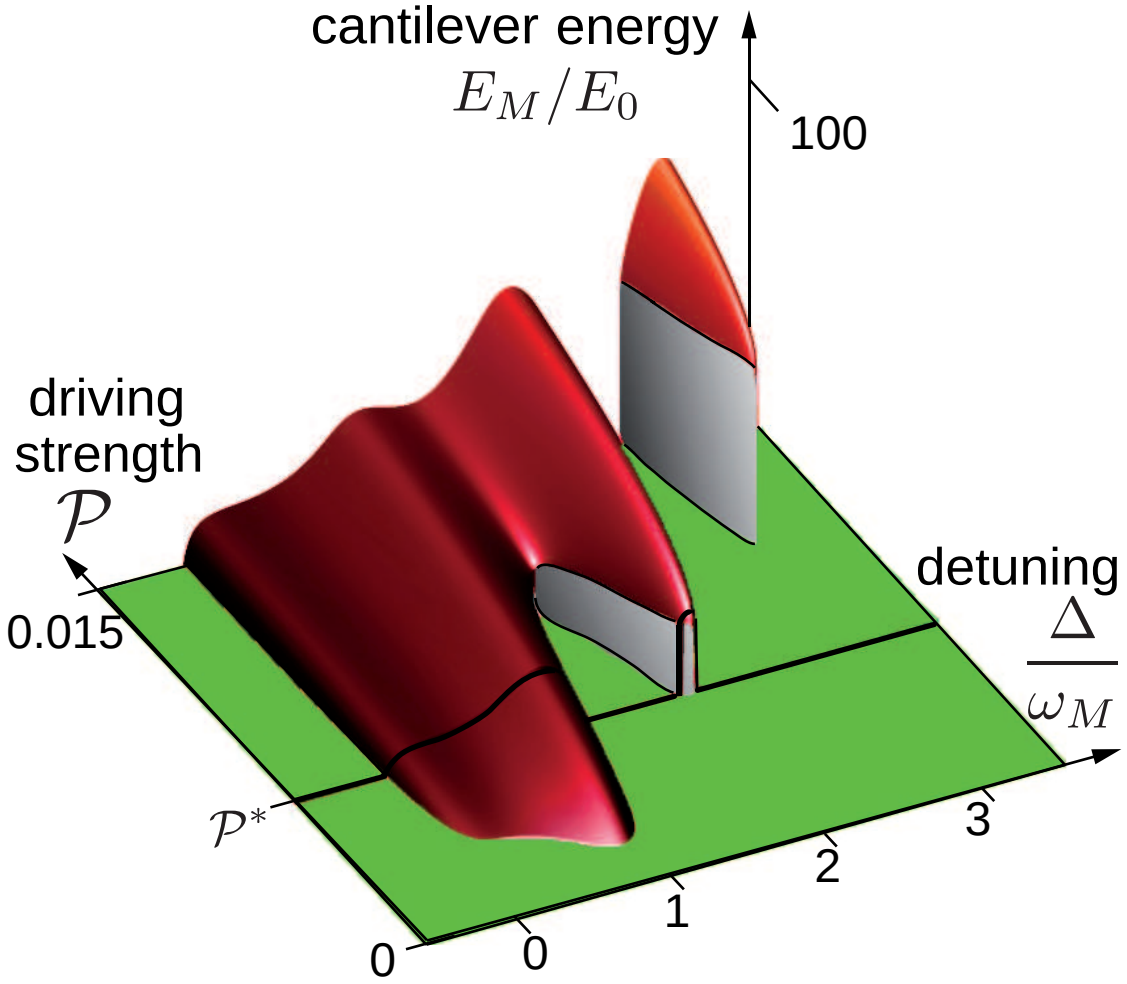

Figure 2.2: Cantilever oscillation energy $E_M \propto A^2$ versus detuning Δ and laser input power $\mathcal{P}$. This plot (in contrast to figure 2.1) shows only the stable oscillation amplitude, but as a function of variable input power. The particular value $\mathcal{P}^*$ corresponding to figure 2.1, and the resulting profile of oscillation amplitudes are indicated by a black line. The green floor of the plot indicates regions without self-induced oscillations. The other system parameters are as in figure 2.1. The continuous onset of the self-oscillations in the sidebands at $\Delta/\omega_M = 0, 1$ (which merge for the present parameter values) represents a super-critical Hopf bifurcation, from $A = 0$ to $A \neq 0$. At higher sidebands, an attractor with a finite $A \neq 0$ appears discontinuously, while $A = 0$ remains a stable solution.

2.2 Rate equation approach

Before embarking on a full quantum-mechanical treatment of the coupled cavity-cantilever system, it is instructive to discuss a more simple method to capture some non-classical effects, in particular the response of the cantilever to the photon shot noise. For that purpose, we consider the shot noise spectrum of the driven cavity, decoupled from the cantilever,

$$S_{FF}(\omega) = \left(\frac{\hbar g}{x_{\mathsf{ZPF}}}\right)^2 S_{nn}(\omega) = \left(\frac{\hbar g}{x_{\mathsf{ZPF}}}\right)^2 \bar{n} \frac{\kappa}{(\omega+\Delta)^2 + (\kappa/2)^2}\,, \tag{2.8}$$

where

$$\bar{n} = \frac{\mathcal{P}}{8\zeta^2} \frac{(\omega_M/\kappa)^2}{(\Delta/\omega_M)^2 + (\kappa/2\omega_M)^2} \tag{2.9}$$

is the mean number of photons in the cavity. The maximum occupation $n_{\mathsf{max}} = \mathcal{P}\omega_M^4/(2\kappa^4\zeta^2) = 4\alpha_L^2/\kappa^2$ occurs at zero detuning.

$$S_{FF}(\omega) = \left(\frac{\hbar g}{x_{\mathsf{ZPF}}}\right)^2 S_{nn}(\omega) = \left(\frac{\hbar g}{x_{\mathsf{ZPF}}}\right)^2 \bar{n} \frac{\kappa}{(\omega+\Delta)^2 + (\kappa/2)^2}\,, \tag{2.10}$$

We note that in using the unperturbed, intrinsic shot noise spectrum for an optical cavity in the absence of optomechanical effects, we neglect the modification of that spectrum due to the back-action of the cantilever motion.

The asymmetry of the shot noise spectrum is important for the dynamics of the cantilever. The spectral density of the radiation-pressure force at positive frequency ω_M (negative frequency $-\omega_M$) yields the probability of the cavity absorbing a phonon from (emitting a phonon into) the cantilever [15].

For a red-detuned laser impinging on the cavity ($\Delta < 0$), the cavity's noise spectrum peaks at positive frequencies and the cavity tends to rather absorb energy from the cantilever. As a consequence, the mechanical damping rate for the cantilever is increased, leading to cooling if one starts with a sufficiently hot cantilever. In the opposite Raman-like process taking place at $\Delta > 0$, a blue-detuned laser beam will preferentially lose energy to the cantilever, so that it matches the cavity's resonance frequency. The effective optomechanical damping rate,

$$\Gamma_{\mathsf{opt}} = \zeta^2\kappa^2[S_{nn}(+\omega_M) - S_{nn}(-\omega_M)]\,, \tag{2.11}$$

is then negative. The corresponding heating of the mechanical cantilever is counteracted by the mechanical damping Γ_M . Simple rate equations for the occupancy of the cantilever yield a thermal distribution for the cantilever phonon occupation number n_M, with [15]

$$\langle \hat{b}^\dagger \hat{b}\rangle = \langle \hat{n}_M\rangle = \frac{\zeta^2\kappa^2 S_{nn}(-\omega_M) + \bar{n}_{\mathrm{th}}\Gamma_M}{\Gamma_{\mathrm{opt}} + \Gamma_M}\,. \tag{2.12}$$

The effective temperature, T_{eff}, is related by $\langle \hat{n}_M + 1\rangle/\langle \hat{n}_M\rangle = \exp[\hbar\omega_M/(k_B T_{\mathsf{eff}})]$ to the mean occupation number. The equilibrium mechanical mode occupation number, $\bar{n}_{\mathrm{th}}$, is determined by the mechanical bath temperature, which is taken as zero in the following. In contrast to first appearance, the mean occupation number of the cantilever given in equation (2.12) does not depend on the quantum parameter ζ, as $\zeta^2 S_{nn}$ is independent of ζ. This is because $S_{nn} \sim \bar{n} \sim 1/\zeta^2$, see equation (2.9). The cantilever energy, therefore, only trivially depends on the quantum parameter as $E_M/E_0 = 4\zeta^2\langle \hat{n}_M\rangle$, so that it vanishes in the classical limit, where $\zeta^2 \propto \hbar \to 0$.

In general, the phonon number in equation (2.12) can increase due to two distinct physical effects: On the one hand, the numerator can become larger, due to the influence of photon shot noise impinging on the cantilever, represented by S_{nn}. On the other hand, the denominator can become smaller due to Γ_{opt} becoming negative. In the latter case, the fluctuations acting on the cantilever (both thermal and shot noise) are amplified. This effect is particularly pronounced just below the threshold of instability, where $\Gamma_M + \Gamma_{\mathrm{opt}} = 0$ (see below).

In the resolved sideband limit $\kappa \ll \omega_M$ (at weak driving) the cantilever occupation $\langle \hat{n}_M \rangle$ will peak around zero detuning, where the number of photons in the cavity is large, and around a detuning of $\Delta = \omega_M$. At the latter value of detuning the aforementioned Raman process is maximally efficient as a photon entering the cavity will exactly match the resonance frequency after exciting a phonon in the cantilever. This dependence of cantilever occupation (or the corresponding energy) on the detuning is shown in figure 2.3.

The approach sketched above can be modified slightly to take account of the modification of the cavity length due to a static shift of the cantilever mirror by radiation pressure. Approaching the resonance of the cavity from below, the increasing number of photons inside the cavity will increase the cavity length due to their radiation pressure on the mirror, bringing the system even closer to the resonance. This effect can be included by considering the equations of motion ((2.2) and (2.1)) in the static case, i.e. for $\frac{d}{dt}\alpha = \frac{d}{dt}x = 0$. We arrive at the coupled equations for the $\bar{x}_M$ and $\bar{n} = |\bar{\alpha}|^2$,

$$\begin{aligned} \bar{n} &= \frac{|\alpha_L|^2}{(\Delta - g\bar{x}_M)^2 + \kappa^2/4}, \\ \bar{x}_M &= \mathcal{P}\bar{n}/\omega_M^2, \end{aligned} \tag{2.13}$$

A self-consistent solution $\bar{n}$ can be readily found numerically and plugged into equation (2.12). The resulting curve of the cantilever occupation shows due to this correction is illustrated in figure 2.3 (a) by the pink, dash-dotted line and shows a tilt of the peak around the resonance. The same figure also includes results of the full quantum mechanical approach, which will be discussed in the next section.

For larger κ, the two peaks in the cantilever excitation merge. Higher-order sidebands are not resolved within this approach, since they would require taking care of the modification of S_{FF} due to the cantilever's motion.

Classical self-induced oscillations occur in a regime of larger driving, where the optomechanical damping rate Γ_{opt} of equation (2.11) becomes negative. They appear once amplification exceeds intrinsic damping, i.e. when $\Gamma_{\mathrm{opt}} + \Gamma_M < 0$. The simple rate equation approach lacks any feedback mechanism to stop the divergence of the phonon number. The classical solution demonstrates how this feedback (i.e. the resulting change in the dynamics of the radiation field) makes the mechanical oscillation amplitude saturate at a finite level. In addition, it shows the onset of self-induced oscillations to occur at a smaller detuning, due to the effective shift of the cantilever position explained above.

In figure 2.3(b) we show results for the detuning dependence of the mean energy of the cantilever above the threshold of classical self-induced oscillations. The coupled cavity-cantilever system acts as an amplifier of fluctuations, increasing the occupation of higher number states of the cantilever well before classical oscillations set in. At the onset of classical self-induced oscillations the rate equation result diverges. A full quantum-mechanical treatment describes the crossover of the cantilever dynamics from quantum-fluctuation induced heating to self-induced oscillations as will be discussed now.

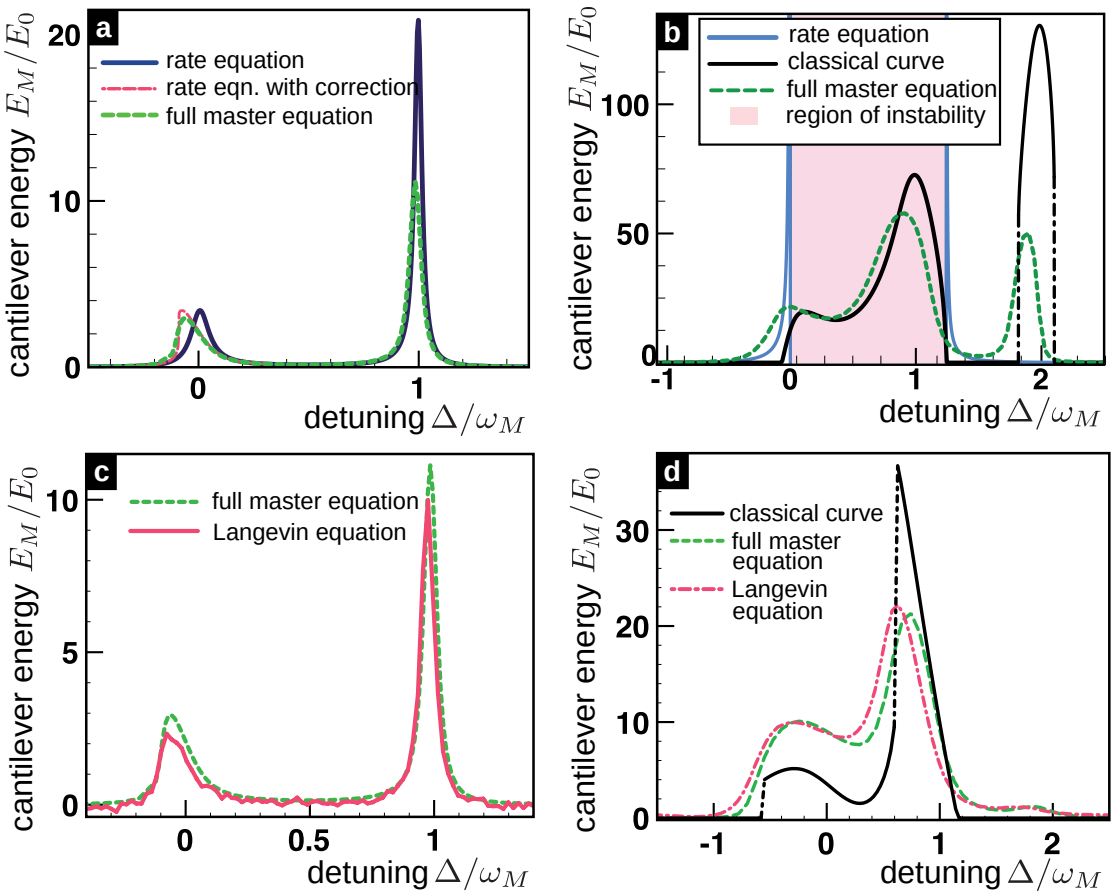

Figure 2.3: Cantilever energy versus detuning for a cavity driven below [(a),(c)] and above [(b), (d)] the onset of self-induced oscillations. Note $E_M/E_0 = 4\zeta^2 \langle \hat{n}_M \rangle$. (a) Below the onset, the cantilever amplitude would vanish according to the classical analysis that does not incorporate fluctuations. However, the cantilever is susceptible to the photon shot noise (the parameters are $\kappa/\omega_M = 0.1$, $\mathcal{P} = 8.4 \cdot 10^{-3}$, $\Gamma_M/\omega_M = 5 \cdot 10^{-3}$, and $\zeta = 1.0$), leading to finite phonon numbers in the cantilever, particularly around the resonance $\Delta = 0$ and at the first sideband $\Delta = \omega_M$ (see main text). This is captured by the full quantum master equation, as well as (approximately) by the rate equation, whose results improve when taking into account the corrections due to the shift of the cantilever position $\bar{x}$. (b) For stronger driving, the classical solution yields self-oscillations (the parameters are $\mathcal{P}^*$, Γ_M^* as in figure 2.2, but $\kappa/\omega_M = 0.3$). The rate equation correctly predicts the onset of the linear instability, but not the nonlinear regime. [The shift in $\bar{x}$ was not taken into account, hence the slight discrepancy vs. the classical solution] The master equation results are shifted to lower detuning and describe sub-threshold amplification and heating as well as self-induced oscillations above threshold, modified and smeared due to quantum effects (as shown for a quantum parameter of $\zeta = x_{\mathrm{ZPF}}/x_{\mathrm{FWHM}} = 1$). (c) Including the zero-point fluctuations in a semi-classical approach via Langevin equations gives results that agree well with both the results from the rate equation and the full master equation, shown here for parameters as in (a). (d) Above the onset of self-induced oscillations the semi-classical approach mimics results from the quantum master equation partially. The parameters for this plot are $\kappa/\omega_M = 0.3$, $\Gamma_M = 50\Gamma_M^*$, $\mathcal{P} = 20\mathcal{P}^*$, $\zeta = 1$.

2.3 Quantum master equation method

The evolution of the coupled quantum system consisting of the cantilever and the optical cavity is described by the Hamiltonian of equation (2.16). Dissipation arises from the coupling of the mechanical mode to a bath and due to the opening of the cavity to the outside. While the former results in mechanical damping with a rate Γ_M, the latter is associated with the ring-down rate of the cavity κ. In this part of the thesis, dealing with the optomechanical instability in the quantum regime, we will assume the mechanical bath to be at zero temperature, where quantum effects are most pronounced in steady state. A future, more realistic treatment should relax this assumption and treat the non-equilibrium dynamics that results when a mechanical system is first cooled optomechanically and then switched to the unstable side.

The system can be described by a reduced density matrix $\hat{\rho}$ for the mechanical cantilever mode and the optical mode of the cavity. In a frame rotating at the laser frequency, the time evolution of the density matrix $\hat{\rho}$ is given by

$$\frac{d}{dt}\hat{\rho} = \frac{[\hat{H}_0, \hat{\rho}]}{i\hbar} + \Gamma_M \mathcal{D}[\hat{b}] + \kappa \mathcal{D}[\hat{c}], \quad (T \equiv 0) \tag{2.14}$$

where $\mathcal{D}[\hat{A}] = \hat{A}\hat{\rho}\hat{A}^\dagger - \frac{1}{2}\hat{A}^\dagger\hat{A}\hat{\rho} - \frac{1}{2}\hat{\rho}\hat{A}^\dagger\hat{A}$ denotes the standard Lindblad operator. The Hamilton operator $\hat{H}_0$ describes the coherent part of the evolution of the coupled cavity-cantilever system,

$$\hat{H} = \hat{H}_0 + \hat{H}_\kappa + \hat{H}_\Gamma . \tag{2.15}$$

By means of the quantum parameter and the set of parameters given in (1.2), we can transform $\hat{H}_0$ from its original shape (1.1) to

$$\hat{H}_0 = \hbar\left(-\Delta - \kappa\zeta\left(\hat{b} + \hat{b}^\dagger\right)\right)\hat{c}^\dagger\hat{c} + \hbar\omega_M\hat{b}^\dagger\hat{b} + \hbar\frac{\sqrt{2\mathcal{P}}\omega_M^2}{4\kappa\zeta}\left(\hat{c} + \hat{c}^\dagger\right). \tag{2.16}$$

For the numerical evaluation, we rewrite equation 2.14 as $d\hat{\rho}/dt = \mathcal{L}\hat{\rho}$, with a Liouvillian super-operator $\mathcal{L}$. We then interpret the density matrix as a vector, whose time evolution is governed by the matrix $\mathcal{L}$. The density matrix at long times (in steady state) is given by the eigenvector of $\mathcal{L}$ with eigenvalue 0. The numerical calculation of this eigenvector is much more efficient than a simulation of the full time evolution. Since we are dealing with large sparse matrices, it is convenient to employ an Arnoldi method that finds a few eigenvalues and eigenvectors of $\mathcal{L}$ by iterative projection. For Hermitean matrices, the Arnoldi method is also known as the Lanczos algorithm.

In practice, the numerical approach used here sets strong limits on the dimension of the Hilbert space. We need to take into account the N_{cav} lowest Fock states of the cavity and the N_M lowest Fock states of the mechanical cantilever, resulting in a Liouvillian super-operator with $(N_M \cdot N_{\mathsf{cav}})^4$ elements. This puts more severe restrictions on our treatment of the coupled cavity-cantilever system than encountered in similar treatments of comparable systems. For example, nanoelectromechanical systems, where an oscillator is coupled to a normal-state or superconducting single-electron transistor (SET), will have to account for only a very limited number of charge states of the SET (namely those few involved in the relevant transport cycle). As a consequence, a larger number of Fock states can be included, e.g., 70 number states of the oscillator were kept in Ref. [28]. In some cases it was furthermore considered sufficient to treat only the incoherent dynamics of the mechanical oscillator, i.e., only the elements of the density matrix diagonal in the oscillator's Fock space, thereby reaching 200 number states of a mechanical mode coupled

to a normal-state SET [36]. The restricted number of Fock states that can be considered here makes it more difficult to fully bridge the gulf to the classical regime of motion of the mechanical cantilever. [$(N_M, N_{\mathsf{cav}}) = (8,16)$ for figure 2.3(a),(c),(d), (4,22) for figures 2.3(b), 2.4 and for the first two panels of 2.6, (3,35) for the last panel of figure 2.6]. More details of the numerical methods and possible improvements are discussed in the appendix (A).

A first comparison of results of the quantum master equation to the classical solution and the results of the rate equation was already shown in figure 2.3. We find that the full quantum results do not qualitatively differ from the rate equation results provided the parameters are chosen sufficiently far from the onset of self-induced oscillations. The parameters of figure 2.3(a) are close to the regime of the instability, though, and the maxima of the cantilever energy are suppressed by nonlinear effects, when compared to the results of the rate equation approach.

In figure 2.4 we demonstrate the influence of the quantum parameter $\zeta = x_{\mathsf{ZPF}}/x_{\mathsf{FWHM}}$ governing the crossover from the quantum regime towards classical behaviour. This crossover occurs actually due to two separate features: First, the usual semi-classical limit (in which $\hbar$ tends to zero and the level spacing becomes small) and, second, the fact that our driven dissipative quantum system does indeed suffer decoherence that tends to restore the classical behaviour.

Figure 2.4(a) shows the cavity photon number, normalized to its value at resonance, n_{max}. For our choice of driving parameter $\mathcal{P}$, the maximal occupation n_{max} is low, so that a small number of Fock states suffices for describing the cavity in the quantum master equation. This allows to account for enough number states of the cantilever to reach the regime of self-induced oscillations. The classical solution (solid black line) consists of the broad Lorentzian of the isolated cavity, on top of which additional peaks appear. These are due to the classical self-induced oscillations occurring at the sidebands $\Delta = \omega_M, 2\omega_M, \ldots$ in the coupled cavity-cantilever system. Figure 2.4(c) displays the cantilever energy E_M/E_0 as a function of the detuning, Δ/ω_M, with features that are in accordance with those found for the photon number. The classical curve in (b), shown in black, corresponds to the cut indicated by the solid line in figure 2.2. For the chosen driving power, the second sideband at $\Delta = \omega_M$ just starts to appear, while the first sideband is merged with the resonance at $\Delta = 0$, which shows up as a slight shoulder. The sharpness and strength of these features also depend on the values of mechanical damping and cavity decay rate. Results of our solution of the quantum master equation are shown for three different values of the quantum parameter $\zeta = x_{\mathsf{ZPF}}/x_{\mathsf{FWHM}}$. Due to restrictions of the numerical resources, it was not feasible to map out a wider range of values of the parameter ζ, although the range analysed here already suffices to describe the quantum-classical crossover.

The quantum master equation shows results that are qualitatively similar to the classical solution in the regime of self-induced oscillations, with the peaks being progressively broadened, reduced in height, and shifted to lower detuning for increasing values of the quantum parameter ζ. Numerical evidence indicates that quantum correlations between the cantilever position operator $\hat{x}_M$ and the photon operators $\hat{b}^\dagger$, $\hat{b}$ may cause the observed shift. As expected, the discrepancy between the quantum mechanical and the classical result reduces with diminishing quantum parameter ζ. In figure 2.4(b), we show the dependence of the cantilever energy on the quantum parameter, for two different values of the detuning. In the sub-threshold regime of amplification/heating the cantilever energy scales as ζ^2, as discussed above. In any case, the classical limit is clearly reached as $\zeta \to 0$.

At the second sideband a classical solution of finite amplitude coexists with a stable zero-amplitude solution (compare figure 2.1 and last panel of figure 2.6). The black curve in figure 2.4(b), showing the finite amplitude solution, may therefore deviate substantially from the $\hbar \to 0$ limit of the quantum mechanical result. In general, the average value of E_M, shown here,

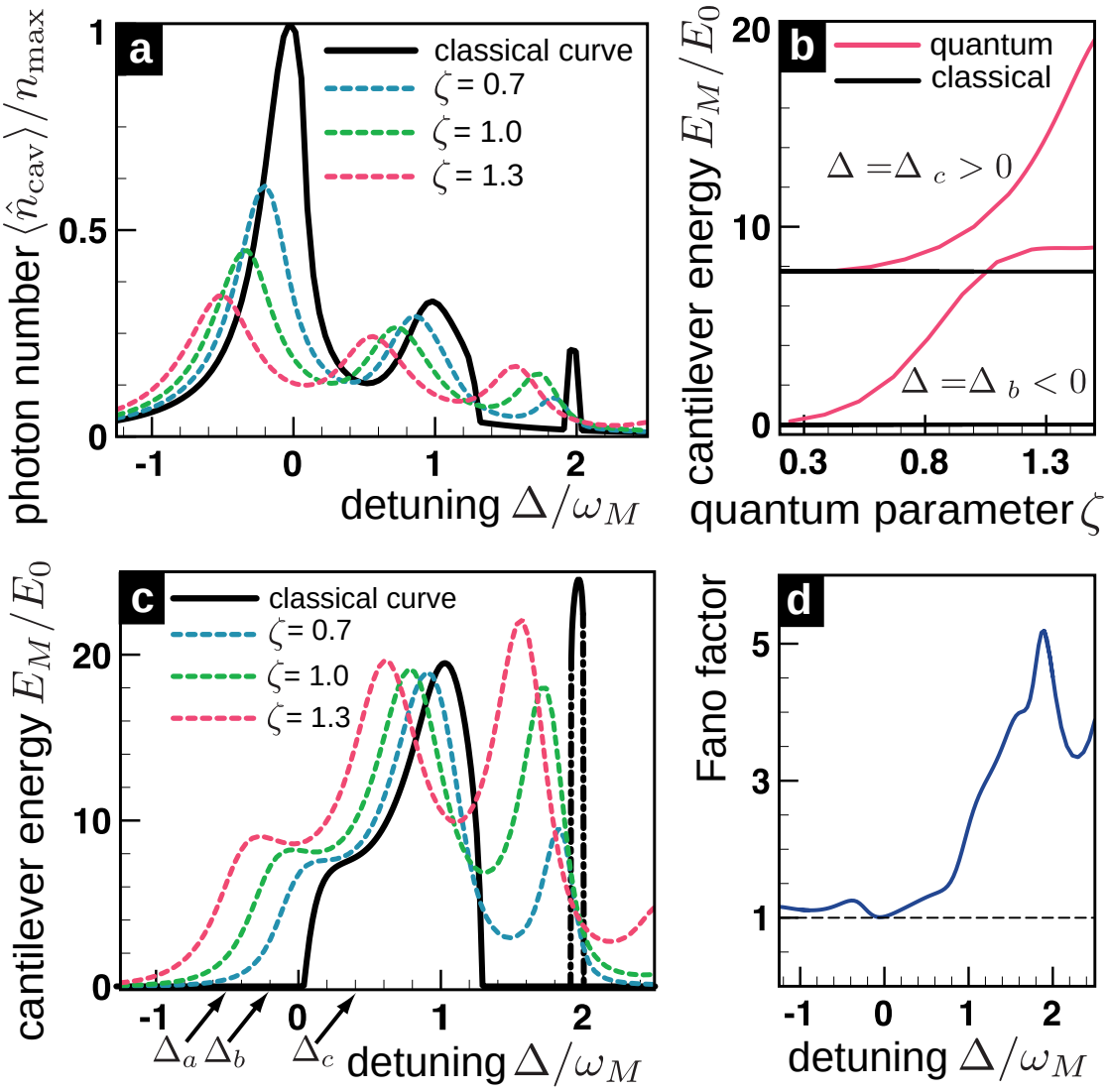

Figure 2.4: Comparison of classical and quantum results. (a) Number of photons inside the cavity as a function of detuning, and (c) energy of the cantilever versus detuning for Γ_M^*, $\mathcal{P}^*$ and $\kappa/\omega_M = 0.5$. The dotted curves show results from the quantum master equation for different values of the quantum parameter $\zeta = 1.3$ (pink) , $\zeta = 1.0$ (green) and $\zeta = 0.7$ (blue), which are compared with the solution of the classical equations of motion (black solid curve). As $\zeta \to 0$, the quantum result approaches the classical curve. See main text for a detailed discussion. (b) The energy of the cantilever as a function of the quantum parameter ζ for fixed detunings $\Delta_b/\omega_M = -0.2$ and $\Delta_c/\omega_M = 0.4$ (the detuning value Δ_a indicated in (b) is used in figure 2.6). (d) Fano factor $(\langle \hat{n}_M^2 \rangle - \langle \hat{n}_M \rangle^2)/\langle \hat{n}_M \rangle$ vs. detuning, for $\zeta = 1$. For a coherent state whose occupation number follows a Poisson distribution, the Fano factor is 1 (dashed black line). Close to the resonance (and far away from it, where $\langle \hat{n}_M \rangle = 0$), the results of the quantum master equation approach this value. The Fano factor becomes particularly large near the second sideband, where we observe coexistence of different oscillation amplitudes (see figure 2.6).

will be determined by the relative weight of the two solutions (which are connected by tunneling due to fluctuations), as well as fluctuations of E_M for each of those two attractors.

In figure 2.5(b) we show the results of the master equation in a different parameter regime, for $\kappa/\omega_M = 0.3$, $\mathcal{P} = 20\mathcal{P}^*$, $\Gamma_M = 50\Gamma_M^*$. Due to the small value of the cavity decay rate, the sidebands of the corresponding attractor diagram (figure 2.4(a)) are even more pronounced than for the parameters of figure 2.1. The increased driving strength $\mathcal{P}$ leads to a strong distortion of the diagram according to the force balance equation (2.6). Subsequently, the classical curve (white contour in figure 2.4(a) and black line in figure 2.4(b)) has discontinuities at the slope to the resonances and at the slope to the first sideband. We note that the jumps do not implicate bistable behaviour in this case.

Both the low value of κ and the high value of $\mathcal{P}$ favour the occurrence of high occupation numbers for cavity and cantilever, we have to chose a rather high mechanical damping rate. In this regime, the scope of our numerics allows us to vary the quantum parameter between $\zeta = 0.9$ and $\zeta = 1.6$ over the whole range of detuning. The oscillation energy of the cantilever as a function of the detuning again shows the characteristics of enhanced quantum fluctuations for large ζ : The resonances are broadened and shifted towards lower values of the detuning parameter. Smooth curves supersede the discontinuities of the classical curve and the slopes at the corresponding flanks scale inversely with the quantum parameter. In view of the attractor diagram, the curves from the master equation for large ζ seem to show features of contour lines for a lower mechanical damping rate (or higher driving strength). The resonance at the second sideband emerges when increasing ζ and the gap between the first and the second sideband disappears.

2.4 Langevin equation

To get an estimate of the influence of quantum fluctuations, we compare the results of the quantum master equation to numerical simulations of classical Langevin equations that try to mimick the quantum noise. The resulting description of the quantum-to-semi-classical crossover is illustrated in figures 2.3(c) and (d). To imitate both the zero-point fluctuations of the mechanical oscillator and the shot-noise inside the cavity, we add white noise terms to equations (2.1) and (2.2):

$$\dot{\alpha} = [i(\Delta + g\frac{x}{x_{\mathrm{ZPF}}}) - \frac{\kappa}{2}]\,\alpha - i\alpha_L + \sqrt{\kappa/2}\,\alpha_{in} \tag{2.17}$$

$$\ddot{x} = -\omega_M^2 x + \frac{\hbar g}{m x_{\mathrm{ZPF}}}\,|\alpha|^2 - \Gamma_M \dot{x} + \sqrt{\hbar\omega_M\Gamma/m}\,\xi, \tag{2.18}$$

where $\langle\alpha_{in}\rangle = \langle\xi\rangle = 0$ and $\langle\alpha_{in}(t)\alpha_{in}^*(t')\rangle = \langle\xi(t)\xi(t')\rangle = \delta(t-t')$. The coefficients in front of the noise terms are chosen such that in the absence of optomechanical coupling we obtain the zero-point fluctuations, i.e. $\langle|\alpha|^2\rangle = 0.5$ away from resonance and $\frac{m\omega_M^2}{2}\langle x^2\rangle = \frac{\hbar\omega_M}{4}$. The mean zero-point energy of the cantilever is subtracted from the curves displayed in figures 2.3 and 2.5.

For parameters below the onset of self-sustained oscillations, this semi-classical approach leads to good qualitative agreement with the quantum mechanical description, as can be seen in figure 2.3(c) for parameters that are the same as those of 2.3(a).

Also in the region of instability the Langevin equation yields results that resemble those of the quantum master equation. The curve in figure 2.3(d), for the parameters $\kappa/\omega_M = 0.3$, $\Gamma_M = 50\Gamma_M^*$, $\mathcal{P} = 20\mathcal{P}^*$, $\zeta = 1$, is similar to the corresponding result of the fully quantum mechanical picture, especially in terms of the slopes and heights of the peaks.

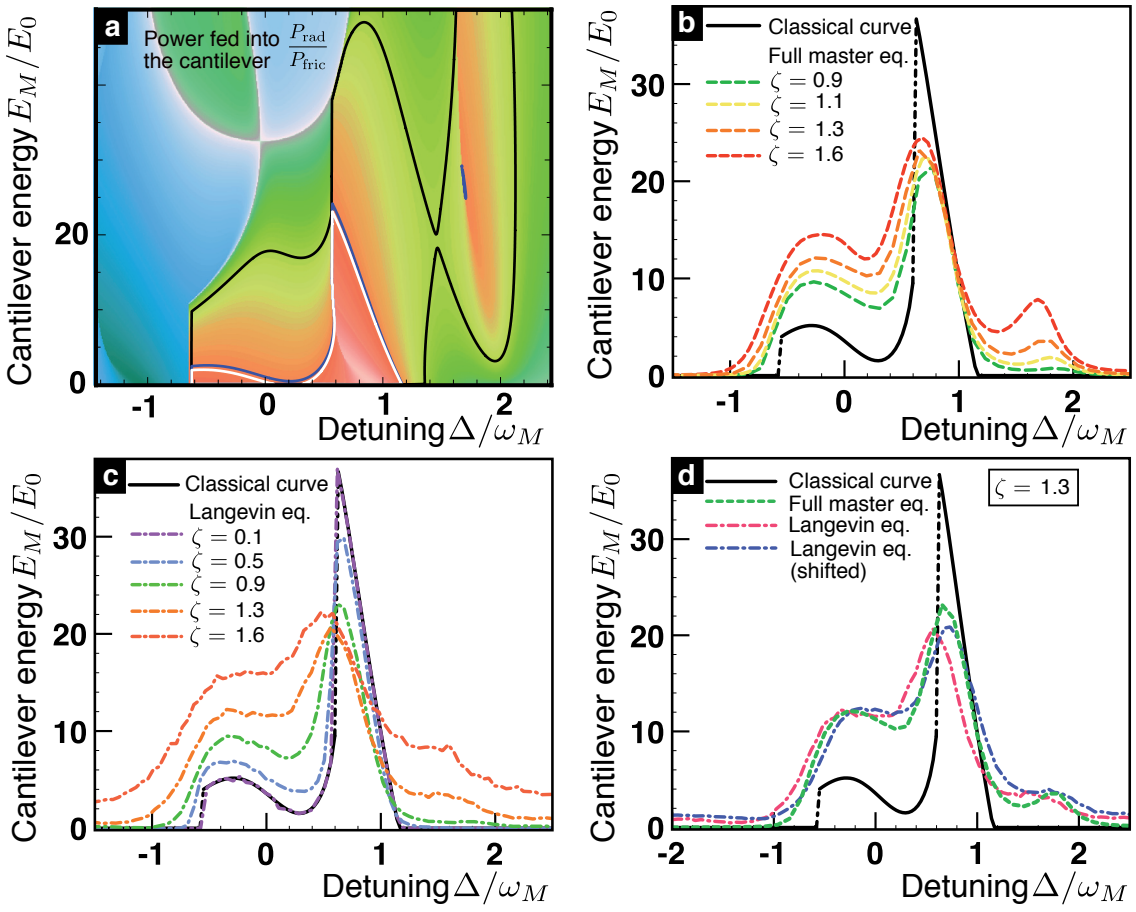

Figure 2.5: Cantilever energy vs. detuning resulting from the Langevin equation in comparison to the classical curve and the results from the quantum master equation. The choice of parameters is the same as for figure 2.4(b), $\kappa/\omega_M = 0.3$, $\Gamma_M = 50\Gamma_M^*$, $\mathcal{P} = 20\mathcal{P}^*$. (a) The classical solution for the oscillation energy is given by the white contour line in the attractor diagram, while the blue and black contours depict the solutions for lower damping rates, $\Gamma_M = 48\Gamma_M^*$ and $\Gamma_M = 13\Gamma_M^*$ respectively. We see, that a bistability at the second sideband occurs already for slightly modified parameters (see the blue. (b) In the solutions of the full master equation, we observe a shift of the resonances towards lower detunings and a smooth behaviour, in contrast to the sharp structures of the classical curve. For high values of the quantum parameter ζ, the curves show features that occur in the classical solution for lower damping rates only: The peak at the second sideband appears and the peaks of the first and second sideband merge. (c) The results of the Langevin equation recover the classical curves for the case of very weak quantum fluctuations, i.e. for $\zeta = 0.1$. They also resume the main features of the curves that come from the master equation. However, this approach fails to match the results of the master equation for large values of ζ and outside the region of instability. (d) Replacing the radiation pressure term of equation (2.18) by $\frac{\hbar g}{m x_{\mathrm{ZPF}}}(|\alpha|^2 - \frac{1}{2})$ shifts the semi-classical curve towards lower detunings, but does not lead to a better agreement with the curve from the quantum master equation.

Still, the Langevin approach can mimick the results from the master equation only partially. The approximation gets worse when dealing with low photon numbers and very large values of the quantum parameter ζ. In particular, the oscillation energy of the cantilever is overestimated by the semi-classical approach in the regions away from or in between the resonances. This is because the Langevin equation introduces artificial fluctuations of the radiation pressure force in the vacuum state. Indeed, $|\alpha|^2$ has a finite variance even in the ground state of the photon field, in contrast to $\hat{c}^\dagger\hat{c}$. To give a few numbers on the occupation numbers of the cavity for the parameters of figures 2.5(c) and (d) and $\zeta = 1.3$, we record that the photon numbers at $\Delta/\omega_M = -1.0$, $\Delta/\omega_M = 1.5$ and $\Delta/\omega_M = 2.0$ has dropped to values below 0.1 from a maximal value of $n_{\mathsf{max}} = 4.4$ at the resonance. The effect, that the semi-classical approach overestimates the quantum fluctuations, becomes more and more apparent for large values of the quantum parameters. We observe, that for $\zeta = 1.6$ the semi-classical curve of 2.5(c) deviates strongly from its fully quantum mechanical counterpart of figure 2.5(b) over the whole range of the detuning parameter.

Another inconsistency of the Langevin approach is the fact that the zero-point occupation of the cavity field does not lead to radiation pressure on the cantilever. To take account of this, we might therefore try and replace the radiation pressure term of equation (2.18) by $\frac{\hbar g}{m x_{\mathsf{ZPF}}}(|\alpha|^2 - \frac{1}{2})$. The resulting curve in figure 2.5(d) is shifted towards higher detunings, but does not improve the comparison to the result from the quantum master equation. As a true artefact of the manipulation of the radiation pressure term, it even shows an increase in the cantilever energy on the cooling side ($\Delta/\omega_M \lesssim -1$), where the real cavity occupation should drop down to zero.

2.5 Wigner density and phonon number distribution

In figure 2.6, we go beyond the average cantilever phonon number and present results for the phonon number probability distribution as well as for the full Wigner density of the cantilever, defined as

$$W(x,p) = \frac{1}{\pi\hbar}\int_{-\infty}^{+\infty} \langle x - y\,|\hat{\rho}|\,x + y\rangle\, e^{2ipy/\hbar}\, dy. \tag{2.19}$$

This figure demonstrates the different nature of the cantilever dynamics in the sub-threshold regime and above threshold, where self-induced oscillations occur. Below the threshold (for a detuning $\Delta_a = -0.45\omega_M$ as indicated in figure 2.4, quantum parameter $\zeta = 1$, and other parameters as in figure 2.4) the occupation of the cantilever is thermal, with an effective temperature determined by the effective optomechanical and mechanical damping rates, cf. equation (2.12). Consequently, the Wigner density shows a broad peak around the origin of the $x-p$ plane of cantilever position and momentum (the static shift of the cantilever due to the radiation pressure is very small). For a detuning of $\Delta_b = -0.2\omega_M$, self-induced oscillations occur. The probability distribution for the phonon number shows some thermal broadening, but an additional peak appears at a finite phonon number. In the Wigner density plot this results in a crater-like feature, which corresponds to a mixture of coherent states with essentially fixed amplitude but arbitrary phases. This captures the fact that the phase of the self-induced oscillations is completely arbitrary also in the classical solution. The energy corresponding to the phonon number at which the distribution peaks, compares fairly well to the oscillation energy obtained from the classical solution. Only the shift towards lower values of detuning as shown in figure 2.4(b) puts restrictions on a detailed quantitative comparison.

For a value of the detuning located in the second sideband, $\Delta_d = 1.72\,\omega_M$, we find a probability distribution with a peak for the occupation of the cantilever ground state, and a broader peak at a finite occupation number (mechanical damping is slightly decreased to display more pronounced features). Likewise, the Wigner density consists of a sharp peak at the origin, surrounded by a broader ring representing finite amplitude oscillations. This corresponds to the existence of two stable attractors in the classical analysis, with vanishing and finite oscillation amplitude, respectively. Similar results for the Wigner densities were found in Ref. [28] for a cantilever driven by a superconducting single-electron transistor.

2.6 Summary and Outlook

We presented a fully quantum mechanical treatment of the coupled cavity-cantilever system and investigated the effects of quantum fluctuations on the instability. To this end we compared the results of the numerical simulation of a quantum master equation to three other approaches: The classical solution, the rate-equation approach and a semiclassical Langevin equation.

Below the threshold of the instability, the influence of the quantum fluctuations and the amplification of the cantilever motion could well be described within the rate equation approach.

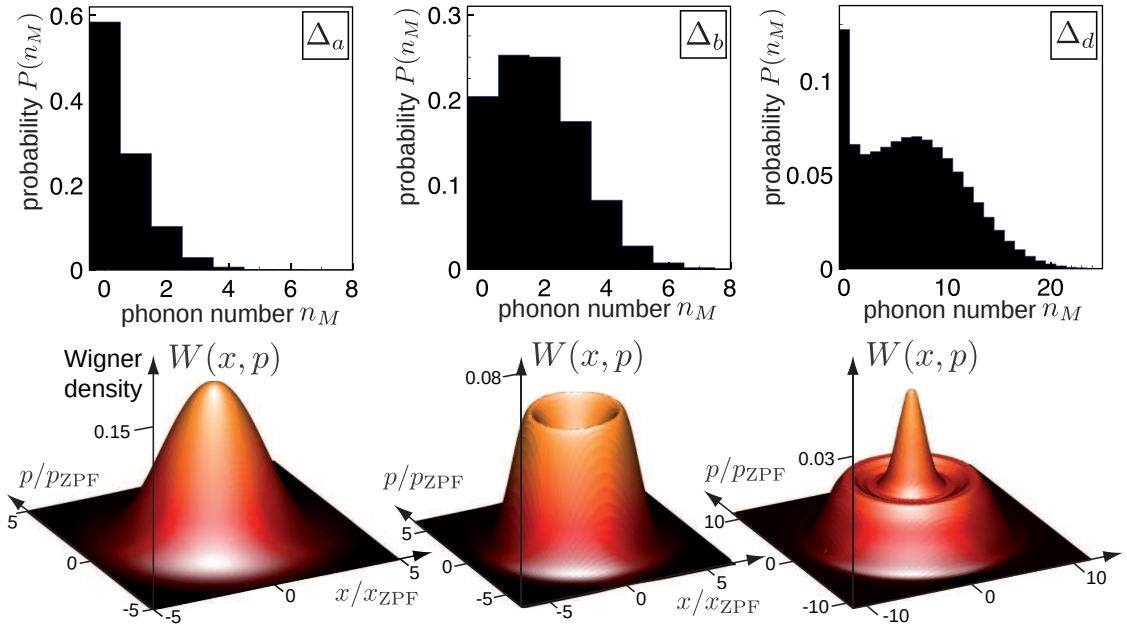

Figure 2.6: Distribution functions $P(n_M)$ of the cantilever occupation and Wigner functions $W(x,p)$ [rescaled by $x_{\rm ZPF}p_{\rm ZPF}$] of the cantilever for $\Delta_a = -0.45\omega_M$, $\Delta_b = -0.2\omega_M$, $\Delta_d = 1.72\omega_M$ [corresponding to the detuning values also indicated in figure 2.4(b); further parameters as in figure 2.4 with $\zeta = 1.0$; for Δ_d the mechanical damping rate is reduced to $\Gamma_M/\omega_M = 1.2{\cdot}10^{-3}$]. Below the threshold of self-induced oscillations, a broadened distribution is found corresponding to an increased effective temperature, cf. equation (2.12) (left panels, Δ_a); self-induced oscillations are visible as a finite amplitude ring in the middle and the right panel. Dynamical multistability (i.e. co-existence of several attractors) in the classical solution becomes apparent both in the distribution and the Wigner density, where a double-peaked structure develops.

In comparison the classical solution, we could find distinct signatures of the quantum fluctuations, including both photon shot noise and mechanical zero-point fluctuations, in the results from the quantum master equation. The quantum parameter determines the strength of these fluctuations and governs the quantum-to-classical transition of the system. In the semiclassical approach the quantum fluctuations were mimicked by classical noise terms. In a certain parameter regime, this semiclassical approach captured the results of the full quantum mechanical treatment fairly well. Finally, we investigated the bistable behaviour that appears in the curves of the oscillation energy at the second sideband. To this end we plotted and discussed the probability distribution of the cantilever occupation number and the Wigner density of the cantilever.

Having done all this, the obvious question arises of whether current optomechanical setups would allow to reach this quantum regime. When considering generic optomechanical setups consisting of a mechanical oscillator and an optical cavity, we have to deny this question. The values for the quantum parameter reach only up to $\zeta \sim 10^{-3}$ (in the Bouwmeester setup [11]), while in our analysis considerable quantum effects only appeared for $\zeta \sim 1$. Nevertheless, in view of the numerous variants of optomechanical systems the answer has to be revised: There are optomechanical systems in the quantum regime already today. In particular, two recent setups that became generally known as "optomechanics with cold atoms", exhibit quantum parameters of $\zeta \sim 1$ [32, 33]. In these systems, the mechanical oscillator is replaced by a cloud of ultracold atoms whose collective motion is coupled to the mode of an optical cavity. It is obviously worthwhile to have a closer look at these systems which we will do in the subsequent part of this thesis.

Chapter 3

Bose-Einstein condensation of trapped atomic gases

This chapter will give a short introduction to the general theory of Bose-Einstein condensates. It will discuss the basic methods to describe the collective motion of Bose-condensed atomic gas. We will employ these methods in Chapter 4, where we focus on optomechanical systems, in which the collective mode of a cloud of ultracold atoms is coupled to the field of an optical cavity. In that sense this chapter is only a preparatory part for the following considerations. For detailed and comprehensive reviews we refer to [37, 38, 39] which this overview is partly based on.

3.1 The Gross-Pitaevskii equation

In the theoretical description of condensates the Gross-Pitaevskii equation plays an exceptional role and is the starting point for various theoretical investigations of problems involving nonuniform dilute Bose gases. The Gross-Pitaevskii equation is a nonlinear Schrödinger equation for the condensate wave function that includes atom-atom interactions in a mean-field approach. It also allows to include stationary or time-dependent external potentials.
A common derivation of the Gross-Pitaevskii equation starts with a many-body Hamiltonian of the form

$$\begin{aligned}\hat{H} &= \int \hat{\Psi}^\dagger(\mathbf{x},t)[-\frac{\hbar^2}{2m_a}\nabla^2 + V_{\text{ext}}(\mathbf{x},t)]\hat{\Psi}(\mathbf{x},t)d^3\mathbf{x} \\ &\quad +\frac{1}{2}\int \hat{\Psi}^\dagger(\mathbf{x},t)\hat{\Psi}^\dagger(\mathbf{x}',\mathbf{t})V_{\text{int}}(\mathbf{x}-\mathbf{x}')\hat{\Psi}(\mathbf{x}',t)\hat{\Psi}(\mathbf{x},t)d^3\mathbf{x}d^3\mathbf{x}', \end{aligned} \tag{3.1}$$

where $V_{\text{ext}}(\mathbf{x},t)$ denotes an external potential and $V_{\text{int}}(\mathbf{x}-\mathbf{x}')$ the two-body interaction that depends on the distance between the atoms only. The mass of a single atom is given by m_a. $\hat{\Psi}^\dagger(\mathbf{x})$ and $\hat{\Psi}(\mathbf{x})$ are the field operators that create and annihilate a single atom at the position $\mathbf{x}$. They obey the canonical commutation relations for bosons: $[\hat{\Psi}(\mathbf{x}),\hat{\Psi}^\dagger(\mathbf{x}')] = \delta(\mathbf{x}-\mathbf{x}')$ and $[\hat{\Psi}(\mathbf{x}),\hat{\Psi}(\mathbf{x}')] = 0$.

The time evolution of the field operator $\hat{\Psi}(\mathbf{x},t)$ according to the Hamiltonian 3.1 is given by

$$i\hbar\frac{\partial}{\partial t}\hat{\Psi}(\mathbf{x},t) = [\hat{\Psi}(\mathbf{x},t),\hat{H}]$$
$$= \Big(-\frac{\hbar^2}{2m_a}\nabla^2 + V_{\text{ext}}(\mathbf{x},t) + \int \hat{\Psi}^\dagger(\mathbf{x}',t)V_{\text{int}}(\mathbf{x}'-\mathbf{x})\hat{\Psi}(\mathbf{x}',t)d^3\mathbf{x}'\Big)\hat{\Psi}(\mathbf{x},t). \tag{3.2}$$

The principles of a mean-field description for the atom gas go back to Bogoliubov [40] and are based on the concept of separating the condensate wave function from the field operator and treat it as a classical function. To this end, the field operator $\hat{\Psi}(\mathbf{x})$ is decomposed by using the eigenbasis of the one-particle density matrix $\{\psi_\alpha(\mathbf{x})\}$:

$$\hat{\Psi}(\mathbf{x}) = \sum_\alpha \psi_\alpha(\mathbf{x})\hat{a}_\alpha. \tag{3.3}$$

$\psi_\alpha(\mathbf{x})$ are normalized single particle wave functions and $\hat{a}_\alpha$ the corresponding annihilation operators such that $\langle\hat{a}_\alpha\hat{a}^\dagger_{\alpha'}\rangle = \delta_{\alpha\alpha'}n_\alpha$, where n_α is the eigenvalue of the density matrix. The Bogoliubov approximation consists of replacing the ground state operators $\hat{a}_0$ and $\hat{a}^\dagger_0$ by the scalar $\sqrt{N_0}$. This approximation is well-suited to describe the macroscopic phenomenon of Bose-Einstein condensation, i.e. the case of a large ground-state occupation $N_0 = \langle\hat{a}_0\hat{a}^\dagger_0\rangle \gg 1$. It follows that

$$\hat{\Psi}(\mathbf{x}) = \sqrt{N_0}\psi_0(\mathbf{x}) + \sum_{\alpha\neq 0}\psi_\alpha\hat{a}_\alpha =: \Psi_0(\mathbf{x}) + \delta\hat{\Psi}(\mathbf{x}). \tag{3.4}$$

$\Psi_0(\mathbf{x})$ is a complex function that plays the role of an order parameter and is often called the wavefunction of the condensate. As a consequence of the Bogoliubov ansatz, we have $\Psi_0(\mathbf{x}) = \langle\hat{\Psi}(\mathbf{x})\rangle$. This expression implies that the expectation value $\langle\hat{\Psi}(\mathbf{x})\rangle$ is not evaluated with respect to a state of fixed particle number but by averaging over physically equivalent states. In that sense a state containing N atoms and the states $|N+1\rangle \propto \hat{a}^\dagger_0|N\rangle$ and $|N-1\rangle \propto \hat{a}_0|N\rangle$ are considered equivalent.

In turn we can already make a general statement on the time evolution of $\langle\hat{\Psi}(\mathbf{x})\rangle$. If the expectation value is taken with respect to stationary states that evolve according to $e^{-iEt/\hbar}$, equation (3.2) yields:

$$\Psi_0(\mathbf{x},t) = e^{-i\mu t/\hbar}\Psi_0(\mathbf{x}). \tag{3.5}$$

This means that the time evolution of the order parameter is given by the difference in energy of physically equivalent states. The chemical potential μ is defined as $\mu = \frac{\partial E}{\partial N} \approx E(N) - E(N-1)$ and is called the chemical potential.

In a dilute gas at low temperatures the interactions between the atoms can to a good approximation be considered as low-energy collisions of point-like particles. In that case, the interaction strength is determined by a single parameter, the s-wave scattering length a_s and the interaction potential is modelled by

$$V_{\text{int}}(\mathbf{x}'-\mathbf{x}) = g\delta(\mathbf{x}'-\mathbf{x}). \tag{3.6}$$

The coupling constant g is related to the scattering length by

$$g = \frac{4\pi\hbar^2 a_s}{m_a}. \tag{3.7}$$

Starting from (3.2), we can now derive an equation that governs the time evolution of the order parameter. Replacing $\hat{\Psi}(\mathbf{x},t)$ by $\Psi_0(\mathbf{x},t)$, and thereby ignoring both quantum and thermal

depletion of the condensate, leads to the well-known Gross-Pitaevskii equation:

$$i\hbar\frac{\partial}{\partial t}\Psi_0(\mathbf{x},t) = (-\frac{\hbar^2}{2m_a}\nabla^2 + V_{\text{ext}}(\mathbf{x},t) + g|\Psi_0(\mathbf{x},t)|^2)\Psi_0(\mathbf{x},t). \tag{3.8}$$

It is a Schrödinger equation with a mean-field interaction term that introduces a nonlinearity. The time-independent Gross-Pitaevskii equation reads

$$\mu\Psi_0(\mathbf{x}) = (-\frac{\hbar^2}{2m_a}\nabla^2 + V_{\text{ext}}(\mathbf{x},t) + g|\Psi_0(\mathbf{x},t)|^2)\Psi_0(\mathbf{x},t). \tag{3.9}$$

The condensate wave function has to be normalized to the total number of particles: $\int |\Psi_0(\mathbf{x})| d^3\mathbf{x} = N$, which also fixes the value of the chemical potential μ in equation (3.9). Recapitulating all the approximations performed so far, we see that the Gross-Pitaevskii equation is valid for a dilute gas with a large particle number and at a very low temperature.

3.2 The Thomas-Fermi limit

A prerequisite for Bose-Einstein condensation is, that the mean interparticle separation becomes comparable to the de Broglie-wavelength of thermal motion. This fact makes a dilute atomic gas an ideal system to study condensation in experiment. Diluteness was also assumed in the derivation of the Gross-Pitaevskii equation (3.8). An atomic gas is considered to be dilute if the average interatomic distance is much larger than the s-wave scattering length: $\bar{n} \ll |a_s|^{-3}$, where $\bar{n}$ denotes the average density. Nevertheless, the interaction between the atoms can dominate the dynamical and stationary properties of the condensate.

In the following we will discuss the role of the interactions for the case of a harmonic trapping potential

$$V_{\text{ext}}(\mathbf{x}) = \frac{m_a}{2}(\omega_x x^2 + \omega_y y^2 + \omega_z z^2). \tag{3.10}$$

A first estimate can be made by comparing the interaction energy E_{int} to the ground state energy of a harmonic oscillator with frequency $\bar{\omega} = (\omega_x\omega_y\omega_z)^{1/3}$: The average density can be approximated by the number of particles N and the ground-state width of the oscillator $a_{\text{ho}} = \sqrt{\hbar/(2m_a\bar{\omega})}$ as $\bar{n} \approx N/a_{\text{ho}}^3$. It follows that the interaction energy is roughly $E_{\text{int}} \approx g\bar{n}N$. On the other hand the kinetic energy in the harmonic potential will be of the order $E_{\text{kin}} \approx \hbar\bar{\omega}N$. The interaction term in the Gross-Pitaevskii equation (3.8) will therefore be dominant for

$$\frac{E_{\text{int}}}{E_{\text{kin}}} \approx \frac{g\bar{n}N}{\hbar\bar{\omega}N} \approx \frac{Na_s}{a_{\text{ho}}} \gg 1. \tag{3.11}$$

The role of the parameter $\frac{Na_s}{a_{\text{ho}}}$ can also be seen by rescaling the Gross-Pitaevskii equation (3.9). Introducing a_{ho}, a_{ho}^{-3}, $\hbar\bar{\omega}$ as the new units of length, density and energy and denoting the rescaled parameters by a tilde leads to:

$$[-\tilde{\nabla}^2 + \lambda_x^2\tilde{x}^2 + \lambda_y^2\tilde{y}^2 + \lambda_z^2\tilde{z}^2 + 8\pi\frac{Na_s}{a_{\text{ho}}}|\tilde{\Psi}_0|^2]\tilde{\Psi}(\tilde{\mathbf{x}}) = \tilde{\mu}\tilde{\Psi}_0(\tilde{\mathbf{x}}), \tag{3.12}$$

where $\lambda_i = (\omega_i/2\bar{\omega})^2$. For a large value of Na_s/a_{ho} the interaction term dominates the left hand side of (3.12) such that - in the so called Thomas-Fermi approximation - the contribution of the

kinetic energy can be neglected. In this limit the time-independent Gross-Pitaevskii equation yields

$$|\Psi_0(\mathbf{x})|^2 = \frac{1}{g}(\mu - V_{\text{ext}}(\mathbf{x})) \tag{3.13}$$

This result is valid for $\mu > V_{\text{ext}}$, i.e. inside an ellipsoid given by $x^2/R_x^2 + y^2/R_y^2 + z^2/R_z^2 = 1$, where $R_i = \sqrt{2\mu/m_a\omega_i^2}$ are the Thomas-Fermi radii. Outside this region the condensate wave function is set to zero.

Up to now, we assumed the Thomas-Fermi approximation to be valid for $Na_s/a_{\text{ho}} \gg 1$. This condition is based on rough approximations, and it turns out that it is not appropriate to describe the crossover to the non-Thomas-Fermi regime. In particular it will fail, if the trap shows a high anisotropy, e.g. for $\omega_x \gg \omega_y, \omega_z$. To get a more accurate defining condition for the Thomas-Fermi regime we therefore turn towards a hydrodynamic description of the condensate. A simple transformation of the Gross-Pitaevskii equation (3.8) leads to an intuitive picture for the superfluid dynamics of the condensate. In addition, this description allows to narrow down the Thomas-Fermi condition.

For that purpose we rewrite the wavefunction $\Psi_0(\mathbf{x}, t)$ in terms of a phase $S(\mathbf{x}, t)$ and a modulus $\sqrt{\rho}$, i.e.

$$\Psi_0(\mathbf{x}, t) = \sqrt{\rho(\mathbf{x}, t)}e^{iS(\mathbf{x},t)/\hbar}. \tag{3.14}$$

Accordingly, the Gross-Pitaevskii equation transforms into two hydrodynamic-like equations, an equation of continuity and an equation for the phase:

$$\frac{\partial \rho}{\partial t} + \nabla \cdot (\rho \mathbf{v}) = 0 \tag{3.15}$$

$$\frac{\partial}{\partial t}S + \Big(\frac{1}{2}m_a\mathbf{v}^2 + V_{\text{ext}} + g\rho - \frac{\hbar^2}{2m_a\sqrt{\rho}}\nabla^2\sqrt{\rho}\Big) = 0 \tag{3.16}$$

Here we introduced the velocity of the condensate flow

$$\mathbf{v} = \frac{1}{m_a}\nabla S = -\frac{i\hbar}{2m_a\rho}(\Psi_0^*\nabla\Psi_0 - \Psi_0\nabla\Psi_0^*). \tag{3.17}$$

Equations (3.15) and (3.16) have the typical structure of equations for the dynamics of a superfluid at zero temperature [38]. The term proportional to the $\nabla^2\sqrt{\rho}$ in equation (3.16) is commonly referred to as the "quantum pressure". If the density profile ρ is smooth this term can be neglected. To capture that effect quantitatively, we introduce a length scale R characterizing the distance over which density variations in the system typically extend. In our case, as we are considering the ground state wavefunction, R is given by the extent of the condensate. When considering excitations of the condensate, the typical length scale would be the wavelength of the oscillations. To proceed, we note that the kinetic pressure term scales as $\frac{1}{\sqrt{\rho}}\nabla^2\sqrt{\rho} \sim R^{-2}$. Its contribution in equation (3.16) can therefore be neglected if $g\bar{n} \gg \frac{\hbar^2}{2m_a}R^{-2}$ or

$$R \gg \xi := \frac{\hbar}{\sqrt{2gm_a\bar{n}}} = (8\pi\bar{n}a_s)^{-\frac{1}{2}}. \tag{3.18}$$

i.e. when the typical length scale R of the density fluctuations is much larger than the so called healing length ξ. To find the ground state density within this approximation we set $\mathbf{v} = 0$, or equivalently $S = \mu t$, and recover the Thomas-Fermi result (3.13):

$$\rho_0(\mathbf{x}) = \frac{1}{g}(\mu - V_{\text{ext}}(\mathbf{x})). \tag{3.19}$$

Most notably, we are now able to find a more reliable condition that determines the validity of the Thomas-Fermi approximation. The system under consideration is in the Thomas-Fermi regime if the Thomas-Fermi radii R_i exceed the healing length:

$$R_i \gg \xi. \tag{3.20}$$

In particular, for highly anisotropic traps, this condition has to be checked for the Thomas-Fermi radius along each of the coordinate axes. For $\omega_x \ll \omega_y, \omega_z$ the condensate will assume the shape of a cigar, for $\omega_x \gg \omega_y, \omega_z$ the shape of a disk. It might even be the case, that the Thomas-Fermi approximation only describes the dynamics along the direction(s) of high elongation correctly, and can not be applied along the direction(s) of strong confinement.

Plugging the definitions $R_i = \sqrt{2\mu/m\omega_i^2}$, $\xi = (8\pi\bar{n}a_s)^{-\frac{1}{2}}$ into the Thomas-Fermi condition (3.20) and using $\mu \approx \bar{n}g$ shows that we could equally demand that the chemical potential has to be much larger than the energy of the harmonic oscillator ground-state:

$$\frac{\mu}{\hbar\omega_i} \gg 1. \tag{3.21}$$

Note that within the Thomas-Fermi approximation the chemical potential is determined by the normalization of $|\Psi_0|^2$ and is given by

$$\mu^{TF} = \frac{\hbar\bar{\omega}}{2}(\frac{Na_s}{a_{ho}})^{\frac{2}{5}}. \tag{3.22}$$

As a final remark, we note that the Thomas-Fermi regime is encountered in a large number of experiments: In the MIT setup from 1995 [4] for example, condensation of $N \sim 10^6$ sodium atoms with $a_s \sim 5 \cdot \mathrm{nm}$ and $a_{\mathsf{ho}} \sim 1\,\mu\mathrm{m}$ was observed.

3.3 The Bogoliubov-de Gennes equations

In the previous section the Gross-Pitaevskii equation for the order parameter was derived by replacing $\hat{\Psi}(\mathbf{x})$ with $\Psi_0(\mathbf{x})$. If instead we substitute $\hat{\Psi}(\mathbf{x}) = \Psi_0(\mathbf{x}) + \delta\hat{\Psi}(\mathbf{x})$ in (3.1) and neglect terms of the order $\mathcal{O}(\delta\hat{\Psi}^3)$ we arrive at a grand canonical Hamiltonian of the form

$$\begin{aligned}
\hat{H} \quad -\mu\hat{N} = & \int \Psi_0^*(\mathbf{x})\Big(-\frac{\hbar^2}{2m_a}\nabla^2 + V_{\mathsf{ext}}(\mathbf{x}) - \mu + \frac{g}{2}|\Psi_0(\mathbf{x})|^2\Big)\Psi_0(\mathbf{x})d^3\mathbf{x} \\
+ & \int \delta\hat{\Psi}^\dagger(\mathbf{x})\Big(-\frac{\hbar^2}{2m_a}\nabla^2 + V_{\mathsf{ext}}(\mathbf{x}) - \mu + 2g|\Psi_0(\mathbf{x})|^2\Big)\delta\hat{\Psi}(\mathbf{x})d^3\mathbf{x} \\
+ & \frac{g}{2}\int \Psi_0^2(\mathbf{x})\delta\hat{\Psi}^{\dagger 2}(\mathbf{x})d^3\mathbf{x} + h.c.,
\end{aligned} \tag{3.23}$$

where we have introduced the number operator $\hat{N} = \int d^3\mathbf{x}\hat{\Psi}^\dagger(\mathbf{x})\hat{\Psi}(\mathbf{x})$.

The grand canonical Hamiltonian $\hat{H} - \mu N$ can be diagonalized by using a Bogoliubov transformation of the form:

$$\delta\hat{\Psi}(\mathbf{x}) = \sum_\alpha (u_\alpha(\mathbf{x})\hat{a}_\alpha - v_\alpha^*(\mathbf{x})\hat{a}_\alpha^\dagger). \tag{3.24}$$

such that

$$\begin{aligned}
\hat{H} - \mu\hat{N} &= H_0 + \sum_\alpha \hbar\omega_\alpha \hat{a}_\alpha^\dagger\hat{a}_\alpha, \\
H_0 &= \int d^3\mathbf{x}\Psi_0^*(\mathbf{x})(-\frac{\hbar^2}{2m_a}\nabla^2 + V_{\mathsf{ext}}(\mathbf{x}) + \frac{g}{2}|\Psi_0(\mathbf{x})|^2)\Psi_0(\mathbf{x}).
\end{aligned}$$

Here $\hat{a}_\alpha$ and $\hat{a}_\alpha^\dagger$ are annihilation and creation operators for the Bogoliubov excitations which obey the canonical commutation relations of bosonic operators. The amplitudes $u_\alpha(\mathbf{x})$ and $v_\alpha(\mathbf{x})$ are normalized as

$$\int d^3\mathbf{x}(u_\alpha u^*_{\alpha'} - v_\alpha v^*_{\alpha'}) = \delta_{\alpha\alpha'} \tag{3.25}$$

and have to satisfy the Bogoliubov-de Gennes equations

$$\begin{aligned}(-\frac{\hbar^2}{2m_a}\nabla^2 + V_{\text{ext}}(\mathbf{x}) - \mu)u_\alpha(\mathbf{x}) + g|\Psi_0|^2(2u_\alpha - v_\alpha) &= \hbar\omega_\alpha u_\alpha \\ (-\frac{\hbar^2}{2m_a}\nabla^2 + V_{\text{ext}}(\mathbf{x}) - \mu)v_\alpha(\mathbf{x}) + g|\Psi_0|^2(2v_\alpha - u_\alpha) &= -\hbar\omega_\alpha v_\alpha.\end{aligned} \tag{3.26}$$

The solutions of (3.26) for $V_{\text{ext}} = 0$ are readily found and give a first impression of the condensate dynamics for the general case. For $u(\mathbf{x}) = ue^{i\mathbf{k}\cdot\mathbf{x}}$ and $v(\mathbf{x}) = ve^{-i\mathbf{k}\cdot\mathbf{x}}$ the Bogoliubov equations reduce to

$$\begin{aligned}\hbar\omega u &= \frac{\hbar^2k^2}{2m_a}u + g\bar{n}(u+v) \\ -\hbar\omega v &= \frac{\hbar^2k^2}{2m_a}v + g\bar{n}(u+v)\end{aligned} \tag{3.27}$$

and yield the well-known Bogoliubov spectrum

$$\begin{aligned}\hbar\omega &= \sqrt{\epsilon_k(g\bar{n} + \epsilon_k)} \\ &= \frac{\hbar^2}{2m_a}\sqrt{\Big(\frac{2\pi}{\lambda_{\text{exc}}}\Big)^2\Big(\Big(\frac{2\pi}{\lambda_{\text{exc}}}\Big)^2 + \frac{1}{\xi^2}\Big)},\end{aligned} \tag{3.28}$$

where $\epsilon_k = \hbar^2k^2/2m_a$ is the free-particle energy and $\lambda_{\text{exc}} = \frac{2\pi}{k}$ denotes the wavelength of the excitations. The low-energy part of this spectrum shows a linear dispersion, $\omega \approx ck$, with a sound velocity of $c = \sqrt{g\bar{n}/m_a} = \sqrt{\mu/m_a}$. The high-energy behaviour, on the other hand, is governed by a quadratic dispersion relation $\hbar\omega \approx \epsilon_k$ as in the case of free particles.

3.4 Collective excitations

When Bose-Einstein condensation of trapped atomic gases became experimentally realizable some ten years ago, the study of its collective excitations immediately came into the focus of several experimental and theoretical groups [41, 42, 43, 44]. For the uniform case the collective excitations had already been studied in the context of superfluid Helium. Even though the case of a trapped gas is in some points analogous, there is an important difference: The spectrum can no longer be expressed by the momentum of the excitation. Instead, new quantum numbers that reflect the symmetries of the problem have to be introduced. The discussion of this section will focus on a spherical symmetric potential, i.e. $V_{\text{ext}}(\mathbf{x}) = \frac{m_a}{2}\omega_0^2\mathbf{x}^2$. In this case, the elementary excitations can be described in terms of the radial quantum number n_r, the angular momentum l and its component in $z-$direction, denoted by m. In his pioneering work [43] Stringari presented an elegant solution for the spectrum and the eigenfunctions within the Thomas-Fermi approximation. It led to a very good agreement with the results of the experiments at JILA [41] and MIT [42]. Here, we give a recapitulation of the results of [43] and discuss general features of the excitation spectrum, as they will become important in later parts of this thesis.

To begin with, we reconsider the hydrodynamic equations (3.15) and (3.16) and concentrate on the low-energy excitations of the condensate. If the wavelength λ_{exc} of these oscillations is much larger than the healing length ξ, the "quantum pressure" term of equation (3.16) can be neglected. Plugging in the ansatz $\rho(\mathbf{x},t) = \rho_0(\mathbf{x},t)+\delta\rho(\mathbf{x},t)$, the hydrodynamic equations (3.15) and (3.16) result in

$$\begin{aligned} \frac{\partial^2}{\partial t^2}\delta\rho + \nabla[(\frac{\partial}{\partial t}\mathbf{v})\rho(\mathbf{x},t) + \mathbf{v}\frac{\partial}{\partial t}\rho(\mathbf{x},t)] &= 0 \\ \frac{\partial}{\partial t}\mathbf{v} + \nabla[\frac{g}{m}\delta\rho + \frac{\mathbf{v}^2}{2}] &= 0 \end{aligned} \tag{3.29}$$

Using the Thomas-Fermi result for the ground state density $\rho_0(\mathbf{x})$ (3.19) and neglecting all terms of the order $\mathcal{O}(\mathbf{v}^2)$, $\mathcal{O}(\delta\rho^2)$, $\mathcal{O}(\mathbf{v}\delta\rho)$ in (3.29), leads to

$$\frac{\partial^2}{\partial t^2}\delta\rho = \nabla\cdot[(\mu - V_{trap})/m\,\nabla\delta\rho]. \tag{3.30}$$

or equivalently,

$$-\omega^2\delta\rho = \nabla\cdot[c^2(\mathbf{x})\nabla\delta\rho], \tag{3.31}$$

where $c(\mathbf{x}) = \sqrt{(\mu - V_{\text{ext}}(\mathbf{x}))/m_a}$ can be interpreted as a local sound velocity. We note that equation (3.31) allows for solution in the form of conventional sound waves, provided their wavelength is much smaller than the extent of the atomic gas, i.e. $\lambda_{\text{exc}} \ll R$, such that the sound velocity can be treated as locally constant. Experimentally such sound waves can be excited by pointing a laser on the trapped condensate. Experiments of this kind have been studied for example in [45]. Their data agreed well with the predictions of the Bogoliubov theory.

For excitations on length scales comparable to the size of the system, $\lambda_{\text{exc}} \approx R$, the spectrum turns out to be discretized. To see this, equation (3.31) can be solved by separation of variables in spherical coordinates. The solution, which is defined for $|\mathbf{x}| < R = \sqrt{2\mu/m_a\omega_a^2}$, is given by

$$\delta\rho(r,\theta,\phi) = P_l^{2n_r}(r/R)r^l Y_{lm}(\theta,\phi). \tag{3.32}$$

The spherical coordinates are introduced in the conventional notation such that $x = r\sin\theta\cos\phi, y = r\sin\theta\sin\phi$ and $z = r\cos\theta$. $P_l^{(2n_r)}(x)$ are polynomials of the form $P_l^{(2n_r)} = 1 + \alpha_2 x^2 + \ldots + \alpha_{2n_r}x^{2n_r}$, with coefficients satisfying $\alpha_{2k+2} = -\alpha_{2k}(n_r - k)\frac{2l+2k+3+2n_r}{(k+1)(2l+2k+3)}$, and $Y_{lm}(\theta,\phi)$ are the spherical harmonic functions.

The corresponding spectrum depends on the radial quantum number n_r and the angular momentum l :

$$\omega(n_r,l) = \omega_0(2n_r^2 + 2n_r l + 3n_r + l)^{\frac{1}{2}}. \tag{3.33}$$

Most strikingly, the eigenfrequencies are independent of both the strength of the interactions g and the density of the atomic gas $\bar{n}$. This can be understood by noting that both the Bogoliubov velocity of sound, $c = \sqrt{\mu/m}$ at the center of the trap, and the size of the condensate, $R = \sqrt{\frac{2\mu}{m\omega_0^2}}$, scale with $\sqrt{\bar{n}g}$.

Still the result reveals distinct signatures of the interactions as can be seen by comparing to the predictions of the non-interacting case. The Gross-Pitaevskii equation (3.8) for $g = 0$ and

$V_{\text{ext}} = \frac{m}{2}\omega_0^2 r^2$ reduces to a Schrödinger equation of a simple harmonic oscillator, whose spectrum is given by

$$\omega(n_r, l) = \omega_0(2n_r + l). \tag{3.34}$$

For $n_r = 0$, the frequencies of the condensate modes, $\omega(n_r = 0, l) = \sqrt{l}\omega_0$, are diminished in value when compared to (3.34). Only the $l = 1$ mode, commonly referred to as the dipole mode, is not influenced by the interactions. We can identify this mode as the center-of-mass oscillation. The excitations closest in energy to the center-of-mass mode is the quadropole mode with $\omega(n_r = 0, l = 2) = \sqrt{2}\omega_0$. Note that all excitations with $n_r = 1$ have smaller excitation energies when compared to the result for the non-interacting case. On the other hand, the lowest mode with $n_r \neq 0$ is the monopole mode with $\omega(n_r = 1, l = 0) = \sqrt{5}\omega_{\text{ho}}$- which is larger than the non-interacting result. This can be understood by noting the the evolution of the monopole mode involves the compression of the condensate.

While for a spherically symmetric trap these results can be derived in a rather straight-forward manner, the case of an anisotropic harmonic trap, $V_{\text{ext}} = \frac{m_a}{2}\omega_{x,y}^2(x^2 + y^2) + \frac{m_a}{2}\omega_z^2 z^2$, is much more involved. An analytic solution based on a separation ansatz in cylindrical elliptical coordinates for the hydrodynamic equations was given in [46]. Equivalent results were found by Öhberg et al. [47] solving the Bogoliubov equations with a polynomial ansatz.

Chapter 4

Cold atoms and optomechanics

In this chapter we will develop and discuss a model setup consisting of a basic optomechanical cavity and a cloud of ultra-cold atoms inside the cavity. It aims at coupling the dynamics of the cantilever motion and the center-of-mass motion of the atoms. In a sense this model is a hybrid combining a setup of the generic optomechanical type (see figure 1.1) and a setup similar to the experiment of Murch et al. [32] where the mechanical motion of a cloud of cold atoms is coupled to a cavity field. As we will see, the model considered here allows for a direct coupling between the cantilever and the atoms, as the spatial structure of the cavity field depends on the position of the cantilever. Moreover, we will discuss a second-order coupling between the cantilever and the atomic cloud that arises due to the fact that both elements interact with the cavity field. This cavity-assisted coupling will turn out to exceed the direct coupling for realistic parameters. We start the analysis by employing a simplified model that treats the atomic cloud in the simplest possible manner. In a later part of this chapter we will confirm the results of the simple model by a calculation that is based on the standard treatment for the dynamics of a Bose-condensed gas.

In view of chapter 2, where we discussed quantum effects in a generic optomechanical setup, we will also investigate the question, if any features of uniquely quantum-mechanical nature can be observed in this model setup. We therefore consider the possibility of generating squeezed states of the cantilever and the atomic cloud. Finally, we address the issue of measuring the Fock state of the atomic collective motion.

4.1 Electromagnetic field mode inside the cavity

Before discussing the interaction between a cloud of atoms and the cavity field, we should preface this part with an investigation of the spatial structure that a standing wave inside an empty cavity exhibits. We consider an optical cavity of length L that is driven by an incoming laser field of wavelength k and amplitude E_0. The transmission and reflection amplitudes of the first and second mirror are denoted by $t_{1,2}$ and $r_{1,2}$. The expression for the electromagnetic field at a specific position along the cavity axis can be derived by summing up all possible paths of the

photons impinging the cavity:

$$\begin{aligned} E(x) &= E_0 t_1 (e^{ikx} + r_2 e^{ik(2L-x)} + r_1 r_2 e^{ik(2L+x)} + r_1 r_2^2 e^{ik(4L-x)} + ...) \\ &= E_0 t_1 \sum_{m=0}^{\infty} (r_1 r_2)^m e^{i2kmL} (e^{ikx} + r_2 e^{ik(2L-x)}) \\ &= E_0 t_1 \frac{e^{ikx} + r_2 e^{ik(2L-x)}}{1 - r_1 r_2 e^{i2kL}} \end{aligned} \tag{4.1}$$

Note that equivalently we could solve the ansatz depicted in figure (4.1) for consistent solutions of the right- and the left-moving wave amplitudes E_1 and E_2. The boundary conditions yield

$$\begin{aligned} E_1 &= E_0 t_1 + E_2 r_1 \\ E_2 e^{-ikL} &= r_2 E_1 e^{ikL}, \end{aligned} \tag{4.2}$$

and the solution $E(x) = E_1 e^{ikx} + E_2 e^{-ikx}$ coincides with (4.1).

The intensity inside the cavity is accordingly given by

$$|E(x)|^2 = |E_0 t_1|^2 \frac{1 + r_2^2 + r_2 \cos(2k(L-x) + \phi_2)}{1 + (r_1 r_2)^2 - 2 r_2 r_2 \cos(2kL + \phi_1 + \phi_2)} \tag{4.3}$$

where the complex reflectivity amplitudes $r_{1,2}$ are rewritten as $r_{1,2} e^{i\phi_{1,2}}$ with real-valued $r_{1,2}$. The phase shift $\phi_{1,2}$ for a reflection on the boundary to a dense medium is π, a result that can be found from Fresnel's formulas for the special case of normal incidence. If we furthermore assume a one-sided cavity, i.e. $|r_2| = 1$ the light intensity reduces to

$$|E(x)|^2 = |E_0 t_1|^2 \frac{4 \sin^2(kx - kL))}{(1 - r_1)^2 + 4 r_1 \sin^2(kL)}. \tag{4.4}$$

In particular, (4.4) shows how the axial intensity profile depends on the wave number k and the cavity length L. We illustrate this dependence in the density plots of figure (4.2).

Regarding the transverse profile of the cavity, we assume an idealized Gaussian beam with constant waist w_0 so that the cavity intensity $|E(x,y,z)|^2$ is given by

$$|E(x,y,z)|^2 = |E(x)|^2 \exp(-\frac{y^2 + z^2}{w_0^2}). \tag{4.5}$$

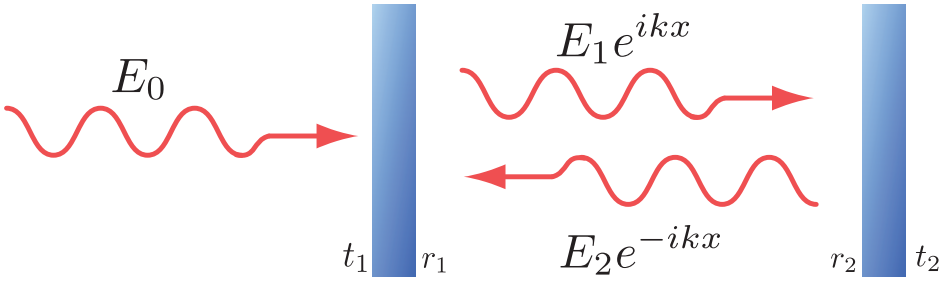

Figure 4.1: The intracavity field is given by the superposition of right- and left-moving waves, whose amplitudes E_1 and E_2 are connected to each other and to the incoming field by appropriate boundary conditions (see equations (4.2)).

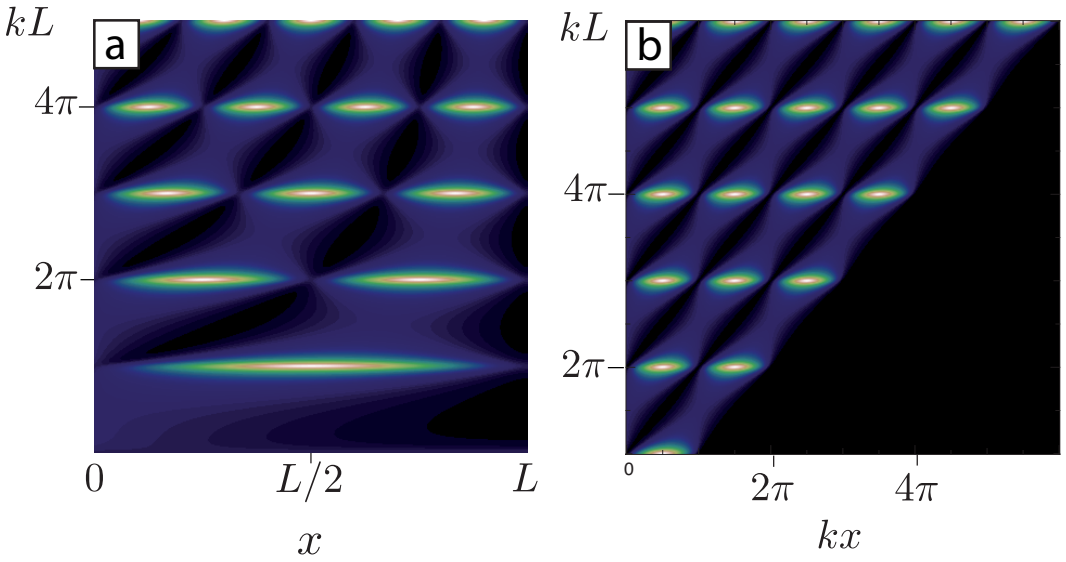

Figure 4.2: Intensity of the electromagnetic field (equation 4.4) as a function of the position x inside the cavity and the wave number k of the incoming laser beam. For this panel we chose the reflectivities of the mirrors to be $r_2 = 1$, $r_1 = 0.7$. The colour scheme is scaled linearly between the maximal value of the intensity, $|E_0 t_1|^2 \frac{4r_2}{(1-r_1 r_2)^2}$, (white) and zero intensity (black). (a) Intensity profile for fixed cavity length L: When the wave number is increased along the vertical axis, the cavity resonances appear at integer multiples of $k = \pi/L$. (b) Intensity profile for fixed wave number k. When increasing the cavity length L, the number of intensity nodes rises by one at $L = n\pi/k$, $n \epsilon \mathbb{N}$.

4.2 Atom-cavity coupling

This section introduces the basic coupling mechanism between a single atom and a single cavity model and follows the corresponding discussion in [48]. We will focus on the case, where the cavity resonance is far detuned from the atomic transition resonance. Note that this model is only valid if the cavity is driven near resonance. This means that the detuning between the laser frequency and the cavity resonance frequency has to be much smaller than the cavity-atom detuning.

The interaction between a single atom and a radiation field can be modelled by the Jaynes-Cummings Hamiltonian

$$\hat{H} = \frac{\hbar\omega_{\mathsf{a,res}}}{2}\hat{\sigma}_z + \hbar\omega_{\mathsf{cav}}\hat{c}^\dagger\hat{c} + \hbar g_0(\mathbf{x})(\hat{\sigma}^+\hat{c} + \hat{\sigma}^-\hat{c}^\dagger) + \hat{H}_\kappa + \hat{H}_{\Gamma_{\mathsf{res}}}. \tag{4.6}$$

Here $\hat{\sigma}_z$, $\hat{\sigma}^+$, $\hat{\sigma}^-$ are Pauli matrices for the effective atomic two level system consisting of ground state and first excited state with energy difference $\hbar\omega_{\mathsf{a,res}}$. $\hat{c}$ and $\hat{c}^\dagger$, on the other hand, are the operators of the cavity field with resonance frequency ω_{cav}. Cavity losses and the finite linewidth of the atomic transition are taken into account by $\hat{H}_\kappa$ and $\hat{H}_{\Gamma_{\mathsf{res}}}$ respectively. The coupling constant $g_0(x)$ along the cavity axis depends on the dipole matrix element of the atom in transverse direction, the atomic transition frequency $\omega_{\mathsf{a,res}}$, the cavity mode volume and the shape of the electromagnetic field inside the cavity. Experimentally, the maximum coupling strength g_0 is determined by a measurement of the Rabi frequency at the atomic resonance ($\Delta_{\mathsf{ca}} = \omega_{\mathsf{cav}} - \omega_{\mathsf{a,res}} = 0$). For large detuning ($|\Delta_{\mathsf{ca}}| \gg g_0, \Gamma_{\mathsf{res}}$), the atomic transitions are suppressed

and the effect of the atom-cavity coupling can be reduced to a shift of the resonance frequencies by $\omega_{\mathsf{cav}} \to \omega_{\mathsf{cav}} + \frac{g_0^2}{\Delta_{\mathsf{ca}}}$ and $\omega_{a,\mathsf{res}} \to \omega_{\mathsf{a,res}} - \frac{g_0^2}{\Delta_{\mathsf{ca}}}$. In the following we neglect the internal degrees of freedom of the atom and focus on its motion that is determined by the dipole force exerted by the cavity field. In doing so, we write down an effective Hamiltonian for the atom-cavity system

$$\hat{H} = \hbar\Big(\omega_{\mathsf{cav}} + \frac{g_0^2(\hat{\mathbf{x}}_a)}{\Delta_{\mathsf{ca}}}\Big)\hat{c}^\dagger\hat{c} + \frac{\hat{\mathbf{p}}_a^2}{2m_a} + \hat{H}_\kappa, \tag{4.7}$$

where we introduced the quantized position operator of the atom $\hat{\mathbf{x}}_a$ and the canonical momentum operator $\hat{\mathbf{p}}_a$, fulfilling the commutation relation $[\hat{\mathbf{x}}_a, \hat{\mathbf{p}}_a] = i\hbar$. This kind of coupling between the dynamics of an atom and the cavity field already resembles the optomechanical coupling that was discussed in the first chapters of this thesis. As we will see in the following section, the Hamiltonian (4.7) can be mapped exactly on the optomechanical Hamiltonian (4.14).

If we now assume the atom to be sitting inside a cavity, we can use the results of the preceding section to deduce the local dependence of the coupling parameter as $\frac{g_0^2(\mathbf{x})}{\Delta_{\mathsf{ca}}} \propto |E(\mathbf{x})|^2$. In view of equation (4.5), we see that

$$\frac{g_0^2(\mathbf{x})}{\Delta_{\mathsf{ca}}} = \frac{g_0^2}{\Delta_{\mathsf{ca}}}\sin^2(kx - kL)\exp(-\frac{y^2+z^2}{w_0^2}). \tag{4.8}$$

By using the result for the field of a cavity in the absence of an atom, we neglect the back-action of the atom on the field. However, for a large number of atoms strongly coupled to the cavity field, the shape of the cavity field will be modified due to the presence of the atoms. This can be most easily understood by modelling the cloud of atoms as a homogeneous medium with a refractive index $n' = 1 + \delta n$. We note that this back-action can lead to interesting dynamics, as for example shown in [34]. Still in the following considerations we will assume parameters for which δn will turn out to be small. We therefore keep the shape of the cavity intensity (4.5), that was derived in the absence of any atoms. Only the number of photons circulating inside the given cavity mode will vary in response to the atomic motion.

4.3 Recent experiments

Within the last year, two groups presented works that can be filed under the label "optomechanics with ultracold atoms". The basic idea behind the set-ups investigated in Berkeley [49, 32] and Zürich [33, 50] is to replace the cantilever of the conventional optomechanical systems by a gas of ultracold atoms inside a cavity. In both cases, a single mode of the atoms' collective dynamics couples to the cavity in a way that is analogous to the typical optomechanical coupling. As already mentioned at the end of chapter 2, these experiments are supposed to be far in the quantum regime.

In the Zürich setup, a Bose-condensed gas of around 10^5 atoms (^{87}Rb) is caught inside a high-finesse cavity by a crossed-beam dipole trap. The condensate stretches over a relatively wide volume given by the Thomas-Fermi radii $(R_x, R_y, R_z) = (3.3, 20.0, 3.5)\,\mu\mathrm{m}$, where the cavity axis is denoted by x. Once a weak, near-resonant pump laser is introduced into the cavity, the condensate couples to the standing wave of the cavity mode whose shape is given by $\sin^2(kx) = (1 - \cos(2kx))/2$. For the parameters of this setup, the condensate is only slightly perturbed by the cavity field and remains connected and continuous in shape. Excitations of the condensate occur primarily into the superposition of the $\pm 2\hbar k$ momentum modes. In view of the Bogoliubov spectrum (3.28), this corresponds to an excitation in the high-energy part of the dispersion relation

($k = 2\pi/\lambda_{\mathsf{exc}} > 1/\xi$ for the given parameters). Defining the annihilation and creation operators of this mode as $\hat{a}$ and $\hat{a}^\dagger$, the coupling term between the excitation mode and the cavity field can be shown to be of the form $\hbar g_{a,c}(\hat{a}^\dagger + \hat{a})\hat{c}^\dagger\hat{c}$. Thereby the basic optomechanical Hamiltonian is recovered. The quantum parameter ζ (1.3), that was introduced and discussed for a generic optomechanical setup in the first chapters of this thesis, can now readily be computed as $\zeta = x_{\mathsf{ZPF}}/x_{\mathsf{FWHM}} = g_{a,c}/\kappa$. For the given cavity decay rate $\kappa = 8.2\,\mathrm{MHz}$ it has a maximal value of $\zeta = 0.6$. This value is already in the regime where quantum effects should affect the system's dynamics substantially. We note that very recently the observation of bistable behaviour in this setup has been reported [50].

A considerably different regime is encountered in the experiments that are performed in the group of D. Stamper-Kurn at Berkeley. Again, a number of about 10^5 Rubidium atoms is confined inside a cavity. In this setup, though, they are trapped by a deep optical lattice. The optical lattice is produced by a strong laser that is off-resonant with the cavity mode. The atoms are spread over more than 300 lattice sites and are confined closely to the center of each trap. As the overlap between neighbouring fractions of the atomic cloud is small, they can be considered as independent. This case is referred to as the Lamb-Dicke regime or deep-lattice limit. We note that in contrast to [33], the Berkeley group has no evidence that the atoms remain in the condensed state, once loaded into the cavity. Nevertheless, the atoms are at ultra-low temperatures $T \approx 0.8\,\mu K$ and the atoms are in the ground state of motion in x-direction, as $\hbar\omega_{\mathsf{trap}} \gg k_B T$, where ω_{trap} is the frequency of the optical trap expanded around a single lattice site. It should also be possible to realize this experiment with a BEC in the near future. So far, the main results of this experiment are a quantification of the measurement back-action [32], i.e. the heating of the atoms due to the photon shot noise of the cavity, and the observation of bistable behaviour of the cavity line shape [49].

To explore the dynamics of the atoms in the Berkeley setup, a second, relatively weak laser beam of wave vector k_p along the cavity axis is introduced. According to (4.7) the coupling of this probe beam to the atoms is given by a term

$$\begin{aligned} \hbar\sum_i \frac{g_0^2(x_i)}{\Delta_{\mathsf{ca}}}\hat{c}^\dagger\hat{c} &= \hbar\sum_i \frac{g_0^2}{\Delta_{\mathsf{ca}}}\sin^2(k_p\bar{x}_i + k_p\delta x_i)\hat{c}^\dagger\hat{c} \\ &\simeq \hbar\sum_i \frac{g_0^2}{\Delta_{\mathsf{ca}}}\big(\sin^2(k_p\bar{x}_i) + k_p\delta x_i \sin(2k_p\bar{x}_i)\big), \end{aligned} \tag{4.9}$$

where the sum goes over all N atoms and transverse motion of the atoms is neglected. Accordingly, the position of a single atom is given by the coordinate x_i along the cavity axis. In the last step the dipole potential $\propto \sin^2(kx_i)$ was expanded for small deviations δx_i around the equilibrium position $\bar{x}_i$ of the the atom in the optical trap. This approximation is justified in the Lamb-Dicke regime, where $k\delta x_i \ll 1$. To grasp the analogy to the optomechanical Hamiltonian, a collective position variable is defined as

$$X = \frac{1}{N_{\mathsf{eff}}}\sum_i \delta x_i \sin(2k_p\bar{x}_i), \tag{4.10}$$

where $N_{\mathsf{eff}} = \sum_i \sin^2(2k_p\bar{x}_i)$. To arrive at a quantum version of the Hamiltonian the collective position variable X can be replaced by the operator $\hat{X} = X_{a,0}(\hat{a}^\dagger + \hat{a}) = \sqrt{\hbar/2N_{\mathsf{eff}}m_a\omega_{\mathsf{trap}}}(\hat{a}^\dagger + \hat{a})$ (see [48]). The corresponding momentum operator is given by $\hat{P} = (1/N_{\mathsf{eff}})\sum_i p_i \sin(2k_p\bar{x}_i)$,and $[\hat{X}, \hat{P}] = i\hbar$. Eventually the coupling term (4.9) can be rewritten as

$$\hbar(\Delta_N + g_{a,c}(\hat{a}^\dagger + \hat{a}))\hat{c}^\dagger\hat{c}. \tag{4.11}$$

Here $\Delta_N = \sum_i \frac{g_0^2}{\Delta_{\mathsf{ca}}} \sin^2(k_p \bar{x}_i)$ generates a shift of the cavity resonance, while the actual coupling between the collective mode and the cavity field is described by $g_{a,c} = k_p N_{\mathsf{eff}} X_{a,0} g_0^2 / \Delta_{\mathsf{ca}}$.

To characterize the coupling of the quantum fluctuations of the collective atomic mode and the optical field, Murch et al. introduced the so called granularity parameter. It compares the momentum that a single cavity photon transfers to the collective motion of the atoms to the zero-point uncertainty in the momentum of the atomic cloud. The granularity parameter is found to have the form

$$\epsilon = \frac{2 N_{\mathsf{eff}} g_0^2 k_p X_{a,0}}{\Delta_{\mathsf{ca}} \kappa}. \tag{4.12}$$

Up to a factor of 2 it is identical to the quantum parameter ζ, which is given by

$$\zeta = \frac{g_{a,c}}{\kappa} = \frac{\epsilon}{2}. \tag{4.13}$$

For the parameters of this setup ($g_0 \approx 9{\cdot}10^7\,\mathrm{Hz}$, $\Delta_{\mathsf{ca}} \approx 6{\cdot}10^{11}\,\mathrm{Hz}$, $X_{a,0} \approx 10^{-10}\,\mathrm{m}$, $k_p \approx 10^7\,\mathrm{m}^{-1}$, $N_{\mathsf{eff}} \approx 10^5\,\mathrm{Hz}$ and $\kappa \approx 4 \cdot 10^6\,\mathrm{Hz}$) the quantum parameter reaches a value of $\zeta \approx 0.3$.

Looking back at the discussion of chapter (2) where we analysed the dynamics of an optomechanical system in the quantum regime ($\zeta \sim 1$), we now have encountered analogous systems that have already reached such high values of the quantum parameter ζ. Therefore these experiments make up an ideal field for studying the effects of measurement back-action and quantum fluctuations or investigating basic features of optomechanical systems like cooling, bistability and self-induced oscillations in the quantum regime.

4.4 A cloud of atoms inside an optomechanical cavity

In this section we introduce a model setup in which both a cloud of cold atoms and a mechanical cantilever are coupled to a cavity field. It consists of a generic optomechanical setup, i.e. a cavity with a movable end mirror, and is extended by placing a Bose-condensed atomic gas inside the cavity. In a way our model is similar to the setups that we discussed in the previous section [32, 33], but comprises the additional feature of the cantilever. To describe the setup we will at first introduce a simplified model that allows us to get a first estimate of the coupling strengths between the the atomic motion, the cavity field and the cantilever. In section (4.7) we will compare these estimates to the results of a more realistic model that treats the dynamics of a cloud of cold atoms by means of the mean-field picture that was introduced in the previous chapter.

In this context we also want to mention recent studies that aim at coupling a mechanical oscillator to one or many atoms: These proposal involve the coupling of a mechanical element to ions [51] or dipolar molecules [52]. By employing an optomechanical cavity additionally, it has been proposed to observe atom-light-mirror entanglement [53, 54, 55, 56] or even perform a Bell measurement [54]. The magnetic coupling of a BEC to a nanomechanical resonator on an atom chip has been studied in [57]. In [31, 58, 59] the dynamics of a movable end mirror of an optomechanical cavity in the presence of a BEC were investigated. This study focused on the adiabatic limit where the motion of the mirror is very slow and the atoms and the cavity field adjust instantaneously to the position of the mirror.

4.4.1 The model

Our model consist of an optical cavity with a movable end mirror, the cantilever. A cloud of N ultracold atoms of mass m_a is placed inside the cavity in such a way that the atoms are confined

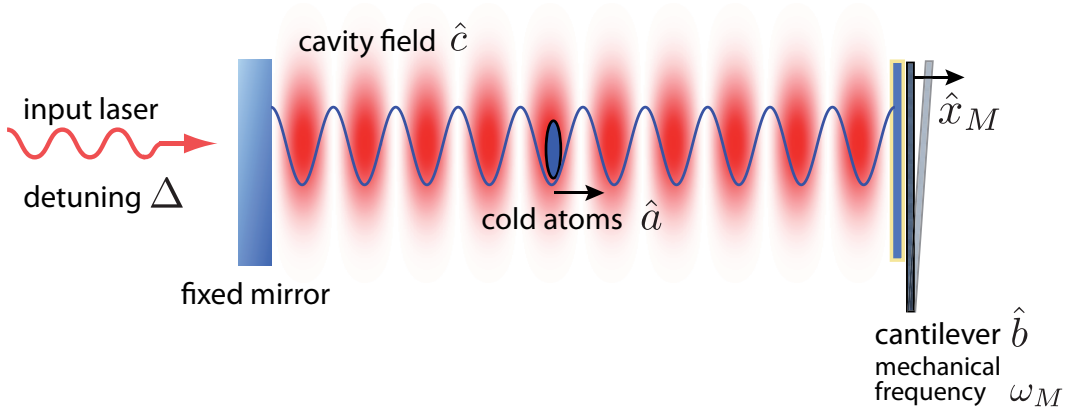

Figure 4.3: The basic model: A cloud of cold atoms is trapped in a single well of an optical lattice that is formed by the standing wave of a cavity. One of the cavity's end mirrors is allowed to oscillate. The dipole force acting on the atoms is proportional to the intensity inside the cavity. Subsequently, the atomic CM position is coupled to both the number of intracavity photons and the position of the cantilever that determines the length of the cavity.

closely to the center of a single lattice well (see figure 4.3). To treat the problem in the simplest possible manner, we neglect transverse motion and describe the dynamics of the atoms by using only their center-of-mass (CM) coordinate along the cavity axis, $\hat{x}_a$. Thereby we essentially replace the cloud of atoms by a 'super-atom' of mass Nm_a sitting at position $\hat{x}_a$.

In the rotating frame with respect to the laser frequency $\omega_L = \Delta + \omega_{\text{cav}}$, the Hamiltonian of this model is given by

$$\begin{aligned}\hat{H} &= \hbar\Big(-\Delta + g_M(\hat{b}+\hat{b}^\dagger) + N\frac{g_0^2}{\Delta_{\text{ca}}}\sin^2\left(k\hat{x}_a - k\hat{x}_M - kL\right)\Big)\hat{c}^\dagger\hat{c} \\ &+ \hbar\omega_M\hat{b}^\dagger\hat{b} + \hbar\alpha_L(\hat{c}+\hat{c}^\dagger) + \frac{1}{2Nm_a}\hat{p}_a^2 + \hat{V}_{\text{trap}} + \hat{H}_\kappa + \hat{H}_{\Gamma_M}. \end{aligned} \tag{4.14}$$

Here, the position and momentum operators of the 'super-atom' are denoted by $\hat{x}_a$ and $\hat{p}_a$. We introduced annihilation and creation operators of the cavity field ($\hat{c}$ and $\hat{c}^\dagger$) and the cantilever ($\hat{b}$ and $\hat{b}^\dagger$). The position operator of the cantilever is given by

$$\hat{x}_M = x_{\text{ZPF}}(\hat{b}^\dagger + \hat{b}) = \sqrt{\hbar/2m_M\omega_M}(\hat{b}^\dagger + \hat{b}), \tag{4.15}$$

where m_M is the mass of the cantilever and ω_M the eigenfrequency. $g_M = -\frac{\omega_{\text{cav}}}{L}x_{\text{ZPF}}$ takes account of the standard optomechanical coupling and α_L of the laser driving. The term $\hat{V}_{\text{trap}}$ denotes an additional external trapping potential. It might be used to shift the equilibrium position of the atoms and will be discussed in more detail below.

We assume the cavity field to be far off-resonant from the atomic resonance frequencies so that we can neglect internal transitions of the atoms. Typical values of this detuning $\Delta_{\text{ca}} = \omega_{\text{cav}} - \omega_{\text{a,res}}$ are a some hundred GHz or more. The detuning of the pump laser with respect to the cavity resonance ($\Delta = \omega_L - \omega_{\text{cav}}$), however, is supposed to be relatively small and in the range of some MHz. We can therefore resume the discussion of the atom-cavity coupling of section 4.2, thereby

neglecting the exact value of Δ when compared to Δ_{ca}. Note that this would not be possible for a far off resonant optical trap (FORT), that we will encounter in a later part.

The coupling of the atomic cloud to the optomechanical system is proportional to the intensity of the intracavity field (4.4). The spatial structure of the intracavity field evokes a coupling of the atomic coordinate to both the photon number and to the cantilever position as in

$$\hat{V}_{\mathsf{dip}} = \hbar N \frac{g_0^2}{\Delta_{\mathsf{ca}}} \sin^2\left(k\hat{x}_a - k\hat{x}_M - kL\right)\hat{c}^\dagger\hat{c} = U_0 N \sin^2\left(k\hat{x}_a - k\hat{x}_M - kL\right)\hat{c}^\dagger\hat{c}. \tag{4.16}$$

We will assume a negative value of Δ_{ca}, i.e. a red-detuned laser frequency with respect to the atomic transition frequency. In that case the atoms are attracted by regions of high intensity.

The coupling between the atomic CM coordinate $\hat{x}_a$ and the cantilever position $\hat{x}_M$, that is induced by the dipole potential $\hat{V}_{\mathsf{dip}}$, can be understood by the following observation: A change of the cavity length ($L \to L + \langle\hat{x}_M\rangle$) shifts the positions of the antinodes of the intracavity field that in turn determine the position of the atomic cloud. We will refer to this coupling term as the direct coupling between the cantilever and the atomic cloud and denote the corresponding coupling constant by $g_{a,M}$.

4.4.2 Estimate of the system parameters

We find it instructive to give an estimate of the values of the parameters that were introduced so far. The numbers of this estimate will be used in the subsequent sections where we continue the investigation of our model setup.

The trapping frequency ω_a can reach values of a few hundreds of kHz. For example in the experiments at Berkeley [32], a far off-resonant optical dipole trap with a frequency of $2\pi \cdot 50\,\mathrm{kHz}$ is used. For our estimates we use $\omega_{\mathsf{trap}} = 10^5\,\mathrm{Hz}$. and discuss possible implementations later. In state-of-the-art experiments with Rb atoms a number of up to $N \approx 10^5$ atoms can be trapped. We assume all N atoms to be confined to a single lattice site. This certainly is an experimental challenge: In the Berkeley setup the atoms were distributed over about 300 lattice sites, for example. However, using additional trapping potentials or integrating micro-fabricated atom-chips [60] should make strong confinement of the atoms possible . We note, that if either the trapping frequency or the number of atoms is increased, the losses due to atomic collisions will get substantially larger. Therefore these quantities are practically limited to the assumed values.

The coupling of the atoms to the cavity field is given by the parameter $U_0/\hbar = g_0^2/\Delta_{\mathsf{ca}}$. The numbers found in the Berkeley setup [32] are $g_0 \approx 2\pi \cdot 15\,\mathrm{MHz}$ and $\Delta_{\mathsf{ca}} \approx 2\pi \cdot 100\,\mathrm{GHz}$, or $U_0 \approx \hbar \cdot 10^4\,Hz$. For reasons that will become apparent later, we assume a value of $U_0 = \hbar \cdot 10^2\,\mathrm{Hz}$. On the other hand, we assume an average number of cavity photons of $|\bar{c}|^2 = 100$, considerably higher than low photon number of the Berkeley setup, where $|\bar{c}|^2 \approx 1$. The dipole forces on the atomic cloud are proportional to $U_0|\bar{c}|^2$ and their value in our assumptions is hence comparable to the one in [32]. For the cavity decay rate we assume a value $\kappa \approx 10^6 s^{-1}$ which is about the value encountered in [32]. Note that generic optomechanical systems that involve a movable end-mirror typically have cavity decay rates that are of the order of $10^7\,\mathrm{Hz}$. We will comment on this point below.

State-of-the-art micromechanical resonators can reach eigenfrequencies of hundreds of kHz or even a few MHz [10, 11, 12] and Q-factors ($Q = \omega_M/\Gamma_M$) between 10^4 and 10^5. We assume a value of $\omega_M \approx 10^5\mathrm{Hz}$ that is of the same order as the atomic CM oscillation frequency ω_a, and a damping rate of $\Gamma_M \approx 1\,Hz$. The masses of the mechanical resonators realized in the relevant experiments vary strongly in their value: The doubly clamped beam in the setup at the LKB

[10] has an eigenfrequency of a few MHz, but its mass is rather large ($m_M \approx 10^{-7}\mathrm{kg}$). In the Bouwmeester group, on the other hand, a cantilever with an attached mirrors is used [11]. The total mass of the resonator ($\omega_M \approx 10\,\mathrm{kHz}$) is $m_M \approx 10^{-11}\mathrm{kg}$. The values for the doubly clamped beam in the Vienna setup [12] are somewhat in between: $\omega_M \approx 2\,\mathrm{MHz}$ and $m_M \approx 4 \cdot 10^{-10}\,\mathrm{kg}$. In view of all these numbers from recent experiments, we assume a mass of $m_M \approx 10^{-10}\,\mathrm{kg}$ for the cantilever in our model. The coupling between cantilever and cavity due to the radiation pressure is determined by the parameter $g_M = -\omega_{\mathsf{cav}} x_{\mathsf{ZPF}}/L$, where ω_{cav} denotes the cavity frequency, L the cavity length and x_{ZPF} the zero-point amplitude of the cantilever. The cavities used in [10, 11, 12] are a few millimeters long. For $L \approx 10^{-3}\,\mathrm{m}$, $x_{\mathsf{ZPF}} = \sqrt{\hbar/2m_M\omega_M} \approx 3 \cdot 10^{-15}\mathrm{m}$ and $\omega_{\mathsf{cav}} \approx 10^{15}\mathrm{Hz}$, the optomechanical coupling is $g_M \approx 10^3\mathrm{Hz}$.

The parameters of our model setup and the corresponding estimates are summarized in Table (4.1). We will refer to this table throughout the subsequent parts of this thesis.

4.5 Coupling constants of the linearized model

In this section we will linearize the basic Hamiltonian of our model setup and discuss the various forms of coupling between the atomic CM mode, the cantilever and the cavity field. At first we will consider the system without an additional trapping potential. In that case the equilibrium position of the atomic cloud is simply given by an antinode of the cavity field. As a consequence the interaction between the atomic motion and the cavity field contains no linear contributions and does not show up in this consideration. Non-vanishing coupling between the atomic cloud and the cavity in this picture can be achieved by a proper external potential that shifts the equilibrium position of the atoms away from a single antinode. We will present the expressions for the coupling constants and frequency shifts of the linearized system and give an estimate of their values.

4.5.1 In the absence of an external trapping potential

In the absence of an external trapping potential, the dipole potential (4.16) is the only source for a trapping of the atoms. The atomic cloud will then have an equilibrium position that is given by the minimum of the dipole potential. We assume the atoms to be "high-field seekers" ($\omega_L - \omega_{\mathrm{a,res}} < 0$), i.e. they are attracted to regions of high intensity. As a consequence, the equilibrium position $\langle \hat{x}_a \rangle = \bar{x}_a$ lies at a local maximum of the electromagnetic field intensity, i.e. $k(\bar{x}_a - \bar{x}_M - L) = (2n+1) \cdot \pi/2$, $n \,\epsilon\, \mathbb{Z}$. Here we already introduced the equilibrium positions of the cantilever ($\bar{x}_M$) and of the atomic CM position ($\bar{x}_a$). The equilibrium position of the cavity field ($\hat{c}$) is denoted by $\bar{c}$. We can now shift the operators $\hat{x}_a$, $\hat{x}_M$ and $\hat{c}$ by their respective steady state solutions:

$$\begin{aligned} \hat{c} &= \bar{c} + \delta\hat{c} \\ \hat{x}_M = \bar{x}_M + \delta\hat{x}_M &= \sqrt{\hbar/2m\omega_M}(\bar{b} + \delta\hat{b}) + h.c. = \bar{x}_M + x_{\mathsf{ZPF}}(\delta\hat{b}^\dagger + \delta\hat{b}) \\ \hat{x}_a &= \bar{x}_a + \delta\hat{x}_a \end{aligned} \tag{4.17}$$

Accordingly, the dipole interaction term the dipole interaction term reduces to

$$\hat{V}_{\mathsf{dip}} = U_0 N \sin^2\!\left(\frac{\pi}{2} + k\delta\hat{x}_a - k\delta\hat{x}_M\right)(\bar{c} + \delta\hat{c})(\bar{c}^* + \delta\hat{c}^\dagger). \tag{4.18}$$

ω_a	CM oscillation frequency of atomic cloud	$10^5\,\mathrm{Hz}$
$\lvert\bar{c}\rvert^2$	average photon number in the cavity	100
$\frac{g_0^2}{\Delta_{\mathsf{ca}}} = \frac{U_0}{\hbar}$	atom-cavity coupling	$-10^3\,\mathrm{Hz}$
$\omega_{\mathrm{dip}} = \sqrt{2U_0k^2\lvert\bar{c}\rvert^2/m_a}$	strength of the dipole potential	$3\cdot10^4\,\mathrm{Hz}$
N	number of atoms	10^5
m_a	mass of a single atom	$10^{-25}\,\mathrm{kg}$
$x_{a,0}^{(N)} = \sqrt{\hbar/2Nm_a\omega_a}$	zero-point width of the CM oscillation	$10^{-10}\,\mathrm{m}$
ω_M	frequency of the cantilever	$10^5\,\mathrm{Hz}$
m_M	mass of the cantilever	$10^{-10}\,\mathrm{kg}$
$x_{\mathsf{ZPF}} = \sqrt{\hbar/2m_M\omega_M}$	zero-point width of the cantilever	$2\cdot10^{-15}\,\mathrm{m}$
Γ_M	damping rate of the cantilever motion	$1\,\mathrm{Hz} = 10^{-5}\,\omega_M$
ω_{cav}	cavity resonance frequency	$10^{15}\,\mathrm{Hz}$
L	cavity length	$10^3\lambda_L \approx 10^{-3}\,\mathrm{m}$
$g_M = -\frac{\omega_{\mathsf{cav}}}{L}x_{\mathsf{ZPF}}$	cantilever-cavity coupling	$10^3\,\mathrm{Hz}$
κ	cavity decay rate	$10^6\,\mathrm{Hz}$

Table 4.1: Assumed parameters for the model of figure (4.3): The estimates on the mechanical properties of the atomic cloud are based on the experiments in Berkeley [32] and Zürich [33]. The assumed properties of the cantilever are in the range of those reached in basic optomechanical setups [10, 11, 12]. The discussion of these parameters can be found in section 4.4, only the definition of ω_{dip}, the strength of the dipole potential, is given in section 4.5. Note that the estimate of the center of mass oscillation frequency ω_a refers to the case, when an additional trapping potential $\hat{V}_{\mathsf{trap}}$ is present.

In the linearized model, the motional excursions of both the cantilever and the atomic cloud are assumed to be small, i.e. $k\sqrt{\langle\delta\hat{x}_M^2\rangle} \ll 1$ and $k\sqrt{\langle\delta\hat{x}_a^2\rangle} \ll 1$. Under these two assumptions, we can approximate the dipole potential (4.18) around a minimum and arrive at

$$\hat{V}_{\mathsf{dip}} \simeq U_0 N(1-(k\delta\hat{x}_a - k\delta\hat{x}_M)^2)(\bar{c}+\delta\hat{c})(\bar{c}^*+\delta\hat{c}^\dagger). \tag{4.19}$$

Let us now discuss the contributions of this expression step by step:

The term quadratic in $\delta\hat{x}_a^2$ takes account of the harmonic confinement of the atoms in the dipole potential of the cavity field:

$$\hat{V}_{\mathsf{dip}} = \frac{Nm_a}{2}\omega_{\mathsf{dip}}^2\delta\hat{x}_a^2, \tag{4.20}$$

where the trapping frequency of the dipole potential is given by

$$\omega_{\mathrm{dip}}^2 \;=\; 2|U_0|k^2|\bar{c}|^2/m_a. \tag{4.21}$$

The validity of the harmonic approximation of the dipole potential is based on the tight confinement of the atomic cloud around its equilibrium position, i.e. $k\sqrt{\langle\delta\hat{x}_a^2\rangle} \ll 1$. This regime is referred to as the Lamb-Dicke regime in atomic physics. As the cloud of atoms is only subject to the harmonic potential of equation (4.20), its CM oscillation frequency ω_a is given by the frequency of the dipole potential, ω_{dip}. We can attribute a zero-point amplitude to the CM motion of the atomic cloud. $x_{a,0}^{(N)} = \sqrt{\hbar/2Nm_a\omega_a}$. The position operator of the "super-atom" can be expressed in terms of the annihilation and creation operators, $\hat{a}$ and $\hat{a}^\dagger$, as $\hat{x}_a = x_{a,0}^{(N)}(\hat{a}^\dagger+\hat{a})$.

For the parameters of the estimate given above (see table 4.1), the frequency of the dipole potential has a value of $\omega_{\mathrm{dip}} \approx 3\cdot 10^4\,\mathrm{Hz}$. Note that the dipole frequency is a useful quantity, even in the presence of an additional external potential. In that case it does no longer determine the CM oscillation frequency ω_a of the atomic cloud. Still the coupling constants will depend on the ratio $\omega_a/\omega_{\mathsf{dip}}$, as we will see below.

Next we examine the the term quadratic in $\delta\hat{x}_M^2$,

$$-U_0Nk^2|\bar{c}|^2\delta\hat{x}_M^2 =: \frac{\hbar\delta\omega_{M,c}}{x_{\mathsf{ZPF}}^2}\delta\hat{x}_M^2, \tag{4.22}$$

It yields a shift of the cantilever frequency due to the presence of the atoms and additionally produces terms of the form $\delta\hat{b}^2 + h.c.$, i.e. terms that involve the annihilation (creation) of two cantilever phonons at the same time.

The coupling between the atomic cloud and the cantilever is taken account of by the term

$$U_0Nk^2|\bar{c}|^2\delta\hat{x}_a\delta\hat{x}_M =: \hbar g_{a,M}(\delta\hat{a}^\dagger+\delta\hat{a})(\delta\hat{b}^\dagger+\delta\hat{b}), \tag{4.23}$$

where we introduced $g_{a,M} = Nk^2|\bar{c}|^2x_{a,0}^{(N)}x_{\mathsf{ZPF}}U_0/\hbar$. We will refer to this term as the direct coupling between the cantilever and the atomic motion. Note that the coupling constant is proportional to the square root of the number of atoms, as $x_{a,0}^{(N)} \propto 1/\sqrt{N}$. This is exactly the direct coupling between the cantilever and the atomic motion that we already discussed above.

Finally, the term $U_0N\delta\hat{c}\delta\hat{c}^\dagger$ corresponds to a shift of the cavity resonance due to the presence of the atoms at the antinodes. Note that it would be absent for if the atoms were "low-field seekers" .

All terms of higher than quadratic order in $\delta\hat{x}_a$, $\delta\hat{x}_M$, $\delta\hat{c}$ and $\delta\hat{c}^\dagger$, are neglected in this approach. Therefore no coupling between the atomic cloud and the cavity field appears in this linearized system.

We can complete the linearization procedure by inserting the operators in the form of equations (4.17) into all parts of the Hamiltonian (4.14) and arrive at

$$\begin{aligned}\hat{H} &= -\hbar\Delta\delta\hat{c}^\dagger\delta\hat{c} \\ &+ \hbar\omega_M\delta\hat{b}^\dagger\delta\hat{b} + \hbar\omega_a\delta\hat{a}^\dagger\delta\hat{a} \\ &+ \hbar\delta\omega_{M,c}(2\delta\hat{b}^\dagger\delta\hat{b} + \delta\hat{b}^2 + \delta\hat{b}^{\dagger 2}) \\ &+ \hbar g_{a,M}(\delta\hat{a} + \delta\hat{a}^\dagger)\delta\hat{b} + h.c. \\ &+ \hbar g_M\bar{c}^*(\delta\hat{b} + \delta\hat{b}^\dagger)\delta\hat{c} + h.c.. \end{aligned} \tag{4.24}$$

The first two lines of this expression comprise the basic contributions of the harmonic oscillators, i.e. the driven cavity, the cantilever and the atomic CM motion. The frequency shift of the cantilever and the two-phonon processes are contained in the third line. The last two lines finally present the direct coupling between the atomic motion and the cantilever, and the basic optomechanical coupling of the cantilever and the coupling via radiation pressure.

Note that we rescaled the detuning parameter $\Delta \to \Delta - \frac{g_0^2}{\Delta_{\mathsf{ca}}}N - g_M\bar{x}_M/x_{\mathsf{ZPF}}$ in order to include the static shift of the cavity resonance due to the presence of the atoms and the equilibrium position of the cantilever.

The definitions of the parameters are given in table (4.2) and the scheme of figure (4.4) illustrates the coupling mechanisms of this Hamiltonian.

To assess the strength of the relevant constants in this model, we turn towards the assumed values of table (4.1) again. The direct coupling between atoms and cantilever, $g_{a,M}$, can be rewritten as $g_{a,M} = (\omega_a/2)\sqrt{Nm_a\omega_a/m_M\omega_M}$. Its strength is therefore limited by the ratio between the mass of the atomic cloud, Nm_a, and the mass of the cantilever m_M. We see that the ratio of the direct coupling term and the atomic CM oscillation frequency is given by $g_{a,M}/\omega_a \approx \sqrt{Nm_a\omega_a/m_M\omega_M} \approx 10^{-5}$ for realistic parameters. This shows that the huge difference in mass impedes a strong direct coupling between the between the atomic cloud ($\sim 10^{-20}\,\mathrm{kg}$)

$\omega_a = \sqrt{2\lvert U_0\rvert k^2\lvert\bar{c}\rvert^2/m_a}$	$3\cdot 10^4\,\mathrm{Hz}$
$g_M = -\frac{\omega_{cav}}{L}x_{\mathsf{ZPF}}$	$10^3\,\mathrm{Hz}$
$g_{a,M} = \frac{\omega_a}{2}\sqrt{\frac{Nm_a\omega_a}{m_M\omega_M}}$	$10^{-1}\,\mathrm{Hz}$
$\Delta_N = N\frac{g_0^2}{\Delta_{\mathsf{ca}}}$	$10^7\,\mathrm{Hz}$
$\delta\omega_{M,c} = -Nk^2x_{\mathsf{ZPF}}^2\lvert\bar{c}\rvert^2U_0/\hbar$	$10^{-7}\,\mathrm{Hz}$

Table 4.2: Definition of the coupling constants and frequency shifts that appear in the Hamiltonian (4.24): The CM oscillation frequency ω_a, the coupling between the cantilever and the cavity via radiation pressure g_M, the direct coupling between the cantilever and the atomic motion $g_{a,M}$, and finally the frequency shifts of the both the cavity resonance (Δ_N) and of the cantilever ($\delta\omega_{M,c}$) due to the presence of the atoms. The estimates on the right-hand side are based on the values of table (4.1).

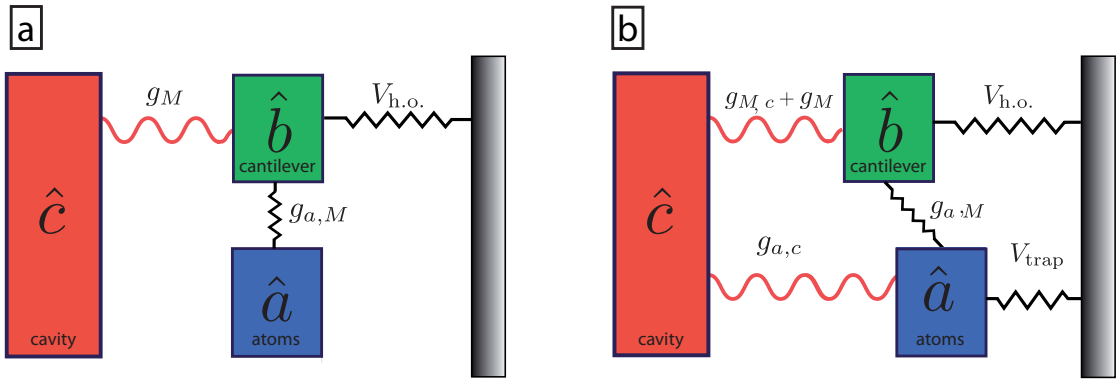

Figure 4.4: Scheme of the coupling mechanisms in a linearized version of the proposed setup (4.3). (a) If the atoms are located around the local minimum of the dipole potential $\hat{V}_{\mathrm{dip}}$, no coupling between the atoms' collective mode ($\hat{a}$) and the cavity field ($\hat{c}$) appears in the Hamiltonian (4.24). Nevertheless, the atomic CM position is linearly coupled to the position of the cantilever ($\hat{b}$) with a coupling strength given by $g_{a,M}$. The cantilever itself is subject to both the harmonic force due to its suspension ($V_{h.o.}$) and the radiation pressure $\propto \hat{c}^\dagger\hat{c}$. The latter results in a cavity-cantilever coupling constant $g_M = -\frac{\omega_{\mathrm{cav}}}{L}x_{\mathrm{ZPF}}$. (b) In the presence of an additional trapping potential (V_{trap}), the atoms' equilibrium position is shifted. Subsequently, a coupling term between the atoms and the cavity field appears in the Hamiltonian (4.28). The cavity-cantilever coupling gets an additional contribution $g_{M,c}$ due to the presence of the atoms.

and the cantilever ($\sim 10^{-10}\,\mathrm{kg}$). The coupling constant $g_{a,M}$ has a value that is about a tenth of the cantilever damping Γ_M rate that we assumed in table 4.1.

The shift of the cavity frequency due to the atoms, $\Delta_N \approx N\frac{g^2}{\Delta_{\mathrm{ca}}}$, can be estimated to be $\Delta_N \approx 10^7\,\mathrm{Hz}$. Δ_N can be converted into a shift of the refractive index, δn by noting that

$$\frac{\Delta_N}{\omega_{\mathrm{cav}}} = \frac{\int \delta n(\mathbf{x})|E(\mathbf{x})|^2 d^3\mathbf{x}}{\int |E(\mathbf{x})|^2 d^3\mathbf{x}}. \tag{4.25}$$

To get a rough estimate we assume that the atoms form a homogeneous medium and spread over a volume of $V \approx w_0^2 x_{a,0}$, where w_0 is the waist of the Gaussian beam and $x_{a,0}$ denotes the zero-point width of a single atom, $x_{a,0} = \sqrt{\hbar/2m_a\omega_a}$. If the cavity mode volume is given by $V_{\mathrm{cav}} \approx w_0^2 L$, equation (4.25) yields $\frac{\Delta_N}{\omega_{\mathrm{cav}}} \approx \delta n \frac{V}{V_{\mathrm{cav}}}$ or $\delta n \approx \frac{L}{x_{a,0}}\frac{\Delta_N}{\omega_{\mathrm{cav}}} \approx 10^{-4}$. Accordingly, the influence of the atoms on the shape of the cavity field is small. This proves the assumption of section (4.2) right where we used the intensity profile of the empty cavity to determine the spatial structure of the cavity-atom coupling $\frac{g_0^2(\mathbf{x})}{\Delta_{\mathrm{ca}}}$.
The shift of the cantilever frequency due to its coupling to the atoms is vanishingly small: $\delta\omega_{M,c} \approx 10^{-7}\mathrm{Hz}$ for the chosen parameters. However, there appears another, stronger frequency shift, $\delta\omega_M = g_M^2|\bar{c}|^2(\frac{1}{\omega_M+\Delta} - \frac{1}{\omega_M-\Delta})$, that stems from the coupling between the cantilever and the cavity. This contribution is commonly referred to as the optical spring and we will derive the expression for $\delta\omega_M$ via second order perturbation theory in section (4.6).

We have seen that in the linearized system without an additional trapping, the atomic motion couples only to the cantilever. This coupling, denoted by $g_{a,M}$, is rather weak, though. The coupling between the atomic motion and the cavity is of higher order and does not appear in this approach. However, this type of coupling might be exploited to measure the Fock states of the

atomic CM mode, which we will discuss in section (4.9).

4.5.2 With an external trapping potential

To achieve non-vanishing coupling between the atoms and the cavity field in the linearized Hamiltonian we have to consider an additional trapping potential $\hat{V}_{\text{trap}}$. It is introduced in order to shift the atomic cloud to a new equilibrium position, a distance $\tilde{x}_a$ away from a minimum of $\hat{V}_{\text{dip}}$. We leave the question of possible implementations to a subsequent discussion and assume for the moment that the atoms gather around $\bar{x}_a$ as they are trapped in an effective potential given by $\hat{V}_{\text{eff}} = \hat{V}_{\text{dip}} + \hat{V}_{\text{trap}}$. We approximate the effective potential locally as

$$\hat{V}_{\text{eff}} \approx \frac{N m_a}{2} \omega_a \delta\hat{x}_a^2, \tag{4.26}$$

where we shifted the atomic CM position operator by the new equilibrium position ($\hat{x}_a = \bar{x}_a + \delta\hat{x}_a$). The dipole interaction term takes the form of

$$\begin{aligned} \hat{V}_{\text{dip}} &= NU_0 \sin^2(\frac{\pi}{2} + \tilde{x}_a + k\delta\hat{x}_a - k\delta\hat{x}_M)(\bar{c} + \delta\hat{c})(\bar{c}^* + \delta\hat{c}^\dagger) \\ &\approx NU_0\big(\cos^2(k\tilde{x}_a) - \sin(2k\tilde{x}_a)(k\delta\hat{x}_a - k\delta\hat{x}_M) \\ &\quad - \cos(2k\bar{x}_a)(k\delta\hat{x}_a - k\delta\hat{x}_M)^2\big)(\bar{c} + \delta\hat{c})(\bar{c}^* + \delta\hat{c}^\dagger). \end{aligned} \tag{4.27}$$

This expression explicitly depends on the shift $\tilde{x}_a$ of the atomic CM equilibrium position away from an antinode of the cavity field.

The linearized Hamiltonian - again we consider terms up to second order in the expansion (4.17) - is given by

$$\begin{aligned} \hat{H} &= -\hbar\Delta\delta\hat{c}^\dagger\delta\hat{c} \\ &+ \hbar\omega_M\delta\hat{b}^\dagger\delta\hat{b} + \hbar\omega_a\delta\hat{a}^\dagger\delta\hat{a} \\ &+ \hbar\delta\omega_{M,c}(2\delta\hat{b}^\dagger\delta\hat{b} + \delta\hat{b}^2 + \delta\hat{b}^{\dagger 2}) \\ &+ \hbar g_{a,c}\bar{c}^*(\delta\hat{a} + \delta\hat{a}^\dagger)\delta\hat{c} + h.c. \\ &+ \hbar(g_{M,c} + g_M)\bar{c}^*(\delta\hat{b} + \delta\hat{b}^\dagger)\delta\hat{c} + h.c. \\ &+ \hbar g_{a,M}(\delta\hat{a} + \delta\hat{a}^\dagger)\delta\hat{b} + h.c.\,. \end{aligned} \tag{4.28}$$

Note that again we shifted the detuning parameter : $\Delta \to \Delta - NU_0\cos^2(2k\tilde{x}_a) - g_M\bar{x}_M/x_{\text{ZPF}}$.

In contrast to the previous form of the linearized Hamiltonian, (4.19), we observe a coupling of both the cantilever position $\delta\hat{x}_M$ and the atomic CM coordinate $\delta\hat{x}_a$ to the cavity field. The interaction terms depend on the strength of the shift $\tilde{x}_a$ and appear in the Hamiltonian as

$$g_{M,c}(\delta\hat{b}^\dagger + \delta\hat{b})(\bar{c}\delta\hat{c}^\dagger + \bar{c}^*\delta\hat{c}) \tag{4.29}$$

and

$$g_{a,c}(\delta\hat{a}^\dagger + \delta\hat{a})(\bar{c}\delta\hat{c}^\dagger + \bar{c}^*\delta\hat{c}). \tag{4.30}$$

A scheme of the couplings involved in the Hamiltonian (4.28) is given in figure (4.4).

Before we can give estimates on these coupling constants, we have to take a closer look at the effective potential $\hat{V}_{\text{eff}}$ for the atomic motion, that is the superposition of the dipole potential

and an additional trapping potential $\hat{V}_{\text{trap}}$. The latter could for example be realized by a far off-resonant optical trap, as it was implemented in the Berkeley setup [32]. Such traps can yield trapping frequencies around a single lattice site of more than $10^5\,\text{Hz}$. Accordingly, the frequency of the effective potential would then reach a value of the same order. Hence we can assume the atomic CM motion in the effective potential to have an oscillation frequency of $\omega_a = 10^5\,\text{Hz}$.

If the trapping potential is realized by using an optical lattice, there is also the following caveat: If the trapping laser is injected along the cavity axis, it will also couple to the cantilever. To avoid possible complications and compensation effects, the trapping laser beam should therefore be inclined with respect to the cavity axis.

Of course one could also think of other trapping mechanisms, like strong magnetic fields. For the purpose of the following considerations we do not have to specify the particular implementation of the trapping potential. It does not take part in the dynamics of the system and we only employ it to yield a large frequency for the atomic CM oscillation and to shift the atomic cloud away from an antinode of the cavity field.

Using the estimates of table (4.1) once again, we find that the coupling between the atomic CM mode and the cavity can reach a value of $\sin(2k\tilde{x}_a)10^4\,Hz$. The interaction between the cantilever and the cavity is dominated by the radiation pressure term since $g_M \approx 10^3\,Hz$ is larger than $g_{M,c} \approx \sin(2k\tilde{x}_a)10^{-1}\,Hz$. We note that the effect of the atoms on the overall cavity-cantilever coupling constant $g_M + g_{M,c}$ will be to either increase (for $\tilde{x}_a > 0$) or decrease (for $\tilde{x}_a < 0$) its absolute value. The atomic cloud and the cantilever interact rather weakly at a rate of $g_{a,M} = 2N(U_0/\hbar)\cos(2k\tilde{x}_a)k^2 x_{\text{ZPF}} x_{a,0}^{(N)} |\bar{c}|^2$ of about $10^{-1}\,Hz$. In table (4.3) we give an overview of the coefficients involved in the Hamiltonian (4.28) and add estimates for $\sin(2k\tilde{x}_a) \approx 10^{-1}$.

As we have seen in this section, the simple model of figure (4.3) allows for a coupling between the cantilever and the atoms' CM position. The corresponding coupling constant $g_{a,M}$ has a relatively low value of $10^{-1}\,Hz$, as it is limited by the ratio of the masses of the atomic cloud and the cantilever. An additional trapping potential enriches the capabilities of the setup. The atomic motion is coupled to the cavity with a relatively large coupling constant $g_{a,c} \approx 10^3\,\text{Hz}$.

$g_{a,M} = \frac{\omega_a}{2}\cos(2k\bar{x}_a)\frac{\omega_{\text{dip}}^2}{\omega_a^2}\sqrt{\frac{Nm_a\omega_a}{m_M\omega_M}}$	$10^{-1}\,Hz$
$g_{a,c} = -N(U_0/\hbar)\sin(2k\tilde{x}_a)kx_{a,0}^{(N)}$	$10^3\,Hz$
$g_{M,c} = N(U_0/\hbar)\sin(2k\tilde{x}_a)kx_{\text{ZPF}}$	$10^{-2}\,Hz$
$g_M = -\frac{\omega_{cav}}{L}x_{\text{ZPF}}$	$10^3\,Hz$
$\delta\omega_{M,c} = -U_0Nk^2x_{\text{ZPF}}^2\|\bar{c}\|^2/\hbar$	$10^{-7}\,\text{Hz}$

Table 4.3: Parameters of the Hamiltonian (4.28) for the case of an additional trapping potential $\hat{V}_{\text{trap}}$: The superposition of $\hat{V}_{\text{trap}}$ and $\hat{V}_{\text{dip}}$ forms an effective potential $V_{\text{eff}} = \frac{Nm_a}{2}\tilde{\omega}_a(\hat{x}_a - \tilde{x}_a)^2$. For the estimates in the right column we assumed $\sin(2k\tilde{x}_a) \approx 10^{-1}$ and refer to the parameters of table (4.1). We note that the value of $\tilde{x}_a$ can be varied over a wide range, depending on the particular implementation of $\hat{V}_{\text{trap}}$.

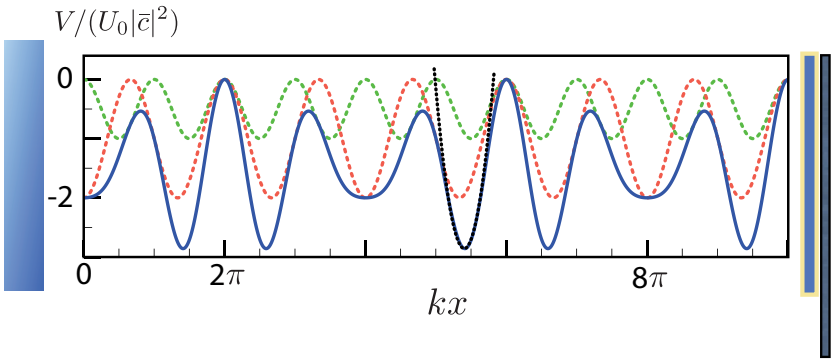

Figure 4.5: The superposition of the dipole potential $\hat{V}_{\text{dip}}$ (green dotted line) and an external trapping potential $\hat{V}_{\text{trap}} = U_{\text{trap}} \sin^2(k_{\text{trap}}\hat{x}_a - k_{\text{trap}}L)$. (red dotted line) in form of an optical lattice. The effective potential $\hat{V}_{\text{eff}}$ (blue solid line) can be approximated locally as a harmonic potential that shifts the equilibrium position of the atomic cloud away from an antinode of the cavity field. This enhances the coupling of the atomic CM coordinate to the cavity. The parameters of this plot are $k_{\text{trap}}/k = 0.75$, $U_{\text{trap}}/(U_0|\bar{c}|^2) = 2$ and $kL = 10\pi$.

4.6 Cavity-assisted coupling of atoms and cantilever

In the preceding section we encountered the direct coupling of the atom's center-of-mass motion and the cantilever. This coupling originates from the term $NU_0 \sin^2(k\hat{x}_a - k\hat{x}_M - \Phi(\Delta))\,\hat{c}^\dagger\hat{c}$ of the basic Hamiltonian (4.14) and leads to the coupling term $\hbar g_{a,M}(\delta\hat{a} + \delta\hat{a}^\dagger)(\delta\hat{b} + \delta\hat{b}^\dagger)$ in the linearized Hamiltonian (4.24). Here we will focus on a different type of coupling between atoms and cantilever that is mediated by the cavity field. An exchange of phonons of the atoms' CM mode and the cantilever can be realized with the assistance of intermediate transitions that involve the creation or annihilation of a cavity photon. These processes can be included by a term of the form $\hbar g_{\text{eff}}\delta\hat{a}\delta\hat{b}^\dagger + h.c.$ in an effective Hamiltonian that comprises the cantilever and the CM mode only. Even though this coupling is second order in the original coupling parameters, we will see that g_{eff} can be orders of magnitude larger than the direct coupling $g_{a,M}$.

At the end of this section we will discuss the relevance of the second-order coupling to our model setup. We will state, that the cavity-assisted coupling will exceed the direct coupling between the cantilever and the atomic motion highly.

4.6.1 Linearized Equations of Motion and Susceptibility

In the first approach we will consider a system in which both the cantilever and the atomic cloud are coupled to the cavity mode, but do not interact directly. We will calculate the response of the system to a test force, i.e. we will evaluate the linear susceptibilities. This result will then be compared to the susceptibility of a reduced system that contains only the cantilever and the atomic CM which are directly coupled to each other. By this comparison we can identify the effective, cavity-assisted coupling constant g_{eff} between the cantilever and the atomic motion.

To start with, we will solve the linearized classical equations of motion of the following system: We consider the center-of-mass mode of an atomic cloud ($\hat{a}$, ω_a, Γ_a) and a mechanical oscillator ($\hat{b}$, ω_M, Γ_M), which are both coupled to a cavity light mode ($\hat{c}$, ω_{cav}, κ). The Hamiltonian in a frame rotating at the laser frequency $\omega_L = \omega_{\text{cav}} + \Delta$ is given by:

$$\begin{aligned}\hat{H} &= \hbar(-\Delta + g_a(\hat{a}+\hat{a}^\dagger) + g_M(\hat{b}+\hat{b}^\dagger))\hat{c}^\dagger\hat{c} + \hbar\omega_a\hat{a}^\dagger\hat{a} + \hbar\omega_M\hat{b}^\dagger\hat{b} \\ &\quad +\hbar\alpha_L(\hat{c}+\hat{c}^\dagger) + \hat{H}_\kappa + \hat{H}_{\Gamma_M} + \hat{H}_{\Gamma_a}. \end{aligned} \tag{4.31}$$

The corresponding classical equations of motions are

$$\begin{aligned}\dot{c} &= (i(\Delta - \frac{\kappa}{2})c - i\alpha_L \\ \ddot{x}_a &= -\omega_a^2 x_a - \Gamma_a\dot{x}_a + \mathcal{P}_a|c|^2 \\ \ddot{x}_M &= -\omega_M^2 x_M - \Gamma\dot{x}_M + P_M|c|^2, \end{aligned} \tag{4.32}$$

where $\tilde{g}_a = \frac{g_a}{x_{a,0}}$, $\tilde{g}_M = \frac{g_M}{x_{\mathsf{ZPF}}}$, $\mathcal{P}_M = \hbar\tilde{g}_M/m_M = 2\omega_M x_{\mathsf{ZPF}} g_M$, $\mathcal{P}_a = \hbar\tilde{g}_a/m_a = 2\omega_a x_{a,0} g_a$. Note that we also rescaled the detuning parameter $\Delta \to \Delta - \tilde{g}_a\bar{x}_a - \tilde{g}_M\bar{x}_M$.

An expansion around the equilibrium values with

$$c = \bar{c} + \delta c,\ x_a = \bar{x}_a + \delta x_a,\ x_M = \bar{x}_M + \delta x_M \tag{4.33}$$

and

$$\bar{c} = \alpha_L/(\Delta + i\kappa/2),\ \bar{x}_{a,M} = \mathcal{P}_{a,M}|\bar{c}|^2/\omega_{a,M}^2 \tag{4.34}$$

yields

$$\delta\dot{c} = (i\Delta - \frac{\kappa}{2})\delta c - i\bar{c}\begin{pmatrix}\tilde{g}_a \\ \tilde{g}_M\end{pmatrix}\cdot\xi \tag{4.35}$$

$$\ddot{\xi} = \begin{pmatrix}-\omega_a^2 & 0 \\ 0 & -\omega_M^2\end{pmatrix}\xi - \begin{pmatrix}\Gamma_a & 0 \\ 0 & \Gamma_M\end{pmatrix}\dot{\xi} + \begin{pmatrix}\mathcal{P}_a \\ \mathcal{P}_M\end{pmatrix}(\bar{c}^*\delta c + c.c.) + \mathbf{f}, \tag{4.36}$$

where $\xi = \begin{pmatrix}\delta x_a \\ \delta x_M\end{pmatrix}$ and $\mathbf{f}$ denotes a test force, whose influence on x_a and x_M we want to observe. Decomposing (4.35) into positive and negative frequency parts ($\delta c = \delta c_+ e^{i\omega t} + \delta c_- e^{-i\omega t}$, $\mathbf{f} = \mathbf{f}_+ e^{i\omega t} + \mathbf{f}_- e^{-i\omega t}$ etc.) leads to

$$\pm\,\omega\delta c_\pm = (\Delta + i\kappa/2)\delta c_\pm - i\bar{c}\begin{pmatrix}\tilde{g}_a \\ \tilde{g}_M\end{pmatrix}\cdot\xi_\pm. \tag{4.37}$$

By introducing the susceptibilities

$$\chi_{ca}(\omega) = \tilde{g}_a\bar{c}/(\omega - \Delta - i\kappa/2), \tag{4.38}$$

$$\chi_{cM}(\omega) = \tilde{g}_M\bar{c}/(\omega - \Delta - i\kappa/2), \tag{4.39}$$

the equations of motion (4.37) can be rewritten as

$$\delta c_\pm = \begin{pmatrix}\chi_{ca}(\pm\omega) \\ \chi_{cm}(\pm\omega)\end{pmatrix}\cdot\xi_\pm. \tag{4.40}$$

We now insert this result into the Fourier-decomposed version of equation (4.36) and arrive at

$$\xi_\pm = \mathbf{M}(\pm\omega)^{-\mathbf{1}}\mathbf{f}_\pm. \tag{4.41}$$

The matrix $M(\omega)$ determines the response of the cantilever and the atoms' CM mode to the test force and is given by

$$\mathbf{M}(\omega) := \begin{pmatrix} -\omega^2 + i\omega\Gamma_a + \omega_a^2 - \mathcal{P}_a\tilde{\chi}_{ca}(\omega) & \mathcal{P}_a\tilde{\chi}_{cM}(\omega) \\ \mathcal{P}_M\tilde{\chi}_{ca}(\omega) & -\omega^2 + i\omega\Gamma_M + \omega_M^2 - \mathcal{P}_M\tilde{\chi}_{cM}(\omega) \end{pmatrix}, \quad (4.42)$$

where we introduced the shortcuts $\tilde{\chi}_{ca}(\omega) := \bar{c}^*\chi_{ca}(\omega) + \bar{c}\chi^*_{ca}(-\omega)$ and $\tilde{\chi}_{cM} = \bar{c}^*\chi_{cM}(\omega) + \bar{c}\chi^*_{cM}(-\omega)$.

In particular the reaction of the mechanical cantilever to a test force $\mathbf{f}_\pm = \begin{pmatrix} 0 \\ f_{M\pm} \end{pmatrix}$ is given by the susceptibility $\chi_M(\omega)$ with $\delta x_{M\pm} = \chi_M(\pm\omega) f_{M\pm}$:

$$\chi_M(\omega) = (\omega_M^2 - \omega^2 + i\omega\Gamma_M + \Sigma_c(\omega) + \Sigma_{ac}(\omega))^{-1} \quad (4.43)$$

The novel features are contained in the "self-energies"

$$\Sigma_c(\omega) = -\mathcal{P}_M(\bar{c}^*\chi_{cM}(\omega) + \bar{c}\chi^*_{cM}(-\omega)), \quad (4.44)$$

$$\Sigma_a(\omega) = -\mathcal{P}_a(\bar{c}^*\chi_{ca}(\omega) + \bar{c}\chi^*_{ca}(-\omega)), \quad (4.45)$$

$$\Sigma_{ac}(\omega) = \Sigma_a(\omega)\Sigma_c(\omega) \,/\, (\omega_a^2 - \omega^2 + i\omega\Gamma_a + \Sigma_a(\omega)) \quad (4.46)$$

The contribution of Σ_c to the susceptibility $\chi_M(\omega_M)$, evaluated at the resonators eigenfrequency, can be interpreted as a shift of the frequency by

$$\begin{aligned} \delta\omega_M &= \mathsf{Re}[\Sigma_c(\omega_M)]/(2\omega_M) \\ &= g_M^2|\bar{c}|^2\Big(\frac{\omega_M + \Delta}{(\omega_M + \Delta)^2 + \kappa^2/4} - \frac{\omega_M - \Delta}{(\omega_M - \Delta)^2 + \kappa^2/4}\Big), \end{aligned} \quad (4.47)$$

plus an optomechanical damping rate

$$\begin{aligned} \Gamma_{\mathsf{M,opt}} &= \frac{\mathsf{Im}[\Sigma_c(\omega_M)]}{\omega_M} \\ &= g_M^2|\bar{c}|^2\Big(\frac{\kappa/2}{(\omega_M - \Delta)^2 + \kappa^2/4} - \frac{\kappa/2}{(\omega_M + \Delta)^2 + \kappa^2/4}\Big). \end{aligned} \quad (4.48)$$

Apparently, both terms are not influenced by the presence of the atoms.

Σ_{ac}, on the other hand, accounts for a coupling of the mechanical oscillator and the condensate motion. This can be seen most easily by a simple comparison. For this purpose we consider a system consisting of the cantilever and the atoms only. We assume that there is a direct coupling between the cantilever and the atomic mode and start from a Hamiltonian of the form

$$\hat{H} = \hbar\omega_a\hat{a}^\dagger\hat{a} \;+\; \hbar\omega_M\hat{b}^\dagger\hat{b} \;+\; \hbar g_{\mathsf{eff}}(\hat{a}^\dagger + \hat{a})(\hat{b}^\dagger + \hat{b}) + \; \hat{H}_{\Gamma_M} + \hat{H}_{\Gamma_a}. \quad (4.49)$$

In a similar procedure as shown above, we can extract the cantilever's susceptibility from the equations of motion:

$$\chi_M(\omega) = (\omega_M^2 - \omega^2 + i\omega\Gamma_M + 2\omega_M(x_{\mathsf{ZPF}}/x_{a,0})g_{\mathsf{eff}}\chi_{aM}(\omega))^{-1}. \quad (4.50)$$

Here the susceptibility $\chi_{aM}(\omega) = 2\omega_a(x_{a,0}/x_{\mathsf{ZPF}})g_{\mathsf{eff}}/(\omega_a^2 - \omega^2 + i\omega\Gamma_a)$ accounts for the response of the atomic CM mode to the cantilever motion.

A comparison of (4.43) and (4.50) shows the following correspondence

$$\frac{4\omega_M\omega_a g_a^2 g_M^2|\bar{c}|^4(\frac{1}{\omega+\Delta-i\kappa/2}-\frac{1}{\omega-\Delta-i\kappa/2})^2}{\omega_a^2-\omega^2+i\omega\Gamma_a+\Sigma_a(\omega)} \leftrightarrow \frac{4\omega_M\omega_a g_{\text{eff}}^2}{\omega_a^2-\omega^2+i\omega\Gamma_a} \tag{4.51}$$

It follows that the effective, cavity assisted coupling between the cantilever and the collective atomic mode is given by

$$g_{\text{eff}} = g_a g_M|\bar{c}|^2(\frac{1}{\omega+\Delta-i\frac{\kappa}{2}}-\frac{1}{\omega-\Delta-i\frac{\kappa}{2}}). \tag{4.52}$$

Note that the coupling rate depends on the frequency ω of the test force. Obviously when the driving by the external force is very fast when compared to the mechanical oscillation frequencies of the cantilever (ω_M) and the atomic motion (ω_a), it will not lead to any response of the system. Moreover, if the driving frequency is larger than the cavity detuning $\omega \gg \Delta$, the effective coupling constant g_{eff} will vanish completely. We therefore state that ω should be comparable to the mechanical oscillation frequencies ω_a and ω_M and smaller than the cavity detuning Δ to reach strong cavity-assisted coupling between the cantilever and the atomic motion.

Furthermore we see that g_{eff} can be strong if both the atomic cloud and the cantilever couple strongly to the cavity field. We will assess its value for the assumed values of table (4.1) below.

4.6.2 Confirmation via Perturbation Theory

The result of the cavity-assisted coupling constant of the previous section already resembles the typical structure of a transition amplitude that was calculated via second-order perturbation theory. The first order couplings of the atomic cloud (g_a) and of the cantilever (g_M) to the cavity appear in the enumerator. The energy needed to create a cavity photon, in this case given by the detuning Δ, shows up in the denominator. Following this observation, we will now derive an expression for the cavity-assisted coupling constant g_{eff} using second order perturbation theory.

Again, we start with linearizing the basic Hamiltonian. Insertion of $\hat{a} = \bar{a}+\delta\hat{a}$, $\hat{b} = \bar{b}+\delta\hat{b}$, $\hat{c} = \bar{c}+\delta\hat{c}$ into (4.31) generates a Hamiltonian of the form

$$\begin{aligned}\hat{H} &= \hbar\omega_a\delta\hat{a}^\dagger\delta\hat{a}+\hbar\omega_M\delta\hat{b}^\dagger\delta\hat{b}-\hbar\tilde{\Delta}\delta\hat{c}^\dagger\delta\hat{c} \\ &\quad -\hbar g_a(\delta\hat{a}^\dagger+\delta\hat{a})(\bar{c}\delta\hat{c}^\dagger+h.c.)-\hbar g_M(\delta\hat{b}^\dagger+\delta\hat{b})(\bar{c}\delta\hat{c}^\dagger+h.c.).\end{aligned} \tag{4.53}$$

In the following we consider the transfer of a single phonon from the cantilever to the atomic cloud. This means that we focus on transitions from a state with one excitation on the mechanical resonator $|i\rangle := |n_a = 0, n_M = 1, n_{\text{cav}} = 0\rangle$ to a state where the condensate has one excitation quantum $|n\rangle := |n_a = 1, n_M = 0, n_{\text{cav}} = 0\rangle$. Note that the notation of the Fock states refers to the shifted operators of the Hamiltonian (4.53), i.e. $\delta\hat{a}|n_a\rangle = \sqrt{n_a}|n_a-1\rangle$, etc..

Given the above Hamiltonian there is no first order transition between these states. According to Fermi's Golden Rule the transition rate thus has the form:

$$\Gamma_{i\to n} = \frac{2\pi}{\hbar}\Big|\sum_{|m_j\rangle}\frac{\langle n|\hat{H}|m_j\rangle\langle m_j|\hat{H}|i\rangle}{E_i-E_{m_j}}\Big|^2\rho(E_n)|_{E_n\simeq E_I} \tag{4.54}$$

The idea is to arrive at an effective Hamiltonian consisting of terms for the atomic cloud, the cantilever and their interaction only. Similar to (4.49), the cavity field does not appear in this

effective Hamiltonian. We will extract the coupling constants from the transition rates. The eigenfrequencies will contain frequency shifts stemming from second order energy corrections. To give an example example, the transition $i \rightarrow n$ will appear with a term $\hbar g_{\text{eff}} \delta\hat{a}^\dagger \delta\hat{b}$ in the effective Hamiltonian.
We can identify two virtual states contribute to this transition: $|n_a = 1, n_M = 1, n_{\text{cav}} = 1\rangle$ and $|n_a = 0, n_M = 0, n_{\text{cav}} = 1\rangle$. The corresponding operators are $\delta\hat{b}\delta\hat{c}\delta\hat{c}^\dagger\delta\hat{a}^\dagger$ and $\delta\hat{a}^\dagger\delta\hat{c}\delta\hat{c}^\dagger\delta\hat{b}$ respectively. The energy level scheme of figure (4.6) illustrates the considered transitions. They contribute to the transition rate with

$$\hbar g_M g_a |\bar{c}|^2 \langle n_{\text{cav}}| \Big(\frac{1}{-\omega_a + \Delta} \delta\hat{c}\delta\hat{c}^\dagger + \frac{1}{\omega_M + \Delta} \delta\hat{c}\delta\hat{c}^\dagger \Big) |n_{\text{cav}}\rangle = \hbar g_M g_a |\bar{c}|^2 \Big(\frac{1}{\Delta + \omega_M} + \frac{1}{\Delta - \omega_a} \Big) \tag{4.55}$$

We can readily find the coupling constant g_{eff} as

$$g_{\text{eff},1} = g_M g_a |\bar{c}|^2 \Big(\frac{1}{\omega_M + \Delta} - \frac{1}{\omega_a - \Delta} \Big). \tag{4.56}$$

Analogously, if we consider transitions from $|n\rangle \rightarrow |i\rangle$, we get an effective coupling $g_{\text{eff},2}\delta\hat{a}\delta\hat{b}^\dagger$:

$$g_{\text{eff},2} = g_M g_a |\bar{c}|^2 \Big(\frac{1}{\Delta + \omega_a} + \frac{1}{\Delta - \omega_M} \Big) \tag{4.57}$$

We see that for $\omega_a = \omega_M = \omega$ we recover the result of the previous section:

$$g_{\text{eff}} = g_M g_a |\bar{c}|^2 \Big(\frac{1}{\omega + \Delta} - \frac{1}{\omega - \Delta} \Big), \tag{4.58}$$

where g_M (g_a) denotes the coupling constant of the cantilever (atomic cloud) to the cavity and Δ is the detuning of the cavity. Moreover, the results (4.56) and (4.57) show an asymmetry for the forward and backward transitions in the case of $\omega_M \neq \omega_a$. This provides additional information that we were not able to obtain from the derivation of (4.52) of the previous section, where we only considered the response of the system due to a test force of frequency ω.

Next we turn towards the diagonal parts of the effective atom-cantilever Hamiltonian. Second order transitions affect the eigenfrequencies of the cantilever and the atoms' collective motion by inducing the shifts $\delta\omega_{M,c}$ and $\delta\omega_{a,c}$. They can be evaluated by noting that

$$\delta\omega = \frac{1}{\hbar} \sum_{k_j} \frac{|\langle k_j | \hat{H}_{eff} | i \rangle|^2}{E_i - E_{k_j}}. \tag{4.59}$$

Applying an analogous procedure as above we arrive at the following expressions for the shift of the atomic CM frequency and the cantilever frequency respectively:

$$\delta\omega_a = g_a^2 |\bar{c}|^2 \Big(\frac{1}{\omega_a + \Delta} - \frac{1}{\omega_a - \Delta} \Big). \tag{4.60}$$

and

$$\delta\omega_M = g_M^2 |\bar{c}|^2 \Big(\frac{1}{\omega_M + \Delta} - \frac{1}{\omega_M - \Delta} \Big). \tag{4.61}$$

These results are in agreement with the frequency shifts extracted from the susceptibility (see equation 4.43) for $\Delta \gg \kappa$. The modification of the frequency of the mechanical resonator in an

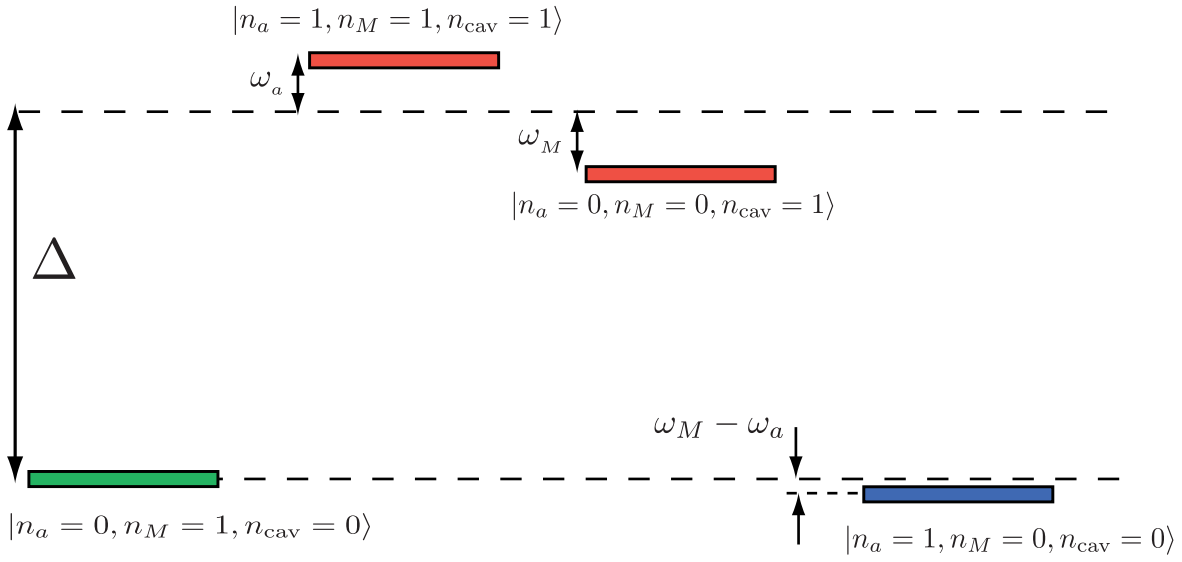

Figure 4.6: Energy level scheme for the cavity-assisted transitions between the states $|i\rangle = |n_a = 0, n_M = 1, n_{\rm cav} = 0\rangle$ and $|n\rangle = |n_a = 1, n_M = 0, n_{\rm cav} = 0\rangle$: A phonon is transferred from the cantilever to the atomic cloud. The transitions involve the creation (annihilation) of a cavity photon. The virtual states are suppressed by an energy of the order of the cavity detuning Δ. The cantilever frequency (ω_M) and the CM oscillation frequency of the atomic cloud (ω_a), are assumed to be much smaller than Δ.

optomechanical setup is commonly referred to as the optical spring effect and has for example been observed in gravitational wave detectors [61]. When assessing the effect of the cavity-assisted coupling $g_{\rm eff}$ in the following section, we have to compare it to both $\delta\omega_a$ and $\delta\omega_M$, as a large frequency shift due to the coupling with the cavity might conceal the coupled dynamics between the cantilever and the atomic motion.

4.6.3 Realization in the proposed setup

In the discussion of section (4.5) we found that the direct coupling between the cantilever and the atomic cloud, $g_{a,M}$, has a value of $10^{-1}\,Hz = 10^{-6}\omega_a$ for realistic parameters. It is limited by the term $\sqrt{\frac{Nm_a\omega_a}{m_M\omega_M}}$, i.e. by the ratio of the mass of the atomic cloud to the cantilever mass. On the other hand, the couplings between cantilever and cavity ($g_M + g_{M,c} \approx g_M$) and between cavity and atomic cloud ($g_{a,c}$) can become considerably large if we introduce an additional trapping potential. This implies that the cavity-assisted coupling $g_{\rm eff}$ can become considerably large. To get the explicit dependence of $g_{\rm eff}$ on the system's parameters, we insert the expressions of (4.28):

$$\begin{aligned} g_{\rm eff} &= g_{a,c}(g_{M,c} + g_M)|\bar{c}|^2\Big(\frac{1}{\omega - \Delta} - \frac{1}{\omega + \Delta}\Big) \\ &= \Big(\frac{NU_0}{4\hbar}\sin(2k\bar{x}_a) + \frac{\omega_{cav}\lambda_L}{8\pi L}\Big)\omega_a \sin(2k\tilde{x}_a)\frac{\omega_{\rm dip}^2}{\omega_a^2}\sqrt{\frac{Nm_a\omega_a}{m_M\omega_M}}\Big(\frac{1}{\omega + \Delta} - \frac{1}{\omega - \Delta}\Big). \end{aligned} \tag{4.62}$$

Again, the ratio of the atoms' mass to the cantilever mass is included by the term $\sqrt{\frac{Nm_a\omega_a}{m_M\omega_M}}$. Furthermore, as the virtual states are energetically suppressed, a factor of $\frac{1}{\Delta}$ enters. Still, the fact

that both the atomic cloud and the cantilever couple strongly to the cavity allows for a large g_{eff}. When assessing the strength of the cantilever-cavity coupling, we note that the standard optomechanical coupling, $g_M = -\frac{\omega_{\text{cav}}}{L} x_{\text{ZPF}}$, turns out to be the dominant contribution. In conclusion this means, that the occurrence of a strong effective coupling g_{eff} is intimately connected to the feature of two independent coupling mechanisms of the system. The atoms couple to the cavity via the dipole interaction, while the cantilever mainly reacts to the radiation pressure via g_M. The contribution of $g_{M,c}$ in equation (4.62) is relatively small and does not lead to a large g_{eff}. For the parameters of table (4.1) and $\sin(2k\tilde{x}_a) \approx 10^{-1}$ we get $g_{\text{eff}} \approx 10^8 \frac{1}{\Delta}\, s^{-2}$.

We can compare this value to the frequency shifts of the atomic cloud and the cantilever respectively. The coupling to the cavity modifies the oscillation frequency of the atomic cloud by $\delta\omega_a$ (see equation (4.60)) and

$$\begin{aligned} \frac{g_{\text{eff}}}{\delta\omega_a} &= -\frac{g_{M,c} + g_M}{g_{a,c}} \\ &= \sqrt{\frac{N m_a \omega_a}{m_M \omega_M}} \Big(1 + \frac{\omega_{\text{cav}} \lambda_L}{2\pi L \sin(2k\bar{x}_a) N U_0/\hbar}\Big) \approx 1. \end{aligned} \tag{4.63}$$

Similarly, the correction of the cantilever frequency due to the cantilever-cavity coupling is given by $\delta\omega_M$ (4.61) and

$$\begin{aligned} \frac{g_{\text{eff}}}{\delta\omega_M} &= -\frac{g_{a,c}}{g_{M,c} + g_M} \\ &= \sqrt{\frac{m_M \omega_M}{N m_a \omega_a}} \Big(1 + \frac{\omega_{\text{cav}} \lambda_L}{2\pi L \sin(2k\bar{x}_a) N U_0/\hbar}\Big)^{-1} \approx 1. \end{aligned} \tag{4.64}$$

In order to observe effects of the coupling between cantilever and atomic cloud in both system, (4.63) and (4.64) should simultaneously be of the order of 1. This can be achieved if $g_{a,c} \approx g_M$ and is one reason why we chose $|U_0| \approx 10^2\, Hz$ in table (4.1), even though it is below the experimentally realizable value of $10^5\, Hz$. We note that there is an additional shift $\delta\omega_{M,c}$ (see table 4.2) which we extracted from the dipole interaction term V_{dip} (4.19). That contribution is negligibly small though.

Finally, we compare the optomechanical damping rates $\Gamma_{\text{a,opt}}$ and $\Gamma_{\text{M,opt}}$ to the effective coupling rate g_{eff}. In this context, the optomechanical damping rate should be kept low in order to avoid heating (or cooling) effects. In addition $\Gamma_{\text{M,opt}}$ ($\Gamma_{\text{a,opt}}$) gives a measure for the coherence time of the cantilever (or the atomic CM) oscillation when subject to the cavity field. The explicit expression for $\Gamma_{\text{M,opt}}$ is given by equation (4.48). For $\Delta \gg \kappa$ this rate is much smaller than $\delta\omega_M$ and $\frac{g_{\text{eff}}}{\Gamma_{\text{M,opt}}} \approx \frac{g_{a,c}}{g_{M,c}+g_M} \frac{\Delta}{\kappa} \approx \frac{\Delta}{\kappa}$. Analogously, we can find an optomechanical damping rate for the atoms' collective motion that is denoted by $\Gamma_{\text{a,opt}}$. Its expression is given by equation (4.48) when replacing ω_M by ω_a and g_M and g_a. For $\Delta \gg \kappa$ it yields that $\frac{g_{\text{eff}}}{\Gamma_{\text{a,opt}}} \approx \frac{g_{M,c}+g_M}{g_a} \frac{\Delta}{\kappa} \approx \frac{\Delta}{\kappa}$. Hence for sufficiently large detuning, the effect of the optomechanical damping rates $\Gamma_{\text{M,opt}}$ and $\Gamma_{a,\text{opt}}$ will be small.

In table (4.4) we summarize the results of this section and give estimates on the strength of the effective coupling and the frequency shifts. In doing so, we assume values for the detuning parameter of $\Delta \approx 10^7\, Hz$ and $\kappa \approx 10^6\, Hz$. With this choice of parameters one can reach a second order coupling between the atoms and the cantilever, $g_{\text{eff}} \approx 10\, Hz$. The frequency shifts of the atomic motion and the cantilever are of the same order, while the optomechanical damping rates are one order below. In this case the detuning is larger than both the cavity decay κ and the

$g_{\text{eff}} = g_{a,c} g_M \lvert\bar{c}\rvert^2 (\frac{1}{\omega+\tilde{\Delta}} - \frac{1}{\omega-\tilde{\Delta}})$	$10\,\text{Hz}$
$\delta\omega_a = g_{a,c}^2 \lvert\bar{c}\rvert^2 (\frac{1}{\omega+\tilde{\Delta}} - \frac{1}{\omega-\tilde{\Delta}})$	
$\delta\omega_M = (g_{M,c} + g_M)^2 \lvert\bar{c}\rvert^2 (\frac{1}{\omega+\tilde{\Delta}} - \frac{1}{\omega-\tilde{\Delta}})$	
$\frac{g_{\text{eff}}}{\delta\omega_a} = -\frac{g_{M,c}+g_M}{g_{a,c}}$	1
$\frac{g_{\text{eff}}}{\delta\omega_M} = -\frac{g_{a,c}}{g_{M,c}+g_M}$	1
$\frac{g_{\text{eff}}}{\Gamma_{a,\text{opt}}} \simeq \frac{g_{M,c}+g_M}{g_{a,c}} \frac{\Delta}{\kappa}$	10
$\frac{g_{\text{eff}}}{\Gamma_{M,\text{opt}}} \simeq \frac{g_{a,c}}{g_{M,c}+g_M} \frac{\Delta}{\kappa}$	10

Table 4.4: Expression for the effective, cavity-assisted coupling constant g_{eff} between cantilever and atomic cloud. It is compared to the frequency shifts due to the optical spring effect ($\delta\omega_a$ and $\delta\omega_M$). Furthermore for the estimates on the right-hand side we assumed the parameters of table (4.1) and additionally $\sin(2k\tilde{x}_a) \approx 10^{-1}$, $\Delta \approx 10^7\,Hz$ and $\kappa \approx 10^6\,Hz$.

frequencies ω_M and ω_a. However, it is not immediately clear if this detuning is sufficiently large. This question certainly has to be checked in a future work.

We also note, that we assumed a relatively low cavity decay rate of $\kappa \approx 10^6\,\text{Hz}$, which we extracted from the parameters of the Berkeley setup [32]. Certainly, it is much harder to reach a high finesse in an optomechanical setup with a movable end mirror than in a setup that has two fixed mirrors, and one might question, if the assumed cavity finesse is realizable. However there is a possible workaround: Resuming the concept of the "membrane-in-the-middle"-setup of [14], we will discuss a setup that features the coupled dynamics of an atomic cloud and a membrane inside in a high-finesse cavity (see section 4.10).

4.7 A BEC coupled to an optomechanical system

To confirm the features of the simple model that we discussed in section (4.4) we consider a more realistic treatment here. If the atomic cloud forms a Bose-Einstein condensate, its dynamics can be described by the Gross-Pitaevskii equation (3.8). The predictions of this equation are reliable for dilute atomic gases ($\frac{N}{V}|a_s|^3 \ll 1$) and they have successfully explained the observations on the collective motion of BECs in the celebrated experiments at the MIT and the JILA ([42, 41, 43, 44]).

Using this approach we now include both the interaction between the atoms in a mean-field description and the full dimensionality of the problem. Furthermore we can get first corrections of the coupling constants and frequency shifts due to the finite extent of the condensate.

4.7.1 Hamiltonian

We recall the setup proposed in section (4.4) and start with a Hamiltonian similar to (4.14), but replace the "super-atom" by a condensate. We also consider the full three dimensional structure of the dipole potential and include the Gaussian decay of the intensity in transverse directions. Furthermore we allow for an additional trapping potential $V_{\text{trap}}(\mathbf{x})$. The Hamiltonian takes the form of

$$\hat{H} = \hbar(-\Delta + g_M(\hat{b} + \hat{b}^\dagger))\hat{c}^\dagger\hat{c} + \hbar\omega_M\hat{b}^\dagger\hat{b} + \hbar\alpha_L(\hat{c} + \hat{c}^\dagger)$$
$$+ \int \hat{\Psi}^\dagger(\mathbf{x})[-\frac{\hbar^2}{2m}\nabla^2 + U_0\sin^2(kx - k\hat{x}_M - \Phi(\Delta))e^{-\frac{y^2+z^2}{w_0^2}}\hat{c}^\dagger\hat{c} + V_{\mathsf{trap}}(\mathbf{x}) + \frac{g}{2}\hat{\Psi}^\dagger\hat{\Psi}\,]\Psi(\mathbf{x})d^3\mathbf{x}$$
$$+\hat{H}_\kappa + \hat{H}_{\Gamma_M}. \tag{4.65}$$

Here $\hat{b}$, $\hat{c}$ are the annihilation operators that represent the mechanical oscillator and the cavity field respectively and that obey the canonical commutation relations for bosonic operators. We can expand the operators $\hat{b}$, $\hat{c}$ for the mechanical oscillator and the cavity respectively around their equilibrium values

$$\hat{c} = \bar{c} + \delta\hat{c},\ \hat{x}_M = \bar{x}_M + \delta\hat{x}_M = \sqrt{\hbar/2m\omega_M}(\bar{b} + \delta\hat{b}) + h.c. = \bar{x}_M + x_{\mathsf{ZPF}}(\delta\hat{b}^\dagger + \delta\hat{b}). \tag{4.66}$$

Subsequently we can approximate the sinusoidal part of the dipole potential around the steady state value $\bar{x}_M$ as

$$\sin^2(kx - k\hat{x}_M - kL) \approx \sin^2(kx - k\bar{x}_M - kL) - k\delta\hat{x}_M\sin(2kx - 2k\bar{x}_M - 2kL)$$
$$+k^2\delta\hat{x}_M^2\cos(2kx - 2k\bar{x}_M - 2kL). \tag{4.67}$$

The field operator of the atoms, $\hat{\Psi}(\mathbf{x})$, is expanded around its ground-state with the help of the Bogoliubov spectrum, as discussed in section3.3:

$$\hat{\Psi}(\mathbf{x}) = \Psi_0(\mathbf{x}) + \delta\hat{\Psi}(\mathbf{x}) = \Psi_0(\mathbf{x}) + \sum_\alpha(u_\alpha(\mathbf{x})\hat{a}_\alpha - v_\alpha^*(\mathbf{x})\hat{a}_\alpha^\dagger). \tag{4.68}$$

This brings the Hamiltonian (4.65) into the following form:

$$\begin{aligned}
\hat{H} - \mu\hat{N} &= H_0 + \sum_\alpha \hbar\omega_\alpha\hat{a}_\alpha^\dagger\hat{a}_\alpha \\
&+ \sum_\alpha \hbar(g_{\alpha,M}\hat{a}_\alpha(\delta\hat{b} + \delta\hat{b}^\dagger) + h.c.) + \sum_\alpha \hbar(g_{\alpha,c}\hat{a}_\alpha(\bar{c}^*\delta\hat{c} + \bar{c}\delta\hat{c}^\dagger) + h.c.) \\
&+ \hbar(-\Delta - \Delta_N)\delta\hat{c}^\dagger\delta\hat{c} \\
&+ \hbar(-\Delta - \Delta_N + (g_{M,c} + g_M)(\delta\hat{b}^\dagger + \delta\hat{b}))(\bar{c}\delta\hat{c}^\dagger + \bar{c}^*\delta\hat{c}) + \hbar\alpha_L(\delta\hat{c}^\dagger + \delta\hat{c}) \\
&+ \hbar(\omega_M + \delta\omega_{M,c})\delta\hat{b}^\dagger\delta\hat{b} + \delta\omega_{M,c}\delta\hat{b}^2 + h.c. \\
&+ \hat{H}_\kappa + \hat{H}_{\Gamma_M},
\end{aligned} \tag{4.69}$$

where

$$
\begin{aligned}
g_{\alpha,M} &= -kx_{\mathsf{ZPF}}\frac{U_0}{\hbar}|\bar{c}|^2\int \Psi_0(\mathbf{x})\sin(2kx-2k\bar{x}_M-2kL)e^{-\frac{y^2+z^2}{w_0^2}}(u_\alpha(\mathbf{x})-v_\alpha(\mathbf{x}))d^3\mathbf{x}\\
g_{\alpha,c} &= (U_0/\hbar)\int \Psi_0(\mathbf{x})\sin^2(kx-k\bar{x}_M-kL)\exp(-\frac{y^2+z^2}{w_0^2})(u_\alpha(\mathbf{x})-v_\alpha(\mathbf{x}))d^3\mathbf{x}\\
g_{M,c} &= -kx_{\mathsf{ZPF}}(U_0/\hbar)\int |\Psi_0(\mathbf{x})|^2\sin(2kx-2k\bar{x}_M-2kL)\exp(-\frac{y^2+z^2}{w_0^2})d^3\mathbf{x}\\
g_M &= -\omega_{\mathsf{cav}}\frac{x_{\mathsf{ZPF}}}{L}\\
\Delta_N &= \int |\Psi_0(\mathbf{x})|^2(U_0/\hbar)\sin^2(kx-k\bar{x}_M-kL)\exp(-\frac{y^2+z^2}{w_0^2})d^3\mathbf{x}\\
\delta\omega_M &= \frac{U_0}{\hbar}k^2x_{\mathsf{ZPF}}^2|\bar{c}|^2\int |\Psi_0(\mathbf{x})|^2\cos(2kx-2k\bar{x}_M-2kL)\exp(-\frac{y^2+z^2}{w_0^2})d^3\mathbf{x}, \qquad (4.70)
\end{aligned}
$$

and where we considered terms up to second order only. Γ_M and κ denote the damping rate for the mechanical motion and the cavity decay respectively. ω_a is the eigenvalue of the Bogoliubov spectrum and has to be determined from equations (3.26).

4.7.2 Different scenarios

It is now our goal to find explicit expressions for the Bogoliubov spectrum (equation 4.68) and to compute the coupling constants (equations 4.70). But before we do so, it is helpful to discuss a few scenarios regarding the confinement of the atoms and the strength of their interactions. This discussion will the lead to approximations so that the later calculations will be straightforward.

The effective potential that confines the atoms in axial direction is given by $V_{\mathsf{eff}}(x) = V_{\mathsf{trap}}(x) + V_{\mathsf{dip}}(x)$ with $V_{\mathsf{dip}}(x) = U_0\sin^2(kx-k\bar{x}_M-kL)|\bar{c}|^2$. As an external potential V_{trap} we employ an optical lattice potential of the form $V_{\mathsf{trap}}(\mathbf{x}) = U_{\mathsf{trap}}\sin^2(k_tx-k_tL)$. We will simplify the discussion by setting $V_{\mathsf{eff}} = V_{\mathsf{trap}}$, i.e. by focusing on the case $U_{\mathsf{trap}} \gg U_0|\bar{c}|^2$. The superposition of V_{trap} and V_{dip} would not change much of the physics but complicate the treatment of the system.

The first classification is given by the strength of the dipole potential. For a very weak lattice potential, $\hbar U_{\mathsf{trap}} \ll \mu$ the dynamics of the condensate is hardly influenced by the lattice. This is the regime encountered in the Zürich setup [33] that we discussed in section 4.3. On the other hand, in the case of a very deep optical lattice with $\hbar U_{\mathsf{trap}} \gg \mu$, the atomic cloud is bound to a single lattice site. The condensate fractions at each site show vanishing overlap and can therefore be considered as independent fractions. The Berkeley setup ([32]) features this limiting case. In the intermediate regime, where the chemical potential μ is comparable to the band width and the lattice strength, the condensate will show features that resemble those of electrons in a solid state. In this case, the condensate would be excited into various mechanical modes and our simple optomechanical picture would become noticeably complicated. Nevertheless we mention that this regime allowed for the observation and study of a number of phenomena that have an analogue in condensed matter physics, most notably the transition from a superfluid to a Mott insulator [62, 63].

If we now focus on the case of a very deep optical lattice along the $x-$axis, the optical potential can be approximated by an expansion around a local minimum. Assuming $U_{\mathsf{trap}} < 0$ this expansion

yields

$$V_{\text{dip}} \simeq U_{\text{trap}}(1 - k^2x^2) = U_{\text{trap}} + \frac{m_a}{2}\omega_a^2 x^2, \tag{4.71}$$

where $\omega_a = \sqrt{2k^2|U_{\text{trap}}|/m_a}$. This approximation is valid in the Lamb-Dicke regime, i.e. if the condensate is confined to a region close to the center of a lattice site and the Thomas-Fermi radius is much smaller than the laser wavelength: $kR_x \ll 1$. By rewriting R_x in terms of k, $R_x = \frac{1}{k}\sqrt{\frac{\mu}{|U_{\text{trap}}|}}$, we see that this condition is already fulfilled if we demand a deep lattice, when $|U_{\text{trap}}| \gg \mu$.

The next step is to determine the role of the atom-atom interactions for a condensed atomic gas trapped in a generic one dimensional optical lattice. As discussed in section (3.2), the interactions dominate the condensate dynamics if $\mu \gg \hbar\omega_i$ or equivalently if $R_i \gg \xi$. A salient feature of optical lattices is the large trapping frequency in axial direction ($\omega_a \sim 10^3...10^5\, Hz$) with moderate frequencies in the transverse directions ($\omega_{y,z} \sim 10...10^3\,\text{Hz}$). For a particular set of parameters the axial trapping frequency can become even larger than $\mu/\hbar$, and $R_{y,z} > \xi > R_x$. In this case the dynamics along the x-axis are determined by the harmonic oscillator terms in the Gross-Pitaevskii equation. Accordingly the condensate shows a Gaussian profile along the $x-$direction. This crossover from the 3D-Thomas-Fermi regime to an effective 2D-regime has been studied for example in [64, 65].

When demanding for a deep lattice and for the Thomas-Fermi regime simultaneously, we impose tight bounds on the chemical potential:

$$|U_{\text{trap}}| \gg \mu \gg \hbar\omega_a. \tag{4.72}$$

To get an estimate we compute the ratio of these two bounds:

$$\left(\frac{|U_{\text{trap}}|}{\hbar\omega_x}\right)^2 \quad = \quad \frac{|U_{\text{trap}}|}{2\hbar^2k^2/m_a}. \tag{4.73}$$

At first sight, it seems as if this ratio could be made arbitrarily large by increasing $|U_{\text{trap}}|$. However, the axial trapping frequency has to be held below some critical value of around $10^5 s^{-1}$ to avoid strong depletion of the condensate. Therefore the value of $|U_{\text{trap}}|$ is limited as well. This is due to the fact that the other parameters in the expression $\omega_a = \sqrt{2|U_{\text{trap}}|k^2/m_a}$, namely k and m_a, are practically fixed. For estimated parameters of table (4.1), the ratio (4.73) takes a value of around 1, and the relation (4.72) can not be fulfilled.

A rough guess on the crossover from the non-interacting to the Thomas-Fermi regime can be made by comparing $\hbar\omega_x$ to the Thomas-Fermi result of the chemical potential, μ^{TF} (3.21). It follows, that $\mu^{TF} > \hbar\omega_a$ for particle numbers larger than

$$N_{2D} = \frac{4}{15}\sqrt{\frac{2\hbar}{m_a a_s^2}}\sqrt{\frac{\omega_x^3}{\omega_y^2\omega_z^2}}. \tag{4.74}$$

This result shows that a strong asymmetry in the trapping potential favors the 2D-regime and that the crossover from the 3D-Thomas-Fermi regime to the 2D-regime can be reached by reducing the number of atoms in the trap ([64]). For a trap with $\omega_a \sim 10^5\, s^{-1}$, $\omega_y \sim \omega_z \sim 10^3\, s^{-1}$ and a gas of ^{87}Rb atoms ($m_a \sim 10^{-25}\,\text{kg}$, $a_s \sim 6 \cdot 10^{-9}\,\text{m}$) the critical atom number is $N_{2D} = 5 \cdot 10^4$. The fact that the transition between the non-interacting and the Thomas-Fermi regime is governed by both the atom number and the ratio of the trapping frequencies can also be seen by rewriting R_x

in terms of the particle density: $R_x = \sqrt{\bar{n}g/m_a\omega_x^2}$. Decreasing the density - by diminishing either N or the transverse trapping frequencies - reduces R_x but increases $\xi = 1/\sqrt{8\pi\bar{n}a_s}$.

In the subsequent section we will restrict our considerations to the case of a deep optical lattice or equivalently the Lamb-Dicke regime. Regarding the role of the interactions, a realistic scenario will be situated in between the Thomas-Fermi limit and the non-interaction regime. We will therefore give results for both of these cases.

4.7.3 Center-of-mass mode

After this preliminary discussion we are now able to evaluate the coupling constants and frequency shifts of equations (4.70). We will compare them to the corresponding expressions that we derived for the simplified model of the "super-atom" and that are here denoted by an upper index A, like for example $g^A_{a,M}$.

Our calculation is based on the following assumptions: We consider a Bose-condensed atomic cloud sitting close to the center of a single lattice site, i.e. $kR_x \ll 1$ and $R_{y,z}/w_0 \ll 1$. At first we assume that the condensate is in the Thomas-Fermi regime and that there is no additional trapping potential, i.e. $V_{\text{trap}} = 0$. Later we will also consider an additional trapping potential $V_{\text{trap}} \neq 0$ and finally the case of a non-interacting atomic gas.

The dipole potential V_{dip} can now be approximated around a local minimum

$$\begin{aligned} V_{\text{dip}}(\mathbf{x}) &\simeq U_0|\bar{c}|^2(1-k^2x^2)(1-\frac{y^2+z^2}{w_0^2}) \\ &\simeq U_0|\bar{c}|^2 + \frac{m_a}{2}\omega_a^2x^2 + \frac{m_a}{2}\omega_y^2y^2 + \frac{m_a}{2}\omega_z^2z^2, \end{aligned} \tag{4.75}$$

where $\omega_a = \sqrt{2|U_0|k^2|\bar{c}|^2/m_a}$ and $\omega_y = \omega_z = \sqrt{2|U_0||\bar{c}|^2/(m_aw_0^2)}$ and x, y and z are measured from the center of the trapping site. Note that the zero-point width along the x-axis for a single atom is given by $x_{a,0} = \sqrt{\hbar/2m_a\omega_a}$.

From symmetry considerations we expect the center-of-mass oscillation in axial direction to be the dominant mode of the atomic collective motion. Focusing on this mode, we set

$$\hat{\Psi}(\mathbf{x}) = \Psi_0(\mathbf{x}) + u_a(\mathbf{x})\hat{a} - v_a^*(\mathbf{x})\hat{a}^\dagger. \tag{4.76}$$

In the Thomas-Fermi approximation the solution of the Bogoliubov equations 3.26 for the center-of-mass excitation in a harmonic potential (see for example [47]) leads to:

$$u_a(\mathbf{x}) - v_a(\mathbf{x}) = \sqrt{\frac{15\hbar\omega_a/\mu}{8\pi R_xR_yR_z}}\Big(1-\frac{x^2}{R_x^2}-\frac{y^2}{R_y^2}-\frac{z^2}{R_z^2}\Big)^{-\frac{1}{2}}\frac{x}{R_x} = \sqrt{\frac{5\hbar\omega_a}{2V\mu}}(1-r'^2)^{-\frac{1}{2}}x', \tag{4.77}$$

where we rescaled the coordinates (x, y, z) with respect to the corresponding Thomas-Fermi radii $R_i = \sqrt{\frac{2\mu}{m\omega_i^2}}$ and introduced the radius $r' = \sqrt{x'^2+y'^2+z'^2}$ and the volume of the ellipsoid $V = \frac{4\pi}{3}R_xR_yR_z$ to shorten the notation. Note that even though the term (4.77) shows a divergence for $r' \to 0$ the correct normalization of $u_a(\mathbf{x})$ and $v_a(\mathbf{x})$ can be achieved by employing equation (3.25).

The Thomas-Fermi result for the condensate wave function has the form

$$\Psi_0(\mathbf{x}) = \sqrt{\frac{\mu}{g}}\sqrt{1-r'^2} = \sqrt{\frac{5N}{2V}}\sqrt{1-r'^2}. \tag{4.78}$$

In the last step we used that the chemical potential is fixed by the normalization of Ψ_0 : $N = \int_V |\Psi_0|^2 d^3\mathbf{x}$.
The direct coupling constant $g_{a,M}$ between the atomic CM mode and the mechanical cantilever can now be computed. In doing so we expand the sinusoidal terms in the equations (4.70) up to second order in kx, $\frac{y}{w_0}$ and $\frac{z}{w_0}$. This expansion is therefore consistent with the approximations in the previous steps (see for example equations (4.75), (4.77) and (4.78)).

$$\begin{aligned} g_{a,M} &= -kx_{\mathsf{ZPF}}\frac{U_0}{\hbar}|\bar{c}|^2\int \Psi_0(\mathbf{x})(u_\alpha(\mathbf{x})-v_\alpha(\mathbf{x}))\sin(\pi+2kx)\exp(-\frac{y^2+z^2}{w_0^2})\,d^3\mathbf{x} \\ &= kx_{\mathsf{ZPF}}(U_0/\hbar)|\bar{c}|^2\int \Psi_0(\mathbf{x})(u_\alpha(\mathbf{x})-v_\alpha(\mathbf{x}))2kx\,d^3\mathbf{x} \\ &= \frac{\omega_a}{2}\sqrt{\frac{Nm_a\omega_a}{m_M\omega_M}} \\ &= g^A_{a,M}. \end{aligned} \tag{4.79}$$

The coupling constant between the condensate CM mode and the cantilever agrees with the expression $g^A_{a,M}$ that was found for the "super-atom". Note that the other coupling constants, $g_{a,c}$ and $g_{M,c}$ are zero. As before, the CM mode does not couple to the cavity field in the linearized Hamiltonian.
The only remaining terms are the frequency shift of the cantilever and the cavity respectively:

$$\begin{aligned} \delta\omega_{M,c} &= (U_0/\hbar)k^2x^2_{\mathsf{ZPF}}|\bar{c}|^2\int|\Psi_0(\mathbf{x})|^2(-1+2k^2x^2)(1-\frac{y^2+z^2}{w_0^2})d^3\mathbf{x} \\ &\approx -\omega_a\frac{m_a}{2\hbar}\frac{\hbar}{2m_M\omega_M}\left(N-\int|\Psi_0(\mathbf{x})|^2(2k^2x^2+\frac{y^2+z^2}{w_0^2})d^3\mathbf{x}\right) \\ &= \delta\omega^A_{M,c}\left(1-\frac{2}{7}k^2R_x^2-\frac{1}{7}\frac{R_y^2+R_z^2}{w_0^2}\right). \end{aligned} \tag{4.80}$$

$$\begin{aligned} \Delta_N &= \int|\Psi_0(\mathbf{x})|^2(U_0/\hbar)(1-k^2x^2)(1-\frac{y^2+z^2}{w_0^2})d^3\mathbf{x} \\ &\approx (U_0/\hbar)\int|\Psi_0(\mathbf{x})|^2(1-k^2x^2-\frac{y^2+z^2}{w_0^2})d^3\mathbf{x} \\ &= \Delta^A_N(1-\frac{1}{7}k^2R_x^2-\frac{1}{7}\frac{R_y^2+R_z^2}{w_0^2}) \end{aligned} \tag{4.81}$$

These terms show corrections due to the extent of the condensate when compared to the corresponding terms for the super-atom ($\delta\omega^A_{M,c}$ and Δ^A_N).

As discussed in section (4.4) non-vanishing coupling between the center-of-mass mode and the cavity field can be obtained with the help of an additional trapping potential $V_{\mathsf{trap}}(\mathbf{x})$ that shifts the condensate to a new equilibrium position $\tilde{x}_a$.
The condensate wave function $\Psi_0(\mathbf{x})$ and the center-of-mass mode $u_a(\mathbf{x})-v_a(\mathbf{x})$ for the total potential $V_{\mathsf{eff}}(\mathbf{x}) = \frac{m_a}{2}\omega_a^2(x-\tilde{x}_a)^2+\frac{m_a}{2}\omega_y^2y^2+\frac{m_a}{2}\omega_z^2z^2$ are then readily found from equations (4.78) and (4.77) by replacing x by $x-\tilde{x}_a$.
The coupling constants and frequency shifts are given by:

$$\begin{aligned} g_{a,M} &= -kx_{\mathsf{ZPF}}\frac{U_0}{\hbar}|\bar{c}|^2\int \Psi_0(\mathbf{x})(u_a(\mathbf{x})-v_a(\mathbf{x}))\sin(\pi+2k\tilde{x}_a+2kx)\exp(-\frac{y^2+z^2}{w_0^2})d^3\mathbf{x} \\ &\approx 2\cos(2k\tilde{x}_a)k^2x_{\mathsf{ZPF}}(U_0/\hbar)|\bar{c}|^2\int \Psi_0(\mathbf{x})(u_a(\mathbf{x})-v_a(\mathbf{x}))\,x\,d^3\mathbf{x} \\ &= g^A_{a,M} \end{aligned} \tag{4.82}$$

$$\begin{aligned} g_{a,c} &= (U_0/\hbar)\int \Psi_0(\mathbf{x})\sin^2(\frac{\pi}{2}+kx+k\tilde{x}_a)\exp(-\frac{y^2+z^2}{w_0^2})(u_a(\mathbf{x})-v_a(\mathbf{x}))d^3\mathbf{x} \\ &\approx -k\sin(2k\tilde{x}_a)(U_0/\hbar)\int \Psi_0(\mathbf{x})(u_a(\mathbf{x})-v_a(\mathbf{x}))x\,d^3\mathbf{x} \\ &= g^A_{a,c} \end{aligned} \tag{4.83}$$

$$\begin{aligned} g_{M,c} &= -kx_{\mathsf{ZPF}}(U_0/\hbar)\int |\Psi_0(\mathbf{x})|^2\sin(\pi+2k\tilde{x}_a+2kx))\exp(-\frac{y^2+z^2}{w_0^2})d^3\mathbf{x} \\ &\approx kx_{\mathsf{ZPF}}(U_0/\hbar)\int |\Psi_0(\mathbf{x})|^2\sin(2k\tilde{x}_a)(1-2k^2x^2)(1-\frac{y^2+z^2}{w_0^2})\,d^3\mathbf{x} \\ &= g^A_{M,c}(1-\frac{2}{7}k^2R_x^2-\frac{1}{7}\frac{R_y^2+R_z^2}{w_0^2}) \end{aligned} \tag{4.84}$$

$$\begin{aligned} \Delta_N &= (U_0/\hbar)\int |\Psi_0(\mathbf{x})|^2\sin^2(\frac{\pi}{2}+k\tilde{x}_a+kx)\exp(-\frac{y^2+z^2}{w_0^2})d^3\mathbf{x} \\ &\approx (U_0/\hbar)\int |\Psi_0(\mathbf{x})|^2(\cos^2(k\tilde{x}_a)(1-\frac{y^2+z^2}{w_0^2})-\cos(2k\tilde{x}_a)k^2x^2)d^3\mathbf{x} \\ &= \Delta_N^A\Big(1-\frac{1}{7}\frac{R_y^2+R_z^2}{w_0^2}\Big)-\frac{1}{7}\frac{g_0^2}{\Delta_{\mathsf{ca}}}Nk^2R_x^2\cos(2k\tilde{x}_a) \end{aligned} \tag{4.85}$$

$$\begin{aligned} \delta\omega_M &= \frac{U_0}{\hbar}k^2x_{\mathrm{ZPF}}^2|\bar{c}|^2\int |\Psi_0(\mathbf{x})|^2\cos(\pi+2kx+2k\tilde{x}_a)\exp(-\frac{y^2+z^2}{w_0^2})d^3\mathbf{x}, \\ &\approx -\frac{U_0}{\hbar}k^2x_{\mathrm{ZPF}}^2|\bar{c}|^2\int |\Psi_0(\mathbf{x})|^2\cos(2k\tilde{x}_a)(1-2k^2x^2-\frac{y^2+z^2}{w_0^2})d^3\mathbf{x} \\ &= \delta\omega^A_{M,c}(1-\frac{2}{7}k^2R_x^2-\frac{1}{7}\frac{R_y^2+R_z^2}{w_0^2}) \end{aligned} \tag{4.86}$$

Again we are able to compare (4.82) - (4.86) to the corresponding results for the "super-atom" of section (see table (4.3)). Up to first order in kR_x the results coincide. This can be understood by the fact, that the dynamics of the center-of-mass mode is not influenced by atom-atom-interactions. Corrections due to the finite extent of the atomic cloud appear for $g_{c,M}$, Δ_N and $\delta\omega_M$. Only if we included higher order terms in the expansions of equations (4.67) and (4.75) and hence in the expression for the CM mode (4.77), we would also get corrections to $g_{a,M}$ and $g_{a,c}$.

So far, the calculations of this section were made for an atomic gas whose dynamics is dominated by the atom-atom-interactions, i.e. in the Thomas-Fermi limit. If we go to the opposite limit of very weak interactions ($g \to 0$), the Gross-Pitaevskii equation (3.8) turns into a linear Schrödinger equation for a harmonic oscillator:

$$i\hbar\frac{\partial}{\partial t}\Psi(\mathbf{x},t) = (-\frac{\hbar^2}{2m_a}\nabla^2 + \frac{m_a}{2}\omega_a^2 x^2 + \frac{m_a}{2}\omega_{yz}^2(y^2+z^2))\Psi(\mathbf{x},t). \tag{4.87}$$

Solutions to this equation are found by separation of variables either in Cartesian coordinates or in spherical coordinates with quantum number (n_x, n_y, n_z) and (n_r, l, m) respectively. We refer to standard textbooks on quantum mechanics for more details.
The energy eigenstates of the problem (4.87), denoted by Ψ_α with $\alpha = (n_x, n_y, n_z)$ and $\alpha = (n_r, l, m)$ respectively, are also solutions of the Bogoliubov equations (3.26) for $g = 0$. In particular, the ground state is found to be

$$\Psi_0(x,y,z) = \sqrt{N}(2\pi)^{-\frac{3}{4}}(x_{a,0}y_{a,0}z_{a,0})^{-\frac{1}{2}}\exp(-\frac{x^2}{4x_{a,0}^2} - \frac{y^2}{4y_{a,0}^2} - \frac{z^2}{4z_{a,0}^2}),$$

where $x_{a,0} = \sqrt{\frac{\hbar}{2m\omega_a}}$, $y_{a,0} = \sqrt{\frac{\hbar}{2m\omega_y}}$ and $z_{a,0} = \sqrt{\frac{\hbar}{2m\omega_z}}$. The center-of-mass mode along the axis is given by the eigenstate corresponding to $\alpha = (n_r = 0, l = 1, m = 0) \leftrightarrow (n_x = 1, n_y = 0, n_z = 0)$ and

$$u_a(x,y,z) = (2\pi)^{-\frac{3}{4}}(x_{a,0}y_{a,0}z_{a,0})^{-\frac{1}{2}}\frac{x}{x_{a,0}}\exp(-\frac{x^2}{4x_{a,0}^2} - \frac{y^2}{4y_{a,0}^2} - \frac{z^2}{4z_{a,0}^2}),$$

while $v_a = 0$. The coefficients are chosen such that $\int|\Psi_0(\mathbf{x})|d^3\mathbf{x} = N$ and $\int|u_a|^2 d^3\mathbf{x} = 1$.
The coupling constants for the non-interacting case in the presence of an additional trapping potential as discussed above are

$$\begin{aligned} g_{a,M} &= -2\cos(2k\tilde{x}_a)k^2 x_{\mathsf{ZPF}}(U_0/\hbar)|\bar{c}|^2\int\Psi_0(\mathbf{x})u_a(\mathbf{x})\,x\,d^3\mathbf{x} \\ &= g_{a,M}^A \end{aligned} \tag{4.88}$$

$$\begin{aligned} g_{a,c} &= k\sin(2k\tilde{x}_a)(U_0/\hbar)\int\Psi_0(\mathbf{x})u_a(\mathbf{x})x\,d^3\mathbf{x} \\ &= g_{a,c}^A, \end{aligned} \tag{4.89}$$

$$\begin{aligned} g_{M,c} &= -kx_{\mathsf{ZPF}}(U_0/\hbar)\int|\Psi_0(\mathbf{x})|^2\sin(2k\tilde{x}_a)(1-2k^2x^2-\frac{y^2+z^2}{w_0^2})\,d^3\mathbf{x} \\ &= g_{M,c}^A(1-2k^2x_{a,0}^2), \end{aligned} \tag{4.90}$$

$$\begin{aligned} \Delta_N &= (U_0/\hbar)\int|\Psi_0(\mathbf{x})|^2(\cos^2(k\tilde{x}_a)(1-\frac{y^2+z^2}{w_0^2}) - \cos(2k\tilde{x}_a)k^2x^2)d^3\mathbf{x} \\ &= \Delta_N^A(1-\frac{y_{a,0}^2+z_{a,0}^2}{w_0^2}) - N\frac{g_0^2}{\Delta_{\mathsf{ca}}}k^2x_{a,0}^2\cos(2k\tilde{x}_a), \end{aligned} \tag{4.91}$$

$$\begin{aligned}\delta\omega_{M,c} &= \frac{U_0}{\hbar}k^2 x_{\mathrm{ZPF}}^2|\bar{c}|^2\int|\Psi_0|^2\big(\cos(2k\tilde{x}_a)(1-\frac{y^2+z^2}{w_0^2})-2k^2x^2\cos(2k\tilde{x}_a)\big)d^3\mathbf{x}\\ &= \delta\omega_{M,c}^A(1-2k^2x_{a,0}^2-\frac{y_{a,0}^2+z_{a,0}^2}{w_0^2}),\end{aligned} \tag{4.92}$$

where we used that $\int\Psi_0(\mathbf{x})u_a(\mathbf{x})xd^3\mathbf{x}=\sqrt{N}x_{a,0}$ and $\int|\Psi_0(\mathbf{x})|^2x^2d^3\mathbf{x}=Nx_{a,0}^2$. The results (4.88) - (4.92) resemble those of the Thomas-Fermi regime and those of the "super-atom". The width of the condensate in axial direction is given by $x_{a,0}$ and correspondingly the corrections of $g_{M,c}$, Δ_N and $\delta\omega_M$ scale with $kx_{a,0}$ instead of kR_x.

To summarize the result of this section very briefly: The expressions for the coupling constants of the model setup that we had found in a simplified picture could be confirmed by employing a more accurate treatment in terms of the Gross-Pitaevskii equation. We considered both the Thomas-Fermi regime as well as the non-interacting case. As already mentioned, we are planning to complement the calculations of the coupling constants (see section 4.7.3) by including the anharmonic term in the expansion of the dipole potential. This would give higher order corrections to the coupling constants due to the finite extent of the condensate.

Speaking of possible continuations of this work, we also have to mention that we have not included any calculations on the influence of other modes yet. We focused exclusively on the center-of-mass mode of the collective atomic motion. Certainly, this mode will be excited first of all, when for example the nodes of the light field are shifted along the cavity axis or when the intensity of the light field changes. However slight asymmetries in such processes can lead to excitations of other collective modes of the condensate. The anharmonic terms in the expansion of the dipole (or trapping) potential might also give rise to excitations into other modes. The dynamics of these excitations are strongly damped and their lifetime is much smaller than that of the center-of-mass oscillations, which - in the ideal case - is only limited by depletion. Still they might couple to the CM mode due to anharmonic terms and might induce a damping of the CM dynamics.

4.8 Coupled dynamics of the cantilever and the atomic CM motion

In this section we briefly sketch, how one could in principle observe the coupled dynamics of the atomic CM motion and the cantilever due to the relatively strong cavity-assisted coupling: One might observe oscillations of the two objects that alternate in time as the energy is swapped in between the two oscillators. The phenomenon is of course nothing else than the well-known beat case for the motion of two linearly coupled pendula. The other observation is a distinct quantum mechanical feature. Once strong coupling has been achieved, one might generate squeezed states of the atomic CM motion and the cantilever.

4.8.1 Swapping excitations between cantilever and atomic cloud

We consider an effective Hamiltonian of the linearly coupled system of cantilever ($\hat{b}$,ω_M) and the atomic CM motion ($\hat{a}$, ω_a):

$$\hat{H}=\hbar\omega_a\hat{a}^\dagger\hat{a}\;+\;\hbar\omega_M\hat{b}^\dagger\hat{b}\;+\;\hbar g_{\mathsf{eff}}(\hat{a}^\dagger+\hat{a})(\hat{b}^\dagger+\hat{b}). \tag{4.93}$$

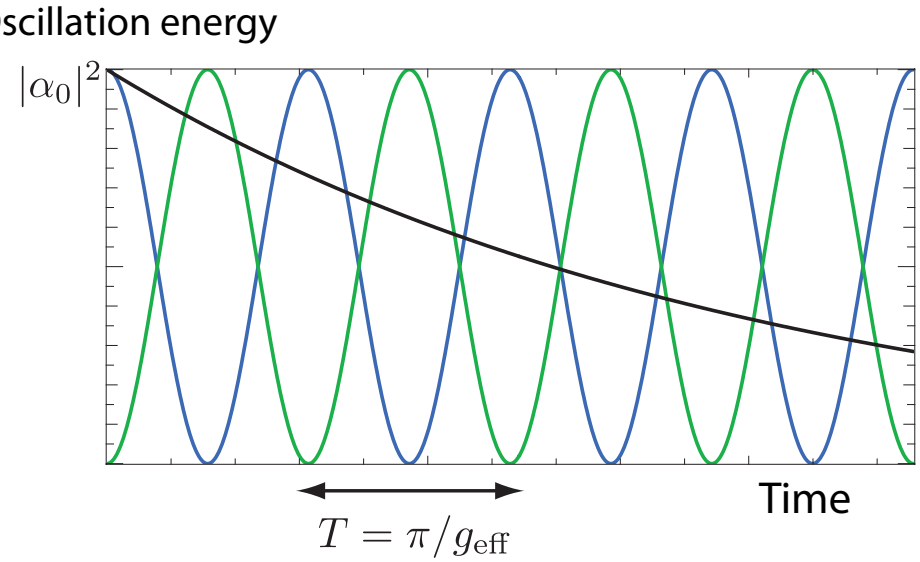

Figure 4.7: Swapping excitations between two oscillators: The energy transfers at a rate $2g_{\rm eff}$, where $g_{\rm eff}$ is the coupling between the two oscillators. The curves correspond to the squared amplitudes $|\alpha|^2$ (blue) and $|\beta|^2$ (green), as given in equation (4.95). The maximal oscillation energy is denoted by $|\alpha_0|^2$. The decay of the energy at rate Γ is sketched by the black line. The parameters chosen here are $\Gamma/g_{\rm eff} = 1/10$.

In order to illustrate the basic idea of the energy swapping in the simplest way, we will consider only the classical amplitudes α and β that correspond to $\hat{a}$ and $\hat{b}$. Furthermore we assume the frequencies of the atomic motion and the cantilever to be equal, $\omega = \omega_a = \omega_M$, and neglect the damping of their motion. In the rotating wave approximation with respect to ω, the equations of motion of the classical amplitudes α and β are given by

$$\begin{aligned} \dot{\alpha} &= -i\omega\alpha - ig_{\rm eff}\beta \\ \dot{\beta} &= -i\omega\beta - ig_{\rm eff}\alpha \end{aligned} \tag{4.94}$$

The solutions of these equations are harmonic oscillations at the frequencies $\Omega_\pm = \omega \pm g_{\rm eff}$. For example, initial conditions like $\alpha(t=0) = \alpha_0$, $\beta(t=0) = 0$ yield

$$\begin{aligned} \alpha(t) &= \frac{1}{2}\alpha_0\left(e^{-i\Omega_+ t} + e^{-i\Omega_- t}\right) \\ \beta(t) &= \frac{1}{2}\alpha_0\left(e^{-i\Omega_+ t} - e^{-i\Omega_- t}\right) \end{aligned} \tag{4.95}$$

Figure (4.7) shows these solutions by plotting the square of their absolute value. As $|\alpha|^2(t)$ and $|\beta|^2(t)$ directly correspond to the energy of the two oscillators, we see that the oscillation energy is swapped from one the other periodically. The rate of this energy transfer is given by $\Omega_+ - \Omega_- = 2g_{\rm eff}$. If the oscillators were subject to damping at a rate Γ, the oscillations would cease out on a time scale set by Γ^{-1}. We therefore see, that the discussed swapping excitations will only be observable, if the coupling $g_{\rm eff}$ is larger than the damping rate Γ. Note that for the assumed values of the proposed model, the cavity-assisted coupling between the cantilever and

the atomic motion was estimated to be $10^2\,\mathrm{Hz}$, larger than the mechanical damping rate of the cantilever. It might therefore be worthwhile to investigate this issue in an accurate treatment and analyse, if the swapping of excitations between the cantilever and the atomic cloud can be observered in such a system.

4.8.2 Squeezing

Let us now discuss a purely quantum mechanical effect that might occur in the case of strong coupling between the cantilever and the atomic motion. We again consider the Hamiltonian

$$\hat{H} = \hbar\omega_a \hat{a}^\dagger \hat{a} \; + \; \hbar\omega_M \hat{b}^\dagger \hat{b} \; + \; \hbar g_{\mathsf{eff}} (\hat{a}^\dagger + \hat{a})(\hat{b}^\dagger + \hat{b}). \tag{4.96}$$

Our goal is to briefly illustrate the very basic idea and treat the system in the simplest possible manner. We therefore neglect damping and any driving terms.

Note that the coupling g_{eff} depends on the intensity of the cavity field $|\bar{c}|^2$. The basic idea is now to modulate the intensity of the light field in the form $|\bar{c}|^2(t) = |\bar{c}|^2 \cos^2(\omega t)$, with a frequency ω that is close to the sum of ω_a and ω_M. The rotating wave approximation with respect to ω allows us to introduce the effective Hamiltonian:

$$\hat{H} = \hbar\Delta_a \hat{a}^\dagger \hat{a} \; + \; \hbar\Delta_M \hat{b}^\dagger \hat{b} \; + \; \hbar g_{\mathsf{eff}} (\hat{a}^\dagger \hat{b}^\dagger + \hat{a}\hat{b}) + \; \hat{H}_{\Gamma_M} + \hat{H}_{\Gamma_a}, \tag{4.97}$$

where $\Delta_a = \omega - \omega_a$ and $\Delta_M = \omega - \omega_M$.
The corresponding Heisenberg equations of motion for the operators $\hat{a}^\dagger$ and $\hat{b}$ are given by

$$\begin{aligned} \frac{d}{dt}\hat{a}^\dagger &= \frac{[\hat{a}^\dagger, \hat{H}]}{i\hbar} \\ &= -i\Delta_a \hat{a}^\dagger + i g_{\mathsf{eff}} \hat{b} \end{aligned} \tag{4.98}$$

$$\begin{aligned} \frac{d}{dt}\hat{b} &= \frac{[\hat{b}, \hat{H}]}{i\hbar} \\ &= i\Delta_M \hat{b} - i g_{\mathsf{eff}} \hat{a}^\dagger. \end{aligned} \tag{4.99}$$

Focusing on the special case of equal frequencies of the cantilever and the atomic motion and $\omega = \omega_a = \omega_M$, i.e. $\Delta_a = \Delta_M = 0$, these equations have the solution

$$\begin{aligned} \hat{a}^\dagger(t) &= \cosh(g_{\mathsf{eff}} t)\hat{a}_0^\dagger - i\sinh(g_{\mathsf{eff}} t)\hat{b}_0, \\ \hat{b}(t) &= \cosh(g_{\mathsf{eff}} t)\hat{b}_0 + i\sinh(g_{\mathsf{eff}} t)\hat{a}_0^\dagger, \end{aligned} \tag{4.100}$$

where $\hat{a}_0 = \hat{a}(t=0)$, $\hat{b}_0 = \hat{b}(t=0)$.

In order to observe a squeezed state in an experiment, one has to look for signatures of squeezing in the correlations of the two oscillators. We therefore turn to a correlator that should in principle be measurable by reading out the spectrum of the cavity field. More precisely we consider the correlator

$$C_{a,b}(t) \;=\; \langle (e^{i\varphi}\hat{a}^\dagger(t) + e^{-i\varphi}\hat{a}(t))(e^{i\varphi}\hat{b}^\dagger(t) + e^{-i\varphi}\hat{b}(t)) \rangle. \tag{4.101}$$

As a first estimate, we try to figure out if any squeezing effects can be observed in a fully thermalized system. In doing so we assume that $\langle \hat{a}^\dagger \hat{a} \rangle_{t=0} = \bar{n}_a$, $\langle \hat{b}^\dagger \hat{b} \rangle_{t=0} = \bar{n}_b$, $\langle \hat{a}\hat{a} \rangle_{t=0} = 0$, $\langle \hat{b}^\dagger \hat{a} \rangle_{t=0} = 0$, etc., and that the coupling g is switched on at $t = 0$. In the simplest case, for $\Gamma_a = \Gamma_M = 0$, the correlator is given by

$$C_{a,b}(t) \quad = \quad \sin(2\varphi)(\bar{n}_a + \bar{n}_b + 1)\sinh(2g_{\mathsf{eff}}t). \tag{4.102}$$

Hence, we see that correlations build up and can even grow exponentially.

Certainly, this discussion only gave a very rough sketch. It can not answer the question, if the generation of squeezed states between the cantilever and the atomic motion is possible. However we illustrated, that a relatively simple mechanism, namely the modulation of the intensity of the cavity field, might allow to study the phenomenon of squeezing in this system.

4.9 Fock state detection

So far we have focused our discussion on the linear coupling between the cavity and the CM position operator of the atoms, $\hat{x}_a$. As we have seen, it leads to an interaction term $\propto \hat{x}_a \hat{c}^\dagger \hat{c}$ and therefore resembles the generic optomechanical coupling between the cavity and the cantilever. However, the proposed setup also allows for a dispersive coupling of the form $\propto \hat{x}_a^2 \hat{c}^\dagger \hat{c}$, if the atomic cloud sits at a minimum of the dipole potential (4.16). An analogous situation can be found in the "membrane-in-the-middle"-setup when the membrane is placed at an extremum of $\omega_{\mathsf{cav}}(x_M)$ (4.116). It has already been shown for this setup, that a detection of the membrane's phonon number should be realizable [14]. In the following we will discuss the possibility of performing a dispersive, quantum-non-demolition measurement of the motional Fock state of the atoms' collective motion.

To begin with, we refresh the basic setup of figure (4.3) by some minor modifications. Again we assume an atomic cloud interacting with the standing wave of a cavity field, but disregard the cantilever for this consideration. In the context of a Fock state detection the cantilever motion would only induce an additional phase shift proportional to its displacement. Regarding the trapping of the atoms we again employ an additional potential such that the atomic cloud is confined by a trapping potential $V_{\mathsf{eff}} \approx \frac{Nm_a}{2}\omega_a \delta\hat{x}_a^2$. However this time we assume that the minimum of V_{eff} coincides with a antinode of the cavity field, i.e. there is no additional shift due to the trapping potential. In the notation of the preceding sections this implies that $\tilde{x}_a = 0$. Accordingly, for small displacements of the atomic cloud the interaction between the atoms and the cavity field is given by a term

$$\hbar N \frac{g_0^2}{\Delta_{\mathsf{ca}}}(1 - k^2\delta\hat{x}_a^2)\hat{c}^\dagger\hat{c} = (NU_0 - \frac{1}{2}\hbar\delta\omega(\hat{a}^\dagger + \hat{a})^2)\hat{c}^\dagger\hat{c}, \tag{4.103}$$

where we defined the coupling constant

$$\delta\omega = 2NU_0k^2(x_{a,0}^{(N)})^2/\hbar. \tag{4.104}$$

This term will later turn out to be the optical frequency shift due to a single phonon of the atoms' oscillation. In this context we recall the explicit expression for the zero-point width of the atomic CM motion: $x_{a,0}^{(N)} = \sqrt{\frac{\hbar}{2Nm_a\omega_a}}$. Plugging it into (4.104) reveals that the frequency shift $\delta\omega$ is independent of the number of atoms N contained in the atomic cloud: $\delta\omega = U_0k^2/(m_a\omega_a)$.

To summarize this preliminary discussion we specify the Hamiltonian as

$$\begin{aligned}\hat{H} &= \hbar(-\Delta+\Delta_N-\frac{1}{2}\delta\omega(\hat{a}^\dagger+\hat{a})^2)\hat{c}^\dagger\hat{c}+\hbar\tilde{\omega}_a\hat{a}^\dagger\hat{a}\\ &+ \hbar\alpha_L(\hat{c}+\hat{c}^\dagger)+\hat{H}_\kappa. \end{aligned} \tag{4.105}$$

We see that the frequency of the cavity depends on $\hat{x}_a^2$. Hence this setup, in principle, allows to extract information about $\hat{x}_a^2$ from the measurement beam. If the cavity ring-down time κ^{-1} is much larger than the period of the atomic CM oscillation, i.e. $\kappa \ll \omega_a$, the cavity field effectively measures the time averaged $\hat{x}_a^2$ which becomes the phonon number:

$$\frac{1}{2}\delta\omega\langle(\hat{a}^\dagger e^{i\omega_a t}+\hat{a}e^{-i\omega_a t})^2\rangle_t = \delta\omega(\hat{a}^\dagger\hat{a}+\frac{1}{2}). \tag{4.106}$$

In the following we illustrate how the phase shift of a single phonon can be extracted from the signal beam, and what requirements have to be fulfilled regarding the measurement time and the phonon lifetime. We start with a description of the cavity field in the standard input-output formalism (see for example [66, 67]):

$$\begin{aligned}\frac{d}{dt}\hat{c} &= i(\Delta-\frac{\delta\omega}{2}(\hat{a}^\dagger+\hat{a})^2)\hat{c}-\frac{\kappa}{2}\hat{c}-\sqrt{\kappa}\hat{\alpha}_{\text{in}}\\ \frac{d}{dt}\hat{c} &= i(\Delta-\frac{\delta\omega}{2}(\hat{a}^\dagger+\hat{a})^2)\hat{c}+\frac{\kappa}{2}\hat{c}-\sqrt{\kappa}\hat{\alpha}_{out}\end{aligned} \tag{4.107}$$

$\hat{\alpha}_{\text{in}}$ and $\hat{\alpha}_{\text{out}}$ denote the operators for the input (output) fields of the cavity. It follows that

$$\hat{\alpha}_{\text{out}}(t)+\hat{\alpha}_{\text{in}}(t)=\sqrt{\kappa}\hat{c}(t) \tag{4.108}$$

and, by solving (4.107) in Fourier space ($\hat{c}(t)=\frac{1}{\sqrt{2\pi}}\int e^{-i\omega t}\hat{c}(\omega)d\omega$ etc.),

$$\hat{\alpha}_{\text{out}}(\omega)=\frac{1+\frac{2i}{\kappa}(\Delta-\frac{\delta\omega}{2}(\hat{a}^\dagger+\hat{a})^2(\omega)+\omega)}{1-\frac{2i}{\kappa}(\Delta-\frac{\delta\omega}{2}(\hat{a}^\dagger+\hat{a})^2(\omega)+\omega)}\hat{\alpha}_{\text{in}}(\omega). \tag{4.109}$$

We introduce a reflection coefficient by defining $r := \frac{|\bar{\alpha}_{\text{out}}|}{|\bar{\alpha}_{\text{in}}|}$, using the classical, time-averaged amplitudes $|\bar{\alpha}_{\text{in}}|$ and $|\bar{\alpha}_{out}|$. As we consider the cavity to be lossless, the absolute value of r is 1 and we can write

$$r := e^{i\theta_{\text{total}}}=\frac{1+\frac{2i}{\kappa}(\Delta-\delta\omega(\langle\hat{a}^\dagger\hat{a}\rangle+\frac{1}{2}))}{1-\frac{2i}{\kappa}(\Delta-\delta\omega(\langle\hat{a}^\dagger\hat{a}\rangle+\frac{1}{2}))}. \tag{4.110}$$

If the measurement beam is resonant with the cavity, i.e. $\Delta = 0$, the phase shift of a single phonon is given by $\theta = \frac{4\delta\omega}{\kappa}$, as can be found by expanding the expression for the reflectivity in the limit $\kappa \gg \delta\omega$:

$$\begin{aligned} r &= \frac{\frac{\kappa}{2}-i\delta\omega(\langle\hat{a}^\dagger\hat{a}\rangle+\frac{1}{2})}{\frac{\kappa}{2}+i\delta\omega(\langle\hat{a}^\dagger\hat{a}\rangle+\frac{1}{2})}\\ &= (\kappa-2i\delta\omega(\langle\hat{a}^\dagger\hat{a}\rangle+\frac{1}{2}))(\frac{1}{\kappa}-2i\frac{\delta\omega(\langle\hat{a}^\dagger\hat{a}\rangle+\frac{1}{2})}{\kappa^2}+...)\\ &\approx 1-i\frac{4\delta\omega(\langle\hat{a}^\dagger\hat{a}\rangle+\frac{1}{2})}{\kappa}. \end{aligned} \tag{4.111}$$

The phase of the cavity output beam can be measured by letting it interfere with a reference beam, a concept which is for example realized in homodyne detection.

Shot noise of the signal beam imposes an uncertainty $\delta\theta$ in the detection of the phase, though. The more photons (N_{phot}) are contained in the output beam, the smaller this uncertainty becomes. This can be seen by employing the common number-phase-uncertainty relation, $\delta N_{\text{phot}}^2 \delta\theta \sim 1$, for a coherent beam with $\delta N_{\text{phot}}^2 \sim N_{\text{phot}}$. It follows that

$$\delta\theta \sim \frac{1}{\sqrt{N_{\text{phot}}}}. \tag{4.112}$$

If we demand a signal-to-noise ratio of $\frac{\delta\theta}{\theta} \sim 1$, a number of $N_{\text{phot}} \sim \frac{1}{\theta^2}$ photons from the measurement beam is needed. For a photon flux of $\dot{N}_{\text{phot}}$ this turns into a required measurement time of

$$\tau = \frac{N_{\text{phot}}}{\dot{N}_{\text{phot}}} = \frac{1}{\theta^2 \dot{N}_{\text{phot}}} = \frac{\kappa^2}{16\delta\omega^2 \dot{N}_{\text{phot}}}. \tag{4.113}$$

An important restriction on this measurement time is given by the preliminary requirement that the atoms' CM motion is not perturbed by the measurement. This yields that we have to demand

$$\omega_a \tau \gg 1. \tag{4.114}$$

To see whether all these requirements can be met in a realistic setup, we now plug in the numbers. Consulting the table (4.1) once again, we see that $U_0 \approx 10^3\,\text{Hz}$, $k^2 \approx 10^7\,\text{m}^{-1}$, $\omega_a \approx 10^5\,\text{Hz}$ and $m_a \approx 10^{-25}\,\text{kg}$ lead to $\delta\omega = U_0 k^2/(m_a\tilde{\omega}_a) \approx 10^3\,\text{Hz}$. We note, that a higher atom-cavity interaction $U_0 \approx \hbar\, 10^5\,\text{Hz}$ is realizable. However, this would make the frequency shift of a single phonon larger than the cavity decay rate, which we assume to be $\kappa \approx 10^4\,\text{Hz}$ in this estimate. Yet we have to demand that $\kappa > \delta\omega$ to stay in the linear regime of equation (4.111), and in order to be able to resolve a single quantum jump between to adjacent Fock states. The relatively low value of κ is probably the most challenging requirement for the implementation. It is necessary to keep $\omega_a > \kappa$.

The condition imposed on the measurement time ($\omega_a\tau \gg 1$) can be fulfilled by tuning the intensity of the signal beam $\dot{N}_{\text{phot}}$:

$$\omega_a \tau = \frac{\omega_a}{\theta^2 \dot{N}_{\text{phot}}} = \frac{\omega_a \kappa^2}{16\delta\omega^2 \dot{N}_{\text{phot}}}. \tag{4.115}$$

Inserting the numbers, we see that $\omega_a\tau = 10^7 \frac{1}{16\dot{N}_{\text{phot}}}\, s^{-1}$ and $\omega_a\tau \gg 1$ can be reached by employing an incoming photon flux $\dot{N}_{\text{phot}} \approx 10^4\, s^{-1}$ or smaller. This would correspond to an incoming laser power of $P_{\text{in}} = \hbar\omega_{\text{cav}}\dot{N}_{\text{phot}} \approx 10^{-15}\, W$ and an average number of intracavity photons of $\bar{n}_{\text{cav}} \approx 1$.

Certainly there is another restriction that we have not considered yet: The measurement time has to be smaller than the lifetime of a phonon in order to resolve quantum jumps between the Fock states. This lifetime is determined by the coupling of the atomic cloud to its environment. However, in this setup it is not immediately which will be the foremost source of decoherence for the atomic motion. For example, it could well be the case that in the presence of the mechanical resonator the atomic motion is heated up due to the thermal motion of the mechanical element.

Even though this investigation has to be continued, we can already state, that very basic requirements for a Fock-state detection can be met in the proposed model. If implemented in

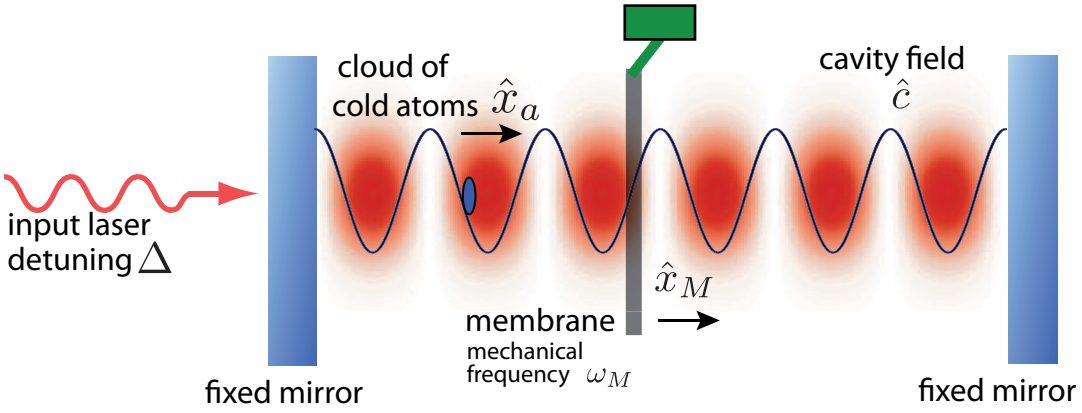

Figure 4.8: "Membrane-in-the-middle"-setup: A membrane and a cloud of cold atoms are coupled to the standing wave of a cavity field. In analogy to the previously considered model (figure 4.3),

an experiment, this would for example allow to observe the quantum jumps in the evolution of the atomic motion as it heats up. Moreover, if the CM mode of the atoms couples to another mechanical oscillator, e.g. a cantilever, one might be able to characterize the effects of the atom-cantilever interaction by reading out the Fock state of the atomic motion.

4.10 Variations of the model

A major technical challenge for general optomechanical setups (figure (1.1)) is imposed by the integration of a highly sensitive mechanical resonator into a high-finesse cavity. It is possible to resolve this difficulty by placing a small micro-mechanical resonator in between two fixed high-finesse mirrors. This concept was implemented by the Harris group in their "membrane-in-the-middle"-setup, that allowed them to cool down the mechanical element, the "membrane", to a temperature of $7\,mK$ [14]. Of course a high cavity finesse is very desirable in our proposed setup (figure (4.3)) as well. Quite generally, it would allow for a better manipulation of the mechanical resonator by the cavity field, especially in terms of ground-state cooling [15, 16]. Moreover, a small cavity decay rate κ allows for strong cavity-assisted coupling between the atoms and the mechanical oscillator as we have seen in section (4.6.3).

Figure (4.8) illustrates our model setup: Both a mechanical resonator and a cloud of cold atoms are inserted in a cavity. We assume the atoms to be trapped by an additional trapping potential which is not depicted here. Accordingly, the atoms' equilibrium (CM) position is shifted away from an antinode of the cavity field. This is a prerequisite for the cavity-assisted coupling between the cantilever and the atomic cloud.

The most striking difference in comparison to the model of figure (4.3) is that the cavity length no longer is determined by the position of the mechanical resonator. Hence the spatial structure of the intracavity light field does no longer depend on the position of the mechanical resonator in the way of equations (4.5) and (4.16). If the membrane is sufficiently thin, we can even neglect the modification of the intensity profile due to its presence. This is analogous to the argument we gave when disregarding the back-action of the atoms on the cavity field. As a consequence there is no direct membrane-atom coupling comparable to $g_{a,M}$.

Nevertheless we can resume the discussion of section (4.6) and consider the effective coupling

$g_{\text{eff}} = g_{a,c} g_M |\bar{c}|^2 \left(\frac{1}{\omega - \Delta} - \frac{1}{\omega + \Delta} \right)$. The coupling of the atomic cloud to the cavity ($g_{a,c}$) will be of the same kind as considered above (see for example table (4.3)) and requires an additional trapping potential. To understand the cavity-membrane coupling of this setup, we adopt the reasoning given in ([14]). The dependence of the cavity resonance frequency on the position x_M of the membrane is given by

$$\omega_{\text{cav}}(x_M) = \frac{c}{L} \cos^{-1} \Big(|r_c| \cos(4\pi x_M / \lambda) \Big), \tag{4.116}$$

where r_c denotes the reflectivity of the membrane and L the length of the cavity. The membrane can be placed at practically any position inside the cavity by using a piezoelectric positioner. An expansion of (4.116) around $x_M = \lambda/8$ produces a term of the form

$$\omega_{\text{cav}}(x_M) \approx \omega_{\text{cav},0} + \frac{g_M}{x_{\text{ZPF}}} (x_M - \bar{x}_M), \tag{4.117}$$

where $g_M = x_{\text{ZPF}} \frac{d\omega_{\text{cav}}}{dx_M}(x_M = \frac{\lambda}{8}) = x_{\text{ZPF}} \frac{\omega_L}{L/2} |r_c|$. This expression reveals that the "membrane-in-the-middle"-setup allows for the standard optomechanical coupling in the form of a term $\hbar g_M (\hat{b}^\dagger + \hat{b}) \hat{c}^\dagger \hat{c}$. The coupling constant differs only by a factor of $2|r_c|$ from the one of the standard setup. In view of the previous estimates on the effective coupling strength g_{eff} we state that strong coupling between the membrane and the atomic clouds seems achievable. We note that this particular setup not only allows for an improved cavity finesse, but also for a smaller mass of the mechanical resonator: The mass of the membrane in the Yale setup is for example $m_M \approx 10^{-11}\,\text{kg}$. As the mass enters the expression of the effective coupling strength in the form $\sqrt{\frac{N m_a \omega_a}{m_M \omega_M}}$, a small value of m_M is in favour of strong coupling.

As a final remark we mention another possible extension of this setup that would involve two atomic clouds at different lattice sites. Again one could make use of the cavity-assisted coupling and observe the coupled dynamics of their center-of-mass motions. In this case the masses of both mechanical objects would be nearly equal and a major obstacle for the achievement of strong coupling would vanish.

4.11 Overview on the various coupling mechanisms

Before concluding this chapter we will give a summary of the coupling mechanisms that we encountered in the investigating of the model setup. This setup comprises an optical cavity, a cantilever and the CM mode of a cloud of cold atoms.

Already in its simplest form, without an additional trapping potential, the proposed setup leads to a direct coupling between the atomic motion and the cantilever. It arises due to the shift of the cavity field when the cantilever moves. The value of the corresponding coupling constant is small compared to typical mechanical damping rates of the cantilever.

A much stronger contribution to the coupling between the cantilever and the CM motion of the atoms is given by a second order term that involves the transitions to virtual cavity-states. This coupling mechanism relies on the fact that both the atomic cloud, when shifted by an external potential, and the cantilever (via the radiation pressure) couple strongly to the cavity.

We note however that the coupling between the atomic cloud and the cavity can not be made arbitrarily large. We can understand this point by reconsidering the discussion of a possible Fock state measurement: If the coupling between the atomic motion and the cavity is very strong, it might induce a phonon measurement even if it is not intended. In this context we can for

example reconsider the swap experiment which we discussed in section (4.8.1). Even though the mechanism of this experiment relies on the linear coupling terms of the system, the quadratic coupling terms also have to be considered and inevitably will lead to a phonon measurement (even if this information is not used). This measurement can destroy the coherent oscillations of the atomic cloud, as the back-action of the measurement on the atomic motion leads to dephasing. Certainly, this unwanted phonon measurement is only one of many points that still have to be checked in terms of measurement back-action. In a sense all these effects are somehow the "backside of the coin": Once a system shows considerable quantum effects, it will be harder and harder to observe them.

Concluding remarks and future perspectives

What we aimed at with this thesis, was to examine and elaborate the specific features of optomechanical systems in the quantum regime. We presented a fully quantum-mechanical treatment of a driven optical cavity coupled to a mechanical oscillator by radiation pressure. It provided insights into the influence of photon shot noise and quantum fluctuations on the coupled dynamics of the cavity-cantilever system. The introduction of a quantum parameter allowed to keep track of the way these results converge towards the classical solutions. Setups that realize a coupling between the mechanical motion of a cloud of cold atoms and a single cavity mode, should allow to observe strong quantum effects. We resumed the basic idea of these experiments and proposed a model setup: It consists of a BEC in a standing light wave of a cavity where one of the cavity's end mirrors is built from an oscillating cantilever.

Let us recapitulate the work in more detail: In the first chapter of this thesis we introduced the basics of optomechanical systems. Such a system consists of a cavity whose resonance frequency depends on the position of a mechanical element, e.g. a cantilever. The interaction between the cavity and the cantilever via radiation pressure leads to an effective contribution to the damping rate of the mechanical resonator. This optical damping rate can reduce the thermal motion of the cantilever and might ultimately cool it to the ground state. On the other hand, if it yields a negative contribution to the damping rate, it can heat the cantilever motion or even induce an instability above some laser power threshold. In the latter case, the full nonlinearity of the system shows up and leads to self-sustained oscillations of the cantilever at fixed amplitude.

We focused on this instability in the second chapter and compared the classical predictions for the amplitude of the cantilever motion to the results from a numerical simulation of a quantum master equation. We studied the crossover between the quantum and the classical regime, which is governed by the quantum parameter, $\zeta = x_{\mathsf{ZPF}}/x_{\mathsf{FWHM}}$, denoting the ratio between the mechanical zero-point fluctuation amplitude and the width of the optical resonance. In regions of dynamical multistability, the different attractors show up simultaneously in the steady state of the cantilever, since the quantum noise can induce transitions between those attractors. By employing semiclassical Langevin equations we were able reproduce the main features of the results from the quantum master equation, at least within a suitable parameter regime. Below the threshold of instability, a simple rate-equation approach compares well to the full quantum results for the cantilever occupation. Finally, we characterized the mechanical motion in the various regimes by discussing the phonon number probability distribution as well as the Wigner density.

In the last two chapters of this thesis we directed our attention towards optomechanical setups that involve the motion of a cloud of cold atoms. A general introduction to basic concepts of the dynamics of a trapped, Bose-condensed gas was presented in chapter 3. We focused on

a particular model setup in chapter 4: Starting with an optomechanical setup of the generic type, i.e. a cavity and a cantilever interacting via radiation pressure, we added a cloud of cold atoms confined to a single well of the cavity field. A linearized Hamiltonian revealed the basic couplings between the cavity field, the cantilever and the center-of-mass mode of the atoms. The corresponding coupling constants and frequency shifts where estimated in a simplified picture. A more accurate calculation based on the mean-field description of a Bose-condensed gas gave only minor corrections to these estimates. Furthermore we were able identify a cavity-assisted coupling between the cantilever and the atomic motion. This coupling turned out to be much stronger than the direct coupling term for realistic parameters.

Once a strong coupling of the cantilever and the atomic cloud is eventually realized in experiment, it will open up several interesting opportunities: One might observe the two oscillators to swing alternately as the oscillation energy swaps between them. Another possibility would be to generate squeezed state of the two oscillators.

We also briefly discussed a possible QND read out for the atomic motion, i.e. a detection of the Fock state of the atomic motion. This would further enhance the possibilities of this setup and might allow to observe uniquely quantum-mechanical effects in this model setup. One might for example watch the evolution of the atomic cloud as it heats up due to the coupling to the cantilever. In the ideal case one should then be able to resolve the quantum jumps of this evolution.

Further extensions of this setup could for example involve the coupling of an atomic cloud to a mechanical membrane. In this case one could even think of a dispersive readout that would detect the sum of phonon numbers of both elements. With such a scheme one could potentially generate entanglement between the atomic motion and the cantilever. Such a scheme for the case of two (or more) mechanical membranes has for example been proposed recently [68].

Before dealing with such future goals however, we certainly have to elaborate on some points of the recent work. The cavity-assisted coupling mechanism has to be contrasted thoroughly with all possible sources of decoherence and dissipation. Possible applications of this coupling (swap, squeezing) were only discussed briefly and a more detailed analysis is certainly needed. Moreover the ongoing experiments in this field will provide new input to our work. In particular, the very recent results of the Esslinger group [50], should bring new insight. Their data, which was published only a few days before this thesis was handed in, shows the observation of bistability in the coupled cavity-BEC system and can now for example directly be compared to the results of the quantum master equation.

The quantum-to-classical transition, that we discussed in the first chapters of this thesis, provides a number of links to new issues. An optomechanical setup can exhibit chaotic behaviour when driven at high laser power (see for instance [18]). The emergence of chaos in a quantum system reveals many interesting questions (see for example [69, 70, 71]) and the analysis of the quantum-to-classical transition of a chaotic, nonlinear oscillator has already provided interesting features [72]. It might therefore be worthwhile to perform a similar analysis for a chaotic optomechanical system.

Appendix A

Numerical methods

In large part the results of chapter 2 are based on the numerical simulation of the master equation for the density matrix. In this appendix we will go into the details of the numerical methods and explain how we represent the density matrix, how we find its steady-state solution and how we extract the quantities of interest from the resulting density matrix.

A.1 Representation of the density matrix

An appropriate representation of the density matrix under consideration is given in the combined Fock space of the cavity-cantilever system. The density matrix elements are given by $\langle n'_M, n'_{\mathsf{cav}}|\hat{\rho}|n_M, n_{\mathsf{cav}}\rangle$, where $|n_M\rangle = \frac{1}{\sqrt{n_M!}}(\hat{b}^\dagger)^{n_M}|0\rangle$ and $|n_{\mathsf{cav}}\rangle = \frac{1}{\sqrt{n_{\mathsf{cav}}!}}(\hat{c}^\dagger)^{n_{\mathsf{cav}}}|0\rangle$ are number states of the cantilever and the cavity field respectively. To arrive at a finite dimensional density matrix we have to truncate the Fock space and consider only the lowest energy eigenstates of the cantilever and the cavity field, i.e. $n_M < N_M$ and $n_{\mathsf{cav}} < N_{\mathsf{cav}}$.

In order be able to access the matrix elements in the common format of rows and columns, we introduce a "super-index" $J(n_M,n_{\mathsf{cav}}) = n_M + n_{\mathsf{cav}}N_M$. Even though this mapping and its inverse are used in all the subsequent steps of the computation, we do not pinpoint that issue in the following but stick to the notation $\langle n'_M, n'_{\mathsf{cav}}|\hat{\rho}|n_M, n_{\mathsf{cav}}\rangle$. We emphasize though, that we are dealing with a density matrix of size $(N \times N)$, where $N = N_M \cdot N_{\mathsf{cav}}$.

A.2 Time-evolution of the density matrix

The coupled cavity-cantilever system is described by the Hamiltonian (1.1)

$$\begin{aligned} \hat{H} &= \hbar\left(-\Delta + g_M\left(\hat{b}+\hat{b}^\dagger\right)\right)\hat{c}^\dagger\hat{c} \;+\; \hbar\omega_M\hat{b}^\dagger\hat{b} \;+\; \hbar\alpha_L(\,\hat{c}+\hat{c}^\dagger\,) \;+\; \hat{H}_\kappa \;+\; \hat{H}_{\Gamma_M} \\ &= \hat{H}_0 + \hat{H}_\kappa + \hat{H}_{\Gamma_M} \end{aligned} \tag{A.1}$$

As already mentioned in section (2.3), the time evolution of the system's density matrix at zero temperature is governed by a master equation of Lindblad form

$$\frac{d}{dt}\hat{\rho} \;=\; \frac{[\hat{H}_0,\hat{\rho}]}{i\hbar} \;+\; \Gamma_M\,\mathcal{D}[\hat{b}] \;+\; \kappa\,\mathcal{D}[\hat{c}], \tag{A.2}$$

where

$$\mathcal{D}[\hat{A}] = \hat{A}\hat{\rho}\hat{A}^\dagger - \frac{1}{2}\hat{A}^\dagger\hat{A}\hat{\rho} - \frac{1}{2}\hat{\rho}\hat{A}^\dagger\hat{A} \tag{A.3}$$

denotes the standard Lindblad operator. The coherent part of the time evolution is given by $\frac{[\hat{H}_0,\hat{\rho}]}{i\hbar}$, while the Lindblad terms take account of the cavity decay and the damping of the mechanical oscillator. The time evolution of the matrix elements can be readily inferred form (A.2) by noting that the right-hand side of (A.2) can be expressed in terms of the operators $\hat{b}$, $\hat{b}^\dagger$, $\hat{c}$ and $\hat{c}^\dagger$ and by using that $\hat{b}|n_M\rangle = \sqrt{n_M}|n_M - 1\rangle$ and $\hat{c}|n_{\mathsf{cav}}\rangle = \sqrt{n_{\mathsf{cav}}}|n_{\mathsf{cav}} - 1\rangle$. The result will be a coupled set of N^2 coupled, linear differential equations

$$\frac{d}{dt}\langle n'_M, n'_{\mathsf{cav}}|\hat{\rho}|n_M, n_{\mathsf{cav}}\rangle = \langle n'_M, n'_{\mathsf{cav}}|\Big(\frac{[\hat{H}_0,\hat{\rho}]}{i\hbar} + \Gamma_M\,\mathcal{D}[\hat{b}] + \kappa\,\mathcal{D}[\hat{c}]\Big)|n_M, n_{\mathsf{cav}}\rangle. \tag{A.4}$$

In particular, the right-hand side of (A.4) will couple the matrix element $\langle n'_M, n'_{\mathsf{cav}}|\hat{\rho}|n_M, n_{\mathsf{cav}}\rangle$ to ten other matrix elements. The set of differential equations can now be written as

$$\frac{d}{dt}\vec{\rho} = \mathcal{L}\vec{\rho}, \tag{A.5}$$

where $\vec{\rho}$ is a vector that consists of all the N^2 elements of the density matrix. Consequently, the Liouvillian $\mathcal{L}$ is a $(N^2 \times N^2)$-matrix. In our case, in the rotating frame with respect to the laser frequency, the Liouvillian $\mathcal{L}$ is time-independent and the formal solution of (A.5) is given by

$$\vec{\rho}(t) = e^{\mathcal{L}t}\vec{\rho}. \tag{A.6}$$

The procedure that brought the master equation (A.2) into the form of a matrix vector equation (A.5) can be summarized in a more formal way. In doing so, we define an operation that transforms a $(N \times N)$ matrix $\hat{A}$ into a N^2 dimensional vector $\overrightarrow{\hat{A}}$:

$$\hat{A} = (A_{ij}) \longrightarrow \overrightarrow{\hat{A}} = (A_{11}, A_{12}, A_{13}, \ldots, A_{21}, A_{22}, \ldots A_{31}, \ldots)^T,$$

where $()^T$ denotes the transpose. It can be shown, that the transformation of a product of three $(N \times N)$ matrices, $\hat{A}\hat{\rho}\hat{B}$, into the vector $\overrightarrow{\hat{A}\hat{\rho}\hat{B}}$ can be rewritten as a matrix-vector multiplication for the vector $\overrightarrow{\hat{\rho}}$:

$$\overrightarrow{\hat{A}\hat{\rho}\hat{B}} = (\hat{B}^T \otimes \hat{A})\,\overrightarrow{\hat{\rho}}\,. \tag{A.7}$$

The right-hand side of equation (A.2) can be represented in terms of the form $\hat{A}\hat{\rho}\hat{B}$, where $\hat{A}$ and $\hat{B}$ can be either $\hat{b}$, $\hat{b}^\dagger$, $\hat{c}$, $\hat{c}^\dagger$ or $\mathbf{1}$. An application of formula (A.7) therefore directly leads to (A.5).

When looking for a solution of this equation, it is instructive to recall its physical meaning: We can assume that the system relaxes to a unique equilibrium. Therefore the spectrum of eigenvalues of $\mathcal{L}$ has to consist of a single eigenvalue 0, while all other eigenvalues have a negative real part. Accordingly, in the long-time limit the density matrix is given by the eigenvector $\vec{\rho}_0$ corresponding to the eigenvalue zero. All other contributions of the eigenvalue decomposition have decayed for $t \to \infty$. To find the stationary solution of the Liouville equation (A.5), it then suffices to evaluate the eigenvector $\vec{\rho}_0$. To this end we employ the Arnoldi method which solves for a few eigenvalues and eigenvectors of $\mathcal{L}$ by iterative projection and thereby makes use of the sparse structure of $\mathcal{L}$. We will comment on the details of that method and on its implementation below in more detail.

Quite generally, an evolution according to the Lindblad master equation preserves the defining properties of the density matrix. For our method of finding the stationary solution this is not the case: it does not preserve the correct normalization. We therefore divide the density matrix, that was output by the eigenvalue solver, by its trace and finally arrive at a steady state density matrix $\hat{\rho}$, with $Tr\{\hat{\rho}\} = 1$.

A.3 The Arnoldi method

By far the biggest obstacle we face when considering the eigenvalue problem of equation (A.5) is the huge size of the Liouvillian matrix $\mathcal{L}$. Even if we take into account only a few energy levels for both the cantilever and the cavity field, i.e. $n_M < N_M$ and $n_{\mathsf{cav}} < N_{\mathsf{cav}}$, the problem turns out to be very challenging, because the size of $\mathcal{L}$ scales as $(N^2 \times N^2) = (N_M^2 \cdot N_{\mathsf{cav}}^2 \times N_M^2 \cdot N_{\mathsf{cav}}^2)$. However, there is a workaround: We can make use of the sparse structure of the Liouvillian matrix. The differential equation for a single density matrix element $\langle n'_M, n'_{\mathsf{cav}}|\hat{\rho}|n_M, n_{\mathsf{cav}}\rangle$ (A.4) contains only ten contributions from other matrix elements. If one of the indices is at the edge of the truncated energy spectrum, e.g. $n_M = N_M - 1$, the differential equation loses one of these contributions from adjacent matrix elements, as $\langle n'_M, n'_{\mathsf{cav}}|\hat{\rho}|N_M, n_{\mathsf{cav}}\rangle \equiv 0$. According to this analysis, the Liouvillian matrix has (less than) $10 \cdot N$ off-diagonal elements and in total (less than) $11 \cdot N$ elements. Therefore the number of floating point operations necessary for a matrix-vector multiplication $\mathcal{L}\vec{\rho}$ is of the order $\mathcal{O}(N)$ instead of $\mathcal{O}(N^2)$ for the case of a dense matrix.

Iterative eigenvalue solvers can make use of this improved scaling behaviour as they are merely composed of a number of elementary matrix-vector multiplications. The basic idea behind this class of solvers relies on the power iteration method: By evaluating $A^k\vec{v}_0$ for a random starting vector $\vec{v}_0$ one can find the largest eigenvalue and corresponding eigenvector of the matrix A which is assumed to be diagonizable. To see this we decompose the starting vector $\vec{v}_i$ in the eigenbasis of A, that is given by the eigenvectors $\{\vec{e}_i\}$ with corresponding eigenvalues $\{\lambda_i\}$. If the largest eigenvalue, λ_1, is simple, i.e. a singular root of the characteristic polynomial, it is straightforward to show that

$$\lim_{k\to\infty} \frac{A^k\vec{v}_0}{\lambda_1^k} = c_1\vec{e}_1, \tag{A.8}$$

where $\{c_i\}$ are the coefficients of the decomposition of the starting vector $\vec{v}_0 = \sum_i c_i\vec{i}$. This scheme leads to the following algorithm for iteratively evaluating the largest eigenvalue and its corresponding eigenvector (see for example [73]).

- Input: A, $\vec{v}_0$
- Put $\vec{v}_0 \to \vec{v}_0/|\vec{v}_0|_\infty$ and define $\vec{v} = \vec{v}_0$
- For $i = 1, 2, \ldots$ until convergence
  $\vec{w} = A\vec{v}$
  $\lambda = \frac{\vec{v}^H\vec{w}}{|\vec{v}|^2}$
  $i = i\_max(\vec{w})$
  $\vec{v} \to \vec{v}/(\vec{e}_i^H\vec{w})$

Here $\vec{v}^H$ denotes the conjugated transpose of $\vec{v}$, $||_\infty$ is the maximum norm and $i\_max(\vec{w})$ is the index of the component of $\vec{w}$ with largest absolute value.

A small modification of this scheme allows to find the eigenvalue that is closest to a complex number μ in absolute value. If one replaces A by $(A-\mu\mathbf{1})^{-1}$, the above algorithm converges to an eigenvalue λ, and the actual eigenvalue of A closest to μ is given by $\mu+\frac{1}{\lambda}$. In practice, the inverse of $(A-\mu\mathbf{1})$ is never calculated explicitly. Instead one solves $(A-\mu\mathbf{1})\vec{w}=\vec{v}$ using an iterative method again.

If one is interested not only in a single eigenvalue but a few eigenvalues close to some number μ, a Krylov subspace or projection method can be employed. To this end we store the vectors $\vec{w}=A^i\vec{v}$ at each step of the iteration and consider the so called Krylov subspace $\mathcal{K}_k$ that is spanned by these vectors: $\mathcal{K}_k=\{\vec{v}_0, A\vec{v}_0, A^2\vec{v}_0, \dots A^k\vec{v}_0\}$. The basic idea is to construct approximate eigenvectors, the so called Ritz vectors, in the Krylov subspace $\mathcal{K}_k$. We refer to [73] for a detailed discussion of such projection methods.

In our implementation of the eigenvalue solver we strongly rely on the ARPACK library, a standard tool that employs elaborate variations of the above mentioned methods. The ARPACK routines are designed to return the desired number of eigenvalues and eigenvectors of a given sparse matrix A. As input data they require the dimension of the problem and the number of Ritz vectors to be calculate at each iteration step. The user can chose between a number of options. Among other things one can specify the starting vector or the convergence criterion. Furthermore the ARPACK routines allow to calculate either the eigenvalues with largest (smallest) absolute value, real part or imaginary part. The ARPACK eigensolver also distinguishes between real- and complex valued matrices, between symmetric and non-symmetric matrices and between double and single precision.

The actual form of A is not handed over to the ARPACK routines, though. The user has to provide all necessary information on the specific eigenvalue problem in the so called reverse communication interface. In practice that means, that one has to implement a sparse matrix-vector multiplication routine that evaluates $A\vec{v}$, for a given input vector $\vec{v}$. This routine is called by the ARPACK routines repeatedly in the course of the iteration procedure. In our implementation the matrix-vector multiplication is realized according to the following scheme:

For $i=0,1,\dots N-1$
For $j=11\cdot i,\dots 11\cdot i+10$
$w[i]+=A[j]\cdot v[\mathrm{col}[j]]$

Here col is an array of length $11\cdot N$ such that col[j] specifies the column of the matrix element $A[j]$.

Before concluding we comment on the performance of the eigensolver for our specific problem and on the choice of parameters and options that turned out to be convenient. Working with an ordinary personal computer, a MacBook with a $2.2\,GHz$ Intel Dual Core chip, allowed to solve eigenvalue problems with dimension $N^2\approx 10^4$ in a reasonable amount of time, i.e. within a few minutes. For most of the plots presented in section (2) the lowest $N_M=16$ and $N_{\mathrm{cav}}=8$ levels of the cantilever and the cavity respectively were taken into account. The relatively small energy spectrum puts strong restrictions on the variation of the parameters and demands to carefully check the validity of the truncation. The simplest test is to monitor the occupation of the highest levels, $n_M=N_M-1$ and $n_{\mathrm{cav}}=N_{\mathrm{cav}}-1$ respectively. A feasible limit of this occupation number turned out to be of the order 10^{-3}. If the truncation was inaccurate one can also find clear signs in the evaluated eigenspectrum and in the Wigner density. Regarding the various options for the ARPACK routines, we rely on empirical values. The eigenvalue solver was most efficient when it was prompted to evaluate only a few eigenvalues (~ 5) but use a slightly higher subspace of

~ 50 vectors. The optimal values of these numbers depend on the exact form of the matrix A and should be reconsidered each time the eigenproblem changes.

In order to allow for a wider applicability, an optimization of the numerical method is definitely worth considering. Clearly, the largest effect will come together with an improved matrix-vector multiplication routine. The performance of such a matrix-vector multiplication is not only restricted by the clock rate of the processor, but also and even more importantly, by the speed of the memory operations. In fact, sparse matrix-vector multiplications perform poorly on modern processors (reportedly reaching only 10% of the peak performance) as they are essentially memory-bounded. The common data structures for sparse matrices require time-consuming data access operations and allow for little data reuse in the cache. In the algorithm discussed above, for example, the elements of the input vector $\vec{v}$ are accessed very irregularly.

Quite generally we can conclude that the sparse matrix-vector multiplication can be efficiently optimized by exploiting information regarding the matrix structure and the processor's architectural characteristics. There are a few libraries that can undertake the task of optimizing the structure of the sparse matrix like the OSKI (Optimized Sparse Kernel Interface) package developed by the Berkeley Benchmarking and Optimization Group. It will be a future goal to address the issue of optimization and possibly apply the simulations to a wider range of parameters and setups.

A.4 Computation of expectation values

Once the steady-state solution of the master equation is found, basically all information on the optomechanical system is at hand. In particular the expectation value of an operator $\hat{A}$ is given by

$$\langle \hat{A} \rangle = Tr\{\hat{\rho}\hat{A}\}. \tag{A.9}$$

In our case, the operators of interest are the position, momentum and occupation number operators of either the cantilever or the cavity. By expressing these operators in terms of the corresponding annihilation and creation operators we can reduce the evaluation of their expectation values to a summation over density matrix elements.

The only peculiarity in this context is that we shift the expectation value of the cantilever's occupation number operator in order to allow for a comparison with the oscillation energy. As explained in more detail in section (1.2) we therefore define $\langle \hat{n}_M \rangle := \langle \hat{b}^\dagger \hat{b} \rangle - \frac{1}{4x_{\mathrm{ZPF}}^2} \langle \hat{x}_M \rangle^2$.

A.5 Evaluation of the probability distributions and Wigner densities

Quite generally, the statistical interpretation of the wave function allows to interpret the density matrix as a complete description of a quantum mechanical ensemble. In that sense we can discuss the statistical properties of the coupled cavity-cantilever system. The results of this analysis are shown in section (2.5) and here we will briefly present a few details of the calculations.

The probability distribution of the cantilever occupation number follows directly from the diagonal parts of the reduced density matrix $\hat{\rho}^{(M)}$ of the cantilever, that is obtained from the density matrix $\hat{\rho}$ of the cantilever-cavity system by tracing over the photon states. The evaluation of the Wigner probability distribution of the cantilever is a bit more costly. By definition the Wigner function is the Weyl transform of the density matrix,

$$W(x,p) = \frac{1}{\pi\hbar} \int_{-\infty}^{+\infty} \left\langle x - y \left| \hat{\rho}^{(M)} \right| x + y \right\rangle e^{2ipy/\hbar}\, dy. \tag{A.10}$$

As we have access to the elements of the density matrix in Fock space only, we rewrite this expression as

$$\begin{aligned} W(x,p) &= \frac{1}{\pi\hbar}\int_{-\infty}^{+\infty}\sum_{n,m}\langle x-y|n\rangle\langle n|\hat{\rho}^{(M)}|m\rangle\langle m|x+y\rangle e^{2ipy/\hbar}dy \\ &= \sum_{n,m} x_{\mathsf{ZPF}}^{-1}\pi^{-\frac{3}{2}}(2^{n+m-1}n!\,m!\,)^{-\frac{1}{2}}\rho_{n,m}^{(M)} \\ &\quad\times\int_{-\infty}^{+\infty} H_n\Big(\frac{x-y}{\sqrt{2}x_{\mathsf{ZPF}}}\Big)H_m\Big(\frac{x+y}{\sqrt{2}x_{\mathsf{ZPF}}}\Big)\exp\big(-\frac{x^2+y^2}{2x_{\mathsf{ZPF}}^2}\big)e^{2ipy/\hbar}dy \end{aligned} \quad \text{(A.11)}$$

where $\rho_{n,m}^{(M)} = \Big\langle n|\hat{\rho}^{(M)}|m\Big\rangle$ is a single matrix element of the cantilever's density matrix in Fock space representation.

$$\Psi_n(x) = \langle x|n\rangle = (2^n n!)^{-\frac{1}{2}}\Big(\frac{\pi}{2}\Big)^{-\frac{1}{4}}\frac{1}{\sqrt{x_{\mathsf{ZPF}}}}H_n\big(\frac{x}{\sqrt{2}x_{\mathsf{ZPF}}}\big)\exp\big(-\frac{x^2}{2x_{\mathsf{ZPF}}^2}\big) \quad \text{(A.12)}$$

denotes the wave function of the nth Fock state and is expressed by means of the Hermite Polynomial $H_n(z)$. Among the various ways to generate the explicit form of the Hermite polynomials $H_n(x)$ we choose the recursion relation $H_{n+1}(x) = 2xH_n(x) - 2nH_{n-1}(x)$, starting with $H_0 = 1$.

Finally we rescale the phase space with respect to the position and momentum zero-point fluctuations, $\tilde{x} = x/x_{\mathsf{ZPF}}$ and $\tilde{p} = p/p_{\mathsf{ZPF}}$, and obtain a Wigner distribution of the form

$$\begin{aligned} \tilde{W}(\tilde{x},\tilde{p}) &= \sum_{n,m}\pi^{-\frac{3}{2}}(2^{n+m-1}n!\,m!\,)^{-\frac{1}{2}}\rho_{n,m}^{(M)} \\ &\quad\times\int_{-\infty}^{+\infty} H_n\Big(\frac{\tilde{x}-\tilde{y}}{\sqrt{2}}\Big)H_m\Big(\frac{\tilde{x}+\tilde{y}}{\sqrt{2}}\Big)e^{-\frac{1}{2}(\tilde{x}^2+\tilde{y}^2)}e^{i\tilde{p}\tilde{y}}d\tilde{y}. \end{aligned} \quad \text{(A.13)}$$

Even though analytical solutions of the integral of equation (A.13) should in principle be possible, we evaluate this part numerically using the Romberg integration routine that is embedded in YORICK. We briefly mention, that we can make use of the symmetries of the integrand of equation and reduce the sum $\sum_{n,m}$ to $\sum_{n,m<n}$.

Bibliography

[1] T. W. Hänsch and A. L. Schawlow. Cooling of gases by laser radiation. *Optics Communications*, 13:68, 1975.

[2] D. Wineland and H. Dehmelt. *Bull. Am. Phys. Soc.*, 20:637, 1975.

[3] M. H. Anderson, J. R. Ensher, M. R. Matthews, C. E. Wieman, and E. A. Cornell. Observation of bose-einstein condensation in a dilute atomic vapor. *Science*, 269:198, July 1995.

[4] K. B. Davis, M. O. Mewes, M. R. Andrews, N. J. van Druten, D. S. Durfee, D. M. Kurn, and W. Ketterle. Bose-einstein condensation in a gas of sodium atoms. *Phys. Rev. Lett.*, 75:3969, Nov 1995.

[5] A. Dorsel, J. D. McCullen, P. Meystre, E. Vignes, and H. Walther. Optical bistability and mirror confinement induced by radiation pressure. *Phys. Rev. Lett.*, 51:1550, 1983.

[6] V.B. Braginsky and A.B. Manukin. Ponderomotive effects of electromagnetic radiation. *Soviet Physics JETP*, 25:653, 1967.

[7] V. B. Braginsky, A. B. Manukin, and M. Yu. Tikhonov. Investigation of dissipative ponderomotove effects of electromagnetic radiation. *Soviet Physics JETP*, 31:829, 1970.

[8] P. F. Cohadon, A. Heidmann, and M. Pinard. Cooling of a mirror by radiation pressure. *Phys. Rev. Lett.*, 83:3174, Oct 1999.

[9] C. Höhberger-Metzger and K. Karrai. Cavity cooling of a microlever. *Nature*, 432:1002, 2004.

[10] O. Arcizet, P. F. Cohadon, T. Briant, M. Pinard, and A. Heidmann. Radiation-pressure cooling and optomechanical instability of a micromirror. *Nature*, 444:71, 2006.

[11] D. Kleckner and D. Bouwmeester. Sub-kelvin optical cooling of a micromechanical resonator. *Nature*, 444:75, 2006.

[12] S. Gigan, H. R. Bohm, M. Paternostro, F. Blaser, G. Langer, J. B. Hertzberg, K. C. Schwab, D. Bauerle, M. Aspelmeyer, and A. Zeilinger. Self-cooling of a micromirror by radiation pressure. *Nature*, 444:67, 2006.

[13] A. Schliesser, P. Del'Haye, N. Nooshi, K. J. Vahala, and T. J. Kippenberg. Cooling of a micro-mechanical oscillator using radiation pressure induced dynamical back-action. *Phys. Rev. Lett.*, 97:243905, 2006.

[14] J. D. Thompson, B. M. Zwickl, A. M. Jayich, Florian Marquardt, S. M. Girvin, and J. G. E. Harris. Strong dispersive coupling of a high-finesse cavity to a micromechanical membrane. *Nature*, 452:900, 2008.

[15] Florian Marquardt, Joe P. Chen, A. A. Clerk, and S. M. Girvin. Quantum theory of cavity-assisted sideband cooling of mechanical motion. *Phys. Rev. Lett.*, 99:093902, 2007.

[16] I. Wilson-Rae, N. Nooshi, W. Zwerger, and T. J. Kippenberg. Theory of ground state cooling of a mechanical oscillator using dynamical backaction. *Phys. Rev. Lett.*, 99:093901, 2007.

[17] C. Höhberger and K. Karrai. Self-oscillation of micromechanical resonators. *Nanotechnology 2004, Proceedings of the 4th IEEE conference on nanotechnology*, page 419, 2004.

[18] T. Carmon, H. Rokhsari, L. Yang, T. J. Kippenberg, and K. J. Vahala. Temporal behavior of radiation-pressure-induced vibrations of an optical microcavity phonon mode. *Phys. Rev. Lett.*, 94:223902, 2005.

[19] T. J. Kippenberg, H. Rokhsari, T. Carmon, A. Scherer, and K. J. Vahala. Analysis of radiation-pressure induced mechanical oscillation of an optical microcavity. *Phys. Rev. Lett.*, 95:033901, 2005.

[20] Constanze Metzger, Max Ludwig, Clemens Neuenhahn, Alexander Ortlieb, Ivan Favero, Khaled Karrai, and Florian Marquardt. Self-induced oscillations in an optomechanical system driven by bolometric backaction. *Phys. Rev. Lett.*, 101:133903, 2008.

[21] Florian Marquardt, J. G. E. Harris, and S. M. Girvin. Dynamical multistability induced by radiation pressure in high-finesse micromechanical optical cavities. *Phys. Rev. Lett.*, 96:103901, 2006.

[22] K. R. Brown, J. Britton, R. J. Epstein, J. Chiaverini, D. Leibfried, and D. J. Wineland. Passive cooling of a micromechanical oscillator with a resonant electric circuit. *Phys. Rev. Lett.*, 99:137205, 2007.

[23] Ya. M. Blanter, O. Usmani, Nazarov, and Yu. V. Single-electron tunneling with strong mechanical feedback. *Phys. Rev. Lett.*, 93:136802, Sep 2004.

[24] A. A. Clerk and S. Bennett. Quantum nanoelectromechanics with electrons, quasi-particles and Cooper pairs: effective bath descriptions and strong feedback effects. *New Journal of Physics*, 7:238, 2005.

[25] M. P. Blencowe, J. Imbers, and A. D. Armour. Dynamics of a nanomechanical resonator coupled to a superconducting single-electron transistor. *New Journal of Physics*, 7:236, 2005.

[26] A. Naik, O. Buu, M. D. LaHaye, A. D. Armour, A. A. Clerk, M. P. Blencowe, and K. C. Schwab. Cooling a nanomechanical resonator with quantum back-action. *Nature*, 443:193, 2006.

[27] S. D. Bennett and A. A. Clerk. Laser-like instabilities in quantum nano-electromechanical systems. *Phys. Rev. B*, 74:201301, 2006.

[28] D. A. Rodrigues, J. Imbers, and A. D. Armour. Quantum dynamics of a resonator driven by a superconducting single-electron transistor: A solid-state analogue of the micromaser. *Phys. Rev. Lett.*, 98:067204, 2007.

[29] T J Harvey D A Rodrigues, J Imbers and A D Armour. Dynamical instabilities of a resonator driven by a superconducting single-electron transistor. *New Journal of Physics*, 9:84, 2007.

[30] C. A. Regal, J. D. Teufel, and K. W. Lehnert. Measuring nanomechanical motion with a microwave cavity interferometer. *Nat Phys*, 4:555, 2008.

[31] D. Meiser and P. Meystre. Coupled dynamics of atoms and radiation-pressure-driven interferometers. *Phys. Rev. A*, 73:033417, 2006.

[32] Kater W. Murch, Kevin L. Moore, Subhadeep Gupta, and Dan M. Stamper-Kurn. Observation of quantum-measurement backaction with an ultracold atomic gas. *Nat Phys*, 4:561, 2008.

[33] Ferdinand Brennecke, Stephan Ritter, Tobias Donner, and Tilman Esslinger. Cavity optomechanics with a bose-einstein condensate. *Science*, 322:235, 2008.

[34] J. K. Asboth, H. Ritsch, and P. Domokos. Optomechanical coupling in a one-dimensional optical lattice. *Physical Review A*, 77:063424, 2008.

[35] A. Schliesser, R. Riviere, G. Anetsberger, O. Arcizet, and T. J. Kippenberg. Resolved-sideband cooling of a micromechanical oscillator. *Nat Phys*, 4:415, 2008.

[36] M. Merlo, F. Haupt, F. Cavaliere, and M. Sassetti. Sub-poissonian phononic population in a nanoelectromechanical system. *New Journal of Physics*, 10:023008, 2008.

[37] L. Pitaevskii and S. Stringari. *Bose-Einstein Condensation*. Clarendon Press Oxford, 2003.

[38] Franco Dalfovo, Stefano Giorgini, Lev P. Pitaevskii, and Sandro Stringari. Theory of bose-einstein condensation in trapped gases. *Rev. Mod. Phys.*, 71:463, Apr 1999.

[39] W. Ketterle, D.S. Durfee, and D.M. Stamper-Kurn. Making, probing and understanding bose-einstein condensates. *Proceedings of the International School of Physics "Enrico Fermi", Course CXL*, pages 67–176, 1999.

[40] N. Bogoliubov. On the theory of superfluidity. *J. Phys. (Moscow)*, 11:23, 1947.

[41] D. S. Jin, J. R. Ensher, M. R. Matthews, C. E. Wieman, and E. A. Cornell. Collective excitations of a bose-einstein condensate in a dilute gas. *Phys. Rev. Lett.*, 77:420, 1996.

[42] M.-O. Mewes, M. R. Andrews, N. J. van Druten, D. M. Kurn, D. S. Durfee, C. G. Townsend, and W. Ketterle. Collective excitations of a bose-einstein condensate in a magnetic trap. *Phys. Rev. Lett.*, 77:988, 1996.

[43] S. Stringari. Collective excitations of a trapped bose-condensed gas. *Phys. Rev. Lett.*, 77:2360, 1996.

[44] Mark Edwards, P. A. Ruprecht, K. Burnett, R. J. Dodd, and Charles W. Clark. Collective excitations of atomic bose-einstein condensates. *Phys. Rev. Lett.*, 77:1671, 1996.

[45] M. R. Andrews, D. M. Kurn, H.-J. Miesner, D. S. Durfee, C. G. Townsend, S. Inouye, and W. Ketterle. Propagation of sound in a bose-einstein condensate. *Phys. Rev. Lett.*, 79(4):553–556, Jul 1997.

[46] Martin Fliesser, András Csordás, Péter Szépfalusy, and Robert Graham. Hydrodynamic excitations of bose condensates in anisotropic traps. *Phys. Rev. A*, 56:R2533, 1997.

[47] P. Öhberg, E. L. Surkov, I. Tittonen, S. Stenholm, M. Wilkens, and G. V. Shlyapnikov. Low-energy elementary excitations of a trapped bose-condensed gas. *Phys. Rev. A*, 56:R3346, 1997.

[48] Kater W. Murch. *Quantum cavity optomechanics with ultracold atoms*. PhD thesis, University of California, Berkeley, 2008.

[49] Subhadeep Gupta, Kevin L. Moore, Kater W. Murch, and Dan M. Stamper-Kurn. Cavity nonlinear optics at low photon numbers from collective atomic motion. *Physical Review Letters*, 99:213601, 2007.

[50] S. Ritter, F. Brennecke, C. Guerlin, K. Baumann, T. Donner, and T. Esslinger. Dynamical coupling between a bose-einstein condensate and a cavity optical lattice. *arXiv:0811.3967*, November 2008.

[51] L. Tian and P. Zoller. Coupled ion-nanomechanical systems. *Physical Review Letters*, 93:266403, 2004.

[52] S. Singh, M. Bhattacharya, O. Dutta, and P. Meystre. Coupling nanomechanical cantilevers to dipolar molecules. *arXiv:0805.3735*, 805, 2008.

[53] C. Genes, D. Vitali, and P. Tombesi. Emergence of atom-light-mirror entanglement inside an optical cavity. *arXiv0801:2266*, 2008.

[54] K. Hammerer, M. Aspelmeyer, E. S. Polzik, and P. Zoller. Quantum interface for nanomechanics and atomic ensembles. *arXiv:0804.3005*, 2008.

[55] H. Ian, Z. R. Gong, Yu xi Liu, C. P. Sun, and Franco Nori. Cavity optomechanical coupling assisted by an atomic gas. *Phys. Rev. A*, 78:013824, 2008.

[56] X. X. Yi, H. Y. Sun, and L. C. Wang. Coupled dynamics of an atom and an optomechanical cavity. *arXiv::0807.2703*, 2008.

[57] Philipp Treutlein, David Hunger, Stephan Camerer, Theodor W. Hansch, and Jakob Reichel. Bose-einstein condensate coupled to a nanomechanical resonator on an atom chip. *Phys. Rev. Lett.*, 99:140403, 2007.

[58] J. K. Asboth and P. Domokos. Comment on "coupled dynamics of atoms and radiation-pressure-driven interferometers" and "superstrong coupling regime of cavity quantum electrodynamics". *Phys. Rev. A*, 76:057801, 2007.

[59] D. Meiser and P. Meystre. Reply to "comment on 'coupled dynamics of atoms and radiation-pressure-driven interferometers' and 'superstrong coupling regime of cavity quantum electrodynamics' ". *Phys. Rev. A*, 76:057802, 2007.

[60] T. Botter, D. Brooks, S. Gupta, Z.-Y. Ma, K. L. Moore, K. W. Murch, T. P. Purdy, and D. M. Stamper-Kurn. Quantum micro-mechanics with ultracold atoms. *arXiv:0810.3841*, 2008.

[61] Benjamin S. Sheard, Malcolm B. Gray, Conor M. Mow-Lowry, David E. McClelland, and Stanley E. Whitcomb. Observation and characterization of an optical spring. *Phys. Rev. A*, 69:051801, 2004.

[62] D. Jaksch, C. Bruder, J. I. Cirac, C. W. Gardiner, and P. Zoller. Cold bosonic atoms in optical lattices. *Phys. Rev. Lett.*, 81:3108, 1998.

[63] M. Greiner, O. Mandel, T. Esslinger, T. W. Hänsch, and I. Bloch. Quantum phase transition from a superfluid to a mott insulator in a gas of ultracold atoms. *Nature*, 415:39, 2002.

[64] A. Görlitz, J. M. Vogels, A. E. Leanhardt, C. Raman, T. L. Gustavson, J. R. Abo-Shaeer, A. P. Chikkatur, S. Gupta, S. Inouye, T. Rosenband, and W. Ketterle. Realization of bose-einstein condensates in lower dimensions. *Phys. Rev. Lett.*, 87:130402, 2001.

[65] I. B. Spielman, P. R. Johnson, J. H. Huckans, C. D. Fertig, S. L. Rolston, W. D. Phillips, and J. V. Porto. Collisional deexcitation in a quasi-two-dimensional degenerate bosonic gas. *Phys. Rev. A*, 73:020702, 2006.

[66] D. F. Walls and G. J. Milburn. *Quantum Optics*. Springer-Verlag, New York, 1994.

[67] A. A. Clerk, M. H. Devoret, S. M. Girvin, F. Marquardt, and R. J. Schoelkopf. Introduction to quantum noise, measurement and amplification. *arXiv:0810.4729*, 2008.

[68] M. Bhattacharya and P. Meystre. Multiple membrane cavity optomechanics. *Phys. Rev. A*, 78:041801, 2008.

[69] T. Bhattachary, S. Habib, and K. Jacobs. The emergence of classical dynamics in a quantum world. *Los Alamos Science*, 27, 2002.

[70] Benjamin D. Greenbaum, Salman Habib, Kosuke Shizume, and Bala Sundaram. Semiclassics of the chaotic quantum-classical transition. *Phys. Rev. E*, 76:046215, 2007.

[71] Salman Habib, Kurt Jacobs, Hideo Mabuchi, Robert Ryne, Kosuke Shizume, and Bala Sundaram. Quantum-classical transition in nonlinear dynamical systems. *Phys. Rev. Lett.*, 88:040402, 2002.

[72] Itamar Katz, Alex Retzker, Raphael Straub, and Ron Lifshitz. Signatures for a classical to quantum transition of a driven nonlinear nanomechanical resonator. *Phys. Rev. Lett.*, 99:040404, 2007.

[73] R. B. Lehoucq, D. C. Sorensen, and C. Yang. *ARPACK User's Guide: Solution of Large-Scale Eigenvalue Problems with Implicitly Restarted Arnoldi Methods*. SIAM, 1998.

Selbstständigkeitserklärung

Hiermit erkläre ich, die vorgelegte Arbeit selbst verfasst und keine anderen als die angegebenen Quellen und Hilfsmittel verwendet zu haben.

München, den 28. November 2008